



PONTIFICIA  
UNIVERSIDAD  
CATÓLICA  
DE CHILE

PONTIFICIA UNIVERSIDAD CATÓLICA DE CHILE  
FACULTAD DE FÍSICA  
Instituto de Física

**CONTROL OF WAVE-PARTICLE DUALITY VIA  
ATOM-FIELD INTERACTION IN DOUBLE-SLIT  
SCHEMES**

**POR MARIO ERNESTO BRAYAN MIRANDA ROJAS**

Tesis presentada al Instituto de Física de la Pontificia Universidad  
Católica de Chile para optar al grado académico de Doctor en  
Física

Profesor Guía: Dr. Miguel Antonio Orszag Posa

Enero 2022

Santiago, Chile

ii

...a mi familia!

# Acknowledgments

We wish to acknowledge the financial support from the project FONDECYT 1180175, Beca Doctorado Nacional CONICYT 21171247 and Vicerrectoría de Investigación UC during the development of this research.

# Contents

<b>Acknowledgments</b>	<b>iii</b>
<b>Contents</b>	<b>iv</b>
<b>List of Figures</b>	<b>vi</b>
<b>Abstract</b>	<b>x</b>
<b>1 Introduction</b>	<b>1</b>
<b>2 Theoretical framework</b>	<b>6</b>
2.1 Experimental and theoretical tests of complementarity . . . . .	6
2.1.1 Which-path detectors and loss of fringe visibility . . . . .	7
2.1.2 Quantum eraser and delayed choice . . . . .	9
2.1.3 Balance among visibility, distinguishability and concurrence . . . . .	14
2.2 Atom-field interaction . . . . .	17
2.2.1 Quantum description . . . . .	17
2.2.2 Atomic location based on atom-field interaction . . . . .	19
<b>3 Controlling the wave-particle duality with quantum fields</b>	<b>28</b>
3.1 Model . . . . .	29
3.1.1 Initial state . . . . .	30
3.1.1.1 Squeezed coherent state . . . . .	30
3.1.1.2 Cat state . . . . .	30
3.1.1.3 Thermal state . . . . .	31
3.1.2 Time evolution . . . . .	31
3.1.3 Which-path information and fringe visibility . . . . .	32
3.2 Results . . . . .	33
3.2.1 Coherent state . . . . .	34
3.2.1.1 Wave-particle duality controlled by the coherent amplitude $\alpha'$ . . . . .	34
3.2.1.2 Wave-particle duality controlled by the coherent phase $\varphi$ . . . . .	36
3.2.2 Squeezed coherent state . . . . .	36
3.2.2.1 Wave-particle duality controlled by the squeeze amplitude $r$ . . . . .	37
3.2.2.2 Wave-particle duality controlled by the squeeze phase $\vartheta$ . . . . .	38
3.2.3 Cat states . . . . .	38
3.2.3.1 Interaction time: $ g ^2 t / \Delta = \pi$ . . . . .	38

3.2.3.2	Interaction time: $ g ^2 t / \Delta = 3\pi/4$ . . . . .	39
3.2.3.3	Interaction time: $ g ^2 t / \Delta = \pi/2$ . . . . .	40
3.2.4	Thermal state . . . . .	41
<b>4</b>	<b>Wave-particle duality controlled by a classical radiation</b>	<b>43</b>
4.1	Model . . . . .	43
4.1.1	Initial state . . . . .	44
4.1.2	Time evolution of the system . . . . .	45
4.1.3	Quadrature measurement . . . . .	47
4.1.4	Particle-wave duality and concurrence . . . . .	50
4.2	Numerical results . . . . .	51
4.2.1	Stage 1: Atom passing through the double slit (no fields) . . . . .	52
4.2.2	Stage 2: Atom passing through the double slit with the quantum field . . . . .	53
4.2.3	Stage 3: Atom passing through the double slit with the quantum and classical fields . . . . .	53
4.3	Effects of the evolution operator on the initial state of the quantum field $ \alpha\rangle$ [ eq. (4.8)]. . . . .	56
<b>5</b>	<b>Partial quantum eraser and delayed choices</b>	<b>59</b>
5.1	Description of the model . . . . .	59
5.2	Partial quantum eraser and delayed choices . . . . .	61
5.2.1	Reading the path information from the quantum field . . . . .	62
5.2.2	Erasing the path information from the quantum field . . . . .	63
5.2.3	Measuring the internal atomic state . . . . .	63
<b>6</b>	<b>Results and conclusions</b>	<b>65</b>
6.1	Controlling the wave-particle duality with quantum fields . . . . .	65
6.2	Wave particle duality controlled by a classical radiation . . . . .	67
6.3	Quantum eraser and delayed choices . . . . .	68
<b>7</b>	<b>Appendix</b>	<b>69</b>
7.1	Appendix subsection 2.1.3 . . . . .	69
7.1.1	Appendix subsection 2.2.1 . . . . .	70
7.1.2	Appendix subsection 2.2.2 . . . . .	73
7.1.3	Appendix chapter 3 . . . . .	80
	<b>Bibliography</b>	<b>82</b>

# List of Figures

2.1	a) Double-slit setup crossed by atoms, in which total interference is obtained due to the interaction of $\psi_1$ with $\psi_2$ , as in a typical Young's experiment. b) External devices used to obtain which-path information and to vanish the interference. . . .	8
2.2	Double-slit setup crossed by atoms, in which interference can be vanished due to the presence of external devices which allows to obtain total which-path information.	8
2.3	Double-slit setup to study the possibilities of implementing a quantum eraser. . . .	10
2.4	Two-level atoms are located in the position 1 and 2. An incident pulse $I_1$ excites one of the atoms to the level $a$ to later emit a $\gamma$ photon. Since the final state of both atoms is the same, no path information can be extracted from them, and total interference is obtained. . . . .	12
2.5	Three-level atoms are located in the position 1 and 2. An incident pulse $I_1$ excites one of the two atoms from the level $c$ to the level $a$ , then it emits a $\gamma$ photon and ends up in the state $b$ . In this case the internal atomic state can reveal which-path information. . . . .	12
2.6	Four-level atoms are located in the position 1 and 2. Two incident pulse, $I_1$ and $I_2$ , excite one of the atoms from the level $c$ to the level $a$ and from $b$ to $b'$ , which allows the emission of the photons $\gamma$ and $\phi$ , respectively. As a consequence, the final atomic state is the same and there is no path-information. . . . .	13
2.7	Theoretical delayed choice quantum eraser scheme. . . . .	14
2.8	Young's two-slit scheme used to study the balance among wave, particle and concurrence . . . . .	15
2.9	Conditional probability $P(\chi x)$ . . . . .	22
2.10	Probability distribution of the atom after an $X$ quadrature measurement of the field with values $\chi_0 = \alpha$ (red) and $\chi_0 = -\alpha$ (blue). . . . .	23
2.11	Probability distribution of the atom after the $X$ quadrature measurement of the field with value $\chi_0 = 0$ . . . . .	23
2.12	Probability distribution in function of $x'$ y $t'$ . . . . .	24
2.13	Postion probability distribution for $t' = 0.015$ . . . . .	24
2.14	Postion probability distribution for $t' = 3$ . . . . .	25
2.15	Atomic probability distribution when the value $\chi_0 = 0$ is obtained after to perform an $X_0$ quadrature measurement. The initial atomic distribution is taken $\kappa(x) = 3\lambda/4$ .	25
2.16	Atomic probability distribution in function of $x'$ y $t'$ after field measurement when $\kappa(x) = 3\lambda/4$ . . . . .	25
2.17	Atomic probability distribution in function of $x'$ for $t' = 0.015$ . . . . .	26
2.18	Atomic probability distribution in function of $x'$ for $t' = 0.05$ . . . . .	26
2.19	Atomic probability distribution in function of $x'$ for $t' = 3$ . . . . .	26

3.1	Double-slit scheme. A two-level atom passes through the atomic beam splitter (ABS) in the ground state. In the upper path $ P_{\uparrow}\rangle$ , the atomic mirror (AM) and Ramsey field (RF) generate the internal atomic state $ \Phi_{\uparrow}\rangle$ , while in the bottom path $ P_{\downarrow}\rangle$ the initial atomic state remains the same. Finally, the atom crosses a node or antinode of the quantum field. . . . .	29
3.2	Unit sphere $D_0^2 + V_0^2 + C_0^2 = 1$ . The cases studied in this article are $C_0 = 1$ (green dot), $C_0 = V_0$ (orange dot) and $V_0 = 1$ (red dot). . . . .	33
3.3	Spread of the atomic distribution once the atom crosses a typical double-slit scheme. In this case, we consider the evolution of the distribution in absence of the quantum field. Therefore, the images (a) – (b), (c) – (d) and (e) – (f) correspond to the cases $C_0 = 1(\phi = \pi/2)$ , $V_0 = C_0(\phi = \pi/4)$ and $V_0 = 1(\phi = 0)$ , respectively. On the left are shown the atomic probability distributions as a function of both, time $t'$ and distance $x'$ , on the right are shown the patterns obtained for a flight time $t' = 3$ . . . . .	35
3.4	Phase-shift (counter-clock wise) produced by the interaction of an atom in the state $ b\rangle$ ( $\phi = 0$ ) and a coherent state with $\alpha' = 3$ and $\varphi = 0$ . An $X$ quadrature measurement [vertical shadows in (c)] can reveal which-path information and no interferences appears. A $Y$ quadrature measurement [horizontal shadow with red edges in (c)] can not distinguish one phase from the other one and total interference is obtained. . . . .	36
3.5	For a coherent state with $\alpha' = 1$ and $\varphi = 0$ there is overlap between both, initial and final phases [vertical shadow with red edges in (c)]. Therefore, an $X$ quadrature measurement becomes ambiguous and partial interference appears. A $Y$ quadrature measurement still shows total interference. . . . .	36
3.6	An atom in the state $ b\rangle$ produces a counter-clockwise phase-shift in a coherent state with $\alpha' = 3$ and $\varphi = \frac{15\pi}{32}$ . The initial and final phases show overlap for an $X$ quadrature measurement [vertical shadows with red edges in (c)] and thus partial interference can be observed. On the contrary, a $Y$ quadrature measurement [horizontal shadows in (c)] can reveal which-path information (no overlap). . . . .	37
3.7	Atomic probability distribution obtained for an $X$ quadrature measurement after atom-field interaction, considering a quantum field represented by a coherent state. The field and atomic parameters are varied in the vertical and horizontal directions, respectively. . . . .	37
3.8	Phase-shift for a squeezed coherent state with $\alpha' = 3$ , $\varphi = 0$ , $r = 2$ and $\vartheta = \pi$ , considering interaction with an atom in the state $ b\rangle$ . For these parameters there is a considerable overlap between the initial and final phases. As a consequence, an $X$ quadrature measurement [vertical shadow in (c)] becomes ambiguous. On the other hand, total interference is obtained if a $Y$ quadrature measurement [horizontal shadow in (c)] is performed. . . . .	38
3.9	The changes in the phases of the field show that for an $X$ quadrature measurement the overlap between the phases decreases when the squeeze phase increases [see (c)]. Therefore, there is more which-path information and less interference, as compared to the previous case. . . . .	39
3.10	Atomic probability distribution obtained for an $X$ quadrature measurement. In this case the quantum field corresponds to a squeezed coherent state. The field parameters are varied vertically while $\phi$ , which defines the atomic state, is varied horizontally. . . . .	39

- 3.11 A phase-shift  $\pi$  just interchanges clockwise or counterclockwise the position of the distributions of the initial phase of the cat state, if the internal atomic state corresponds to  $|a\rangle$  or  $|b\rangle$  [see (b)], respectively. Therefore, it is not possible to obtain path-information if an  $X$  or  $Y$  quadrature measurement is performed [see (c)]. . . . 40
- 3.12 A phase-shift equal to  $3\pi/4$  allows to differentiate the initial phase from the final one for certain results of the quadrature measurements. Therefore, partial path-information can be obtained with an  $X$  or  $Y$  quadrature measurement [see (c)]. . . 40
- 3.13 A phase-shift equal to  $\pi/2$  allows a better phase differentiation. In this case, path-information can be obtained for most results of an  $X$  or  $Y$  quadrature measurement. Red lines in (c) represent the possible results for which these measurements become ambiguous. . . . . 41
- 3.14 Atomic probability distribution obtained for an  $X$  quadrature measurement considering different interaction times between an atom and a cat state with  $\alpha' = 3$  and  $\varphi = 0$ . The atomic parameter  $\phi$  is varied horizontally and the interaction time vertically. . . . . 41
- 3.15 For different values of  $\langle n \rangle_{th}$  the phase of the thermal state remains in the center of the  $XY$  plane. Therefore, the possible phase-shifts in the evolution operator can not be detected after the interaction. . . . . 42
- 4.1 Scheme of the possible paths followed by the atom. ABS: Atomic Beam Splitter, AM: Atomic Mirror, RF: Ramsey Field. The atom is either reflected or transmitted by the ABS by taking the upper or lower path, respectively. Finally, the atom crosses the double-slit and both, quantum (red) and classical (blue) fields. . . . . 44
- 4.2 Initial phase of the quantum field  $|\alpha\rangle$  for an amplitude  $\alpha = \sqrt{8}$ , where  $X$  and  $Y$  correspond to the amplitude and phase quadrature of the field, respectively. . . . . 45
- 4.3 A three-level atom crosses the double cavity with a quantum (red) and a classical (blue) field. . . . . 46
- 4.4 If the internal atomic state in the top path is  $|b\rangle$ , there is no phase-shift in the quantum field for  $\alpha = \sqrt{8}$  and  $\varepsilon = 0$ . Therefore, no path-information is record on the field. However, the own internal atomic states in the top and bottom path can give information about which slit the atom passed through. . . . . 48
- 4.5 If the internal atomic state in the top path is  $|c\rangle$ , it produces a phase-shift of  $\pi$  in the quantum field, which reveals path-information. We consider  $\alpha = \sqrt{8}$  and  $\varepsilon = 0$ . In this case the most probable result for an  $X$  quadrature measurement is  $\chi_{\theta=0} = -\alpha$ . 49
- 4.6 A  $Y$  quadrature measurement does not reveal path information, because the most probable result is obtained regardless of quantum field state. . . . . 50
- 4.7 Unit sphere  $D_0^2 + V_0^2 + C_0^2 = 1$ . The extreme cases  $V_0 = 1$ ,  $D_0 = 1$ ,  $C_0 = 1$  and intermediate ones are shown on the surface by red dots. . . . . 51
- 4.8 *Stage I*: Atomic probability distribution obtained for each case shown on the sphere  $V_0^2 + D_0^2 + C_0^2 = 1$  for  $t' = 3$ . The distance  $x'$  is expressed in units of  $\lambda = \lambda_{CF}$ . a)  $V_0 = 1$ , b)  $V_0 = D_0$ , c)  $D_0 = 1$ , d)  $D_0 = C_0$ , e)  $C_0 = 1$ , f)  $C_0 = V_0$ , g)  $V_0 = D_0 = C_0$ . 52

4.9 Stage 2: Atomic probability distribution obtained for each case shown on the sphere  $V_0^2 + D_0^2 + C_0^2 = 1$  in presence of the quantum field for  $t' = 3$  with  $\alpha = \sqrt{8}$  (blue) and  $\alpha = 1$  (red).  $x'$  is expressed in units of  $\lambda = \lambda_{CF}$ . The choice of the parameters  $c_{\uparrow,\downarrow}$  and  $\gamma$  satisfies: a)  $V_0 = 1$ , b)  $V_0 = D_0$ , c)  $D_0 = 1$ , d)  $D_0 = C_0$ , e)  $C_0 = 1$ , f)  $C_0 = V_0$ , g)  $V_0 = D_0 = C_0$ . . . . . 54

4.10 Internal atomic state  $|b\rangle$  in the top path: As the value of  $\varepsilon$  rises, the phase of the quantum field begins to differentiate from the initial phase. Thus, now a  $X$  quadrature measurement can reveal path-information. . . . . 55

4.11 Internal atomic state  $|c\rangle$  in the top path: In this case, as  $\varepsilon$  increases, the phase of the quantum field approaches to its initial value. So now, the  $X$  quadrature measurement becomes ambiguous and the path-information decreases. . . . . 56

4.12 Stage 3: When  $\varepsilon = 3$ , the effects of the atomic states  $|b\rangle$  and  $|c\rangle$  on the phase of the quantum field are similar [see figure 4.10b and figure 4.11b]. Therefore, an  $X$  quadrature measurement cannot reveal completely path-information and the atomic distributions show partial interference in some cases and a faster evolution in other ones (red lines). Blue lines correspond to the results obtained for  $\varepsilon = 0$  in the *stage 2*. The cases a)  $V_0 = 1$ , b)  $V_0 = D_0$ , c)  $D_0 = 1$ , d)  $D_0 = C_0$ , e)  $C_0 = 1$ , f)  $C_0 = V_0$ , g)  $V_0 = D_0 = C_0$  represent the choice of the parameters used in the *stage 1*. The flight time is taken  $t' = 3$  with  $x'$  in units of  $\lambda = \lambda_{CF}$ . . . . . 57

5.1 Scheme of the possible paths followed by the atom. ABS: Atomic Beam Splitter, AM: Atomic Mirror, RF: Ramsey Field. The atom is either reflected or transmitted by the ABS by taking the upper or lower path, respectively. Finally, the atom crosses the double-slit and the quantum field. . . . . 60

5.2 Phase shifts for maximum atom-field interaction considering  $|g|^2 t / \Delta = \pi$ . If the atom crosses the upper slit is in the state  $|b\rangle$  ( $|a\rangle$ ) there is a counter-clock (clock) wise phase shift in the coherent state. If an amplitude quadrature measurement (black dotted lines) is performed, the results can give information about the path followed by the atom, but cannot always reveal the internal its internal state. On other hand, a phase quadrature measurement becomes ambiguous and it does not reveal path information or the atomic state. . . . . 61

5.3 Patterns observed depending on the measurements performed on the atom and field. We consider different values of the atomic parameter  $\phi$ , in order to show more possibilities of partial fringe visibility. . . . . 64

# Abstract

The dual nature of light and matter represents an important challenge for science. Since the origins of quantum mechanics, several theoretical and experimental works have studied the wave and corpuscular properties of photons, atoms, electrons, etc. The main model that has been considered in the development of them has been the Young's double-slit scheme, by means of which the wave nature of light was demonstrated. However, it also can be used to obtain the particle-like properties of the systems. In case of considering identical slits, this model allows to obtain total fringe visibility on a screen located at a certain distance from the double-slit, and thus, null knowledge about the path followed by the object that crosses the scheme. Therefore, the system shows a wave behavior.

In order to obtain information about the path taken by the objects (photons, atoms, electrons, etc), several authors have studied the coupling of external systems to double-slit schemes, which allows to know the path followed by the particle. As a consequence, the implementation of any type of path-detector results in the loss of fringe visibility, according to the principle of complementarity postulated by Bohr.

In this research, we have considered the use of double-slit schemes and atom-field interactions to control the balance between fringe visibility and which-path information. We consider field cavities which act as path-detectors and they are represented by different quantum states. Instead of photons, our schemes are crossed by atoms, whose internal levels are correlated to the paths of the schemes. Therefore, based on the preparation of both, field and atom, we can study the balance between distinguishability, visibility and the concurrence present in the system.

Our results show that the wave-particle duality can be controlled by atomic and field parameters, depending on the behavior that the experimenter wishes to observe, wave-like or particle-like. Additionally, we present a model in which a classical field can control the quantum atom-field interaction. Therefore, the amplitude of the classical field can also be considered as a controlling parameter of the wave-particle duality.

Finally, based on our results, we propose a theoretical model to be implemented in quantum eraser and delayed choice experiments, which nowadays arouses great interest among researchers. Our results suggest that the wave-particle duality can be controlled even at times after the atom is registered on a screen, which allows us to choose the behavior of the system, wave-like or particle-like, at any moment.

# Chapter 1

## Introduction

Particle-wave duality represents one of the most important concepts within physics, and it has played an essential role in the study of the behavior of light and matter in experimental and theoretical contexts. Nowadays, different works associated to the duality are mainly focused on the development of models based on quantum mechanics, in order to offer alternatives to discussions that have been held for years. This is because the dual behaviour of light and matter has been an interesting way to explain how the quantum world works around us, but at the same time it has been a continuous source of controversy based on different proposals and the results that have been obtained over the years, even at times giving rise to paradoxes hard to address.

To understand the evolution of the ideas related to the wave-particle duality, we must go back to the first studies and observations that sought to understand the composition and nature of light. As early as the 3rd century B.C. Euclid (325 B.C.-265 B.C) developed his studies on the behavior of light, and how it propagated in different media, which led to one of his main findings about the way in which light interacted with certain objects changing its direction of propagation [8]. His observations led him to raise the law of reflection of light, establishing that the angle with which a beam of light falls on a certain reflective surface, is the same with which it is reflected [9]. Behind his results, we can note that Euclid's vision of the nature of light was to consider it simply as rays propagating in a straight line, which in the presence of a reflective object could change its direction. That is, in no case was light considered as a wave or a particle.

Despite the development of various studies seeking understanding of the behavior of light, it was not until several centuries later that wave-particle duality became a problem to be discussed among the scientific community. In the 17th century, the way in which light propagated remained a topic of interest, which led to the carrying out of several works by different scientists, including Willebrord Snell van Royen (1580-1626) and René Descartes (1596-1650), who sought to understand the refraction of light, phenomenon that occurs when the beam passes from one medium to another. As a result, light changes its direction, depending on the densities of both media [40]. The results obtained led to an expression in terms of the angles of incidence  $\theta_i$  and refraction  $\theta_r$ , and the refraction index of the media of propagation,  $n_i$  and  $n_r$ , respectively, which today is called Snell's Law:

$$n_i \sin \theta_i = n_r \sin \theta_r, \quad (1.1)$$

where the refraction indexes are defined as  $n = \frac{c}{v}$  with  $c$  being the speed of light in the vacuum and  $v$  the speed of light in a given medium. Therefore, the way the light spreads from one medium to another will depend on the density of them [11].

Up to this point the concepts of particle or wave had not been considered as essential to study the behavior of light or to describe it. However, other phenomena such as the diffraction of light, studied by Francesco María Grimaldi (1618-1663), gave hints of its wave behavior, which was not well received by the rest of the researchers of the time, who attributed these results to possible experimental errors [41, 44]. Despite this, the fact that light had a wave-like nature was not entirely discarded by other scientists like Christian Huygens (1629-1695), who proposed that light propagated as waves traveling in a medium denominated ether. This led to a better interpretation of phenomena such as diffraction, reflection and refraction of light through the method of analysis that today we now know as the Huygens-Fresnel Principle [29, 30], due to the mathematical complement made by Jean Fresnel (1788-1827) years later [60].

Despite Huygens' contributions, the wave behavior of light had not been thoroughly studied to establish it as definitive in the description of the nature of light. Between the 17th and 18th centuries, Isaac Newton (1643-1727) postulated his ideas regarding the corpuscular nature of light, which was based on the assumption that light could be understood as a set of particles that propagated from a certain source to the human eye through the ether. Thus, the colors that could be observed corresponded to different types of particles or combinations of these [48]. Although the novelty of the proposal, it was discussed by another scientist of the time, like Robert Hooke (1635-1703), who supported the idea that the nature of light had a wave behaviour [10], to which Newton argued that, in fact, light was constituted by particles that generated waves in the propagation medium, making the analogy with the waves created by stones in the water. Newton argued that light could not be only wave-like, referring to the fact that the waves had a spherical propagation, whereas the rays of light propagated in a straight line, which suggested a corpuscular behavior [1, 47]. The above was largely accepted for several years despite the contrary beliefs that certain scientists had with regard to Newton's arguments, such as Huygens, who held that light was actually the movement of the ether particles, that is, the results of oscillations of the propagation medium.

More than a hundred years later, it was Thomas Young (1773-1829), who contributed the debate on the nature of light by revalidating the, then, discarded wave theory, which was put aside for a long time because of the figure that Newton represented and the great support that his theory maintained. Young developed several experiments that showed that light interfered, the results of which were attributable to wave behaviour [36, 66, 69]. However, his ideas were not fully accepted due to the lack of a solid mathematical development for his proposals and the still-extant respect for the corpuscular theory proposed by Newton. The work done by Young was later considered by Augustin Fresnel (1788-1827), who also relied on Huygens' ideas about the wave behavior of light to explain different optical phenomena [20]. Fresnel's contribution helped significantly to make ideas about the dual nature of light widely accepted. This also was supported by the work of other researchers, such as the Christian Doppler (1803-1853), who used these ideas to explain the shifts of stellar frequency spectra [14], or James Clerk Maxwell (1831-1879), who considered that the phenomena associated with electromagnetism propagated

as waves, coming to the conclusion that light was an electromagnetic phenomenon [3, 42]. This idea would later be demonstrated by Heinrich Hertz (1857-1894) [28].

Finally, it seemed that the wave theory of light managed to prevail and be widely accepted by the scientific community thanks to the work done by scientists such as Huygens, Young, Maxwell, Fresnel and Hertz, which put the corpuscular theory imposed by Newton in an awkward position in front of the new advances made under the premise that light was actually a wave and not a set of traveling particles, although this idea had not been refuted in any way. Therefore, the coexistence of both theories could not yet be ruled out. However, we would have to wait until the beginning of the 20th century to understand, with the birth of quantum mechanics, the behavior of light.

In 1890 Max Planck (1858-1947) was working on the study of black body radiation, based on Wien's law [52] and making use of his prior knowledge of Boltzmann's theory about the second law of thermodynamics [37]. As a result, Planck proposed a new constant (Planck's constant  $\hbar$ ), postulating that radiation energy was divided into small portions of energy which he called quantum of energy, which was in complete agreement with the experimental results of the time [38, 39]. Planck's work is considered as the beginning of quantum mechanics and gave an account of the corpuscular behavior of light. His ideas were subsequently considered by Albert Einstein (1879-1955), who used them as a basis for his research on the photoelectric effect [59, 64, 65], in which it demonstrated the importance of light frequency in that process [15]. With this, Einstein further endorsed Planck's results, assuming that the processes of emission and absorption of radiation were produced in small packets of energy, just as light was propagated through space. Although Einstein's work was still poorly accepted by some researchers, in 1922 Arthur Compton (1892-1962) conducted an experiment based on X-ray scattering, whose results could be explained taking into consideration the idea of a corpuscular nature of light [19], with which he could understand how light and matter related by exchanging moments as small particles would, which was evident in their experimental results.

With the above, the idea of a corpuscular nature of light was again gaining strength among scientists. However, it was still difficult to explain some observed phenomena using only corpuscular theory, such as interference, since these kinds of phenomena found a solid explanation in the idea that radiation should have a wave behaviour. In this context, quantum mechanics would play a leading role in the final understanding of the nature of light. In 1924, Louis de Broglie (1892-1987) raised the idea that, as well as light, the rest of matter also presents a corpuscular behavior on certain occasions and undulatory in others [13]. That is, the idea of a duality could also be extended to other entities such as atoms and electrons. Although this idea was not entirely convincing in principle, it was subsequently tested on an experimental basis [12, 18]. With this, the concept of a wave-particle duality began to become increasingly present among scientists seeking to explain the behavior of light and matter at the quantum level. However, this implied the unfriendly idea that the world around us was actually particle and wave at the same time.

Some time later, Niels Bohr (1885-1962) attempted to unify the idea of the corpuscular and undulatory nature by establishing the Principle of Complementarity, which stated that both, light and matter had a sometimes wave-like and sometimes particle-like behavior, and that both be-

haviors cannot be observed simultaneously [7]. This idea also seemed to be supported by Werner Heisenberg (1901-1976) through the uncertainty principle, which referred to the impossibility of simultaneously measuring characteristics such as the position and momentum of quantum mechanical objects [55]. Since then the dual behavior of light and matter has been studied through different works that seek to better understand how the nature around us behaves.

The Bohr's Principle of Complementarity [7] states that two complementary properties of a given quantum system cannot be obtained simultaneously. This implies that in a measurement process of two complementary observables of a quantum-mechanical object, the total knowledge of the first one makes that all possible outcomes of the second one are equally probable. The wave-particle duality of nature represents the best example of mutually exclusive properties of quantum systems, and several experimental and theoretical works have been developed in order to study this behaviour [4, 16, 68]. For instance, in a double-slit Young-type scheme, the particle-like properties are attributed to the knowledge of the path followed by the particle, i.e to the distinguishability ( $D$ ). On other hand, the wave-like properties are associated to the fringe visibility ( $V$ ) on the screen.

The obtaining of path-information can be achieved using an external device which acts like a which-path detector [57, 58]. For instance, if an atom passes through the slits, a quantum field can be located immediately after them and store path-information [61, 62]. This is because the atom-field interaction affects the initial phase of the quantum field depending on the atom's position with respect to the nodes and antinodes of the wave. Thus, if path-information is recorded on the field, it can be extracted by performing a proper measurement in order to know the path followed by the atom and obtain the particle-like properties of the system. However, the stored path-information can also be erased [56, 58, 62] in order to restore the wave-like behaviour of the system and thus observing the typical interference pattern on the screen.

In the wave-particle duality the wave-like and the particle-like properties are determined via path-information or fringe visibility and has been quantified mathematically through the inequality

$$V^2 + D^2 \leq 1, \quad (1.2)$$

which has been demonstrated by Englert [17] and also derived in other ways [25, 32]. Several works have shown that depending on the initial setup of a double-slit experiment, the wave-particle duality can be controlled in order to analyse the complementarity between distinguishability and visibility [31, 35]. Furthermore, it is possible to establish correlations between an intrinsic degree of freedom of the particle passing through the double-slit and the possible paths of the scheme. This implies that the inequality which controls the complementarity between particle and wave, must be modified as to include this correlation as a third parameter. Recently, concurrence has been considered in a double-slit experiment with single-photons, in order to quantify the established correlations between the paths of the double-slit and the polarization of the photons [33, 34, 53, 67]. The results have demonstrated that the inequality (1.2) in presence of the concurrence turns into the equality:

$$V^2 + D^2 + C^2 = 1, \quad (1.3)$$

where  $C$  represents the degree of quantum entanglement between the polarization of photons

and the possible paths of the scheme. Therefore, as a result of the new equality, the definitions of distinguishability and visibility may simultaneously vanish depending on the degree of correlation present in the scheme.

In this research, instead of photons, we have atoms passing through a double slit schemes and immediately after, crossing cavity fields, in order to study how the wave-particle duality can be controlled depending on the choice of the atomic and field parameters. In addition, we show that discussions based on duality still continue to this day, when we consider concepts such as quantum eraser and delayed-choice experiments.

# Chapter 2

## Theoretical framework

### 2.1 Experimental and theoretical tests of complementarity

Particle-wave duality has been from the beginning of quantum mechanics one of the most interesting topics among the scientific community, being to this day a source of controversy for which answers have been sought through different experiments. In this sense, it is considered that the systems can exhibit either wave or particle properties, provided that they can be attributed a certain characteristic that defines their behavior, which will in many cases depend on the configuration established in each experiment or theoretical proposal. In most cases, they are considered Young-type models in order to analyze the duality. In these models, the wave-like behavior of light or matter is defined based on the visualization of interference patterns on a screen. On the other hand, the corpuscular behavior of the systems is typically defined based on the knowledge of the path followed by the object under study that crosses the double-slit scheme.

Even though in the 1920s, with the emergence of quantum mechanics, the discussion among those who embraced the idea of an undulatory or corpuscular nature that explain the behavior of light seemed to reach a consensus, the interpretation of a dual nature of the microscopic world seemed not yet to convince scientists at all. In this sense, a common example to describe and analyze complementarity was the impossibility of obtaining simultaneously some properties of the quantum systems under study, such as position and momentum. Knowledge of the position of the object involves immediately determining its corpuscular behavior, while a measurement of momentum leads to attributing wave properties to it. Therefore, both behaviors cannot be obtained simultaneously because two complementary properties, in this case position and momentum, cannot be observed at the same time. This is because the knowledge of one of them has as a consequence the fact that all possible results of the other property to be measured become equally probable.

From the point of view of the optics, the dual behaviour of light has been studied to this day through the famous Young's double-slit experiment, which was one principal works that contributed to determine the wave behaviour of light. In this experiment the wave properties of light become evident due to the presence of fringe visibility upon a screen located at a certain distance

from the double-slit through which the beam crosses. With this observation in the the Young's experiment, there was no doubt that the nature of light responded to a wave phenomenon, similar to the typical example of the propagation of waves in the water, where waves coming from different sources can interact causing constructive or destructive interference. In the 20th century Louis de Broglie proposed that the rest of the particles, as electrons or atoms, also could exhibit a dual behaviour since it was possible to attribute them a certain momentum. With his results, and inspired also in the previous ideas proposed by Planck and Einsten, de Broglie postuled the idea that not only light can be treated in a quantum way, but also all particles. Therefore, the wave-particle duality could be considered to describe the behaviour of the whole matter, and it was not an exclusive property of light.

In this section, instead of photons, we consider the study of the wave and corpuscular properties of a beam of atoms, which cross a double-slit scheme. This allows us to analyze different possibilities in order to determine the behaviour of the atoms, depending on the use or not of which-path detectors. In this sense, we will consider cases in which the fringe visibility vanishes when an external device is correlated with de system, and thus the corpuscular properties are obtained.

### 2.1.1 Which-path detectors and loss of fringe visibility

As we have seen in the previous section, in Young-type double-slit setup we always obtain an interference pattern due to the wave nature of light or atoms, as appropriate. In sections later, we will see that the interference can be modified if, for example, we vary the width of the slits or establish some correlation in the system, in which properties of the atoms or photons are involved. However, it is also possible to modify the interference pattern by adding an external device which is correlated with the entire system, in such a way that it acts as which-path detector. In fact, we can even achieve the total loss of the fringe visibility at the expense of obtaining the path followed by the atom or photon.

In this section, we will explain a model proposed by Scully et al., [57, 58] in which the slits are crossed by atoms and an external device is used to determine the path followed by them. As a consequence, the interference is completely lost. On the left side of the figure 2.1 we can observe a typical double-slit setup, in which the atoms are collimated before going through the slits. In that case, since there is no external devices in the setup, we would hope to obtain a typical interference pattern. However, in order to modify the observed pattern, we can consider a laser beam and cavities micromasers , which are shown on the right side of the figure 2.1.

Let us analyze the setup in which the laser and micromasers are not included in the system yet. In this case, the state which describes the atom after it crosses the double-slit corresponds to

$$\psi(\vec{r}) = \frac{1}{\sqrt{2}} [\psi_1(\vec{r}) + \psi_2(\vec{r})] |i\rangle, \quad (2.1)$$

where  $|i\rangle$  represents the initial atomic state. The probability density for a position  $\vec{r} = \vec{R}$  of the

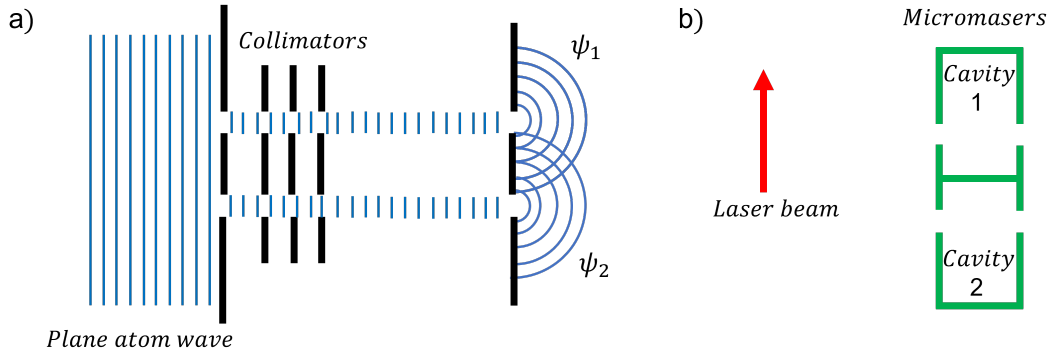


Figure 2.1: a) Double-slit setup crossed by atoms, in which total interference is obtained due to the interaction of  $\psi_1$  with  $\psi_2$ , as in a typical Young's experiment. b) External devices used to obtain which-path information and to vanish the interference.

center-of-mass is given by the square modulus of  $\psi(\vec{R})$ , such that

$$P(\vec{R}) = \frac{1}{2} [|\psi_1|^2 + |\psi_2|^2 + \psi_1^* \psi_2 + \psi_2^* \psi_1] \langle i|i \rangle. \quad (2.2)$$

Therefore, from the red terms, it is clear that an interference pattern is obtained on the screen. As a consequence, we have a wave-like behaviour for the atom, since we cannot determine which slit it passed through. However, if we want to know the path followed by the atom we can include the laser and micromasers considering the scheme shown in the figure 2.2

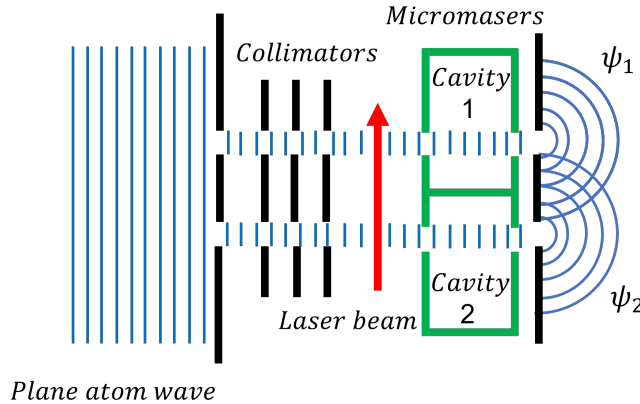


Figure 2.2: Double-slit setup crossed by atoms, in which interference can be vanished due to the presence of external devices which allows to obtain total which-path information.

When the set laser-micromasers is included in the system, the cavities 1 and 2 are located after the laser beam in the upper and lower paths, respectively. The task of the beam laser is to excite the atoms to the long-lived Rydberg state  $|a\rangle$ . Once the atom is excited, it crosses the cavities making a transition  $|a\rangle \rightarrow |b\rangle$  by spontaneous emission of a photon. Therefore, the state of the total system is now given by

$$\psi(\vec{r}) = \frac{1}{\sqrt{2}} [\psi_1(\vec{r})|1_1 0_2\rangle + \psi_2(\vec{r})|0_1 1_2\rangle] |b\rangle, \quad (2.3)$$

where the state  $|1_1 0_2\rangle$  ( $|0_1 1_2\rangle$ ) denotes the presence of a photon in cavity 1(2) and no photon in cavity 2(1). It is important to note that the initial system (Young-type setup) and the which-path detector have become entangled. In this case, the new probability density for a position of the center of mass given by  $\vec{r} = \vec{R}$  corresponds to

$$\begin{aligned} P(\vec{R}) &= \frac{1}{2} [|\psi_1|^2 + |\psi_2|^2 + \psi_1^* \psi_2 \langle 1_1 0_2 | 0_1 1_2 \rangle + \psi_2^* \psi_1 \langle 0_1 1_2 | 1_1 0_2 \rangle] \langle b | b \rangle \\ &= \frac{1}{2} [|\psi_1|^2 + |\psi_2|^2], \end{aligned} \quad (2.4)$$

because  $\langle 1_1 0_2 | 0_1 1_2 \rangle = \langle 0_1 1_2 | 1_1 0_2 \rangle = 0$ . As a consequence, the terms (in red) which produce interference are cancelled and no fringe visibility is observed on the screen. Therefore, we can conclude that the cavities act as a which-path detector, since the atom leaves a photon in one of them depending on the slit that it crossed, i.e. the path-information is available in the micromasers and it can be extracted by performing a proper measurement of the number of photons. However, we must keep in mind that the change produced by the extra photon left in the cavity, should be detectable. In this sense, we can consider that the easier way to achieve that is to prepare a cavity with no photon initially. This allow us to detect the emitted photon and determine the path followed by the atom.

### 2.1.2 Quantum eraser and delayed choice

Through the years, several works have studied the dual behaviour of light and matter considering different models both, theoretical and experimental. Although in the most of cases the results have helped to better understand the properties of photon, atoms, electrons, etc, and the way these behave under certain conditions, some results have increased discrepancies among scientists. In this section, we consider theoretical setups in which we study the concepts quantum eraser and delayed choice, and the controversial ideas on which they are based.

Let us go back to the last scheme studied in the previous section. In that case, we saw how the interference can be completely removed by introducing a path detector device in the system, which allows us to distinguish unambiguously the path followed by the atom based on the measurement of the number of photons in the micromaser cavities. Therefore, at this point we wonder whether it is possible to retrieve the interference by erasing the which-path information contained in the detectors (cavities). This is precisely the purpose behind of the concept of the quantum eraser, which we will study considering the setup shown in the figure 2.3.

In this case, the atoms also cross a laser beam and immediately after enter in the micromasers, where they can leave a photon which can reveal the path followed by the atom. However, now we consider that the which-path detector (cavities) are separated by a shutters-detector wall combination. Therefore, after the atom leaves a photon in one of the cavities, we can choose to “erase” the path-information, since as long as shutters are closed, the radiation remains contained either in the upper or the lower cavity. However, if the shutters are opened, the radiation will interact with the photodetector wall. Thus, the photon that was initially left in the upper or lower cavity is absorbed. As a consequence, the memory of the passage of the atom is erased.

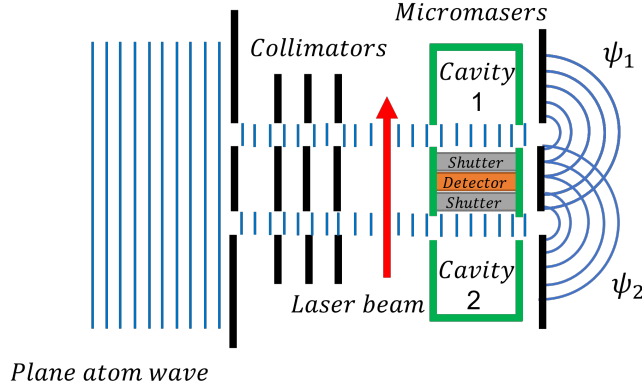


Figure 2.3: Double-slit setup to study the possibilities of implementing a quantum eraser.

The interesting point here is that one can open the shutters even long after the atom crosses the entire system. That is, once the atom is away from the micromaser cavities, no physical influence on the wave function of the atomic center of mass can be thought of. Therefore, one could define the behavior of the system during the time of flight of the atom by erasing or keeping the path information in the cavities. In this sense, the patterns are formed considering the events in which a photocount is produced in the detector wall or not, which can be controlled by the experimenter through the shutters. This is precisely the paradox in this and other quantum eraser models.

In order to study the previously presented model, we analyze the mathematical description of the problem considering that the detector wall is a two-level atom initially in its ground state  $|d\rangle$  and it can be found in the excited state  $|e\rangle$  when the shutters are opened. Thus, the state of the system immediately after the atom crosses the micromasers can be described as

$$\psi(\vec{r}) = \frac{1}{\sqrt{2}} [\psi_1(\vec{r})|1_1 0_2\rangle + \psi_2(\vec{r})|0_1 1_2\rangle] |b\rangle |d\rangle, \quad (2.5)$$

where  $|b\rangle$  is the internal atomic state. Moreover, we can introduce symmetric and antisymmetric states of the atom and the radiation fields contained in the cavities, which are defined respectively as  $\psi_{\pm}$  and  $|\pm\rangle$ :

$$\psi_{\pm}(\vec{r}) = \frac{1}{\sqrt{2}} [\psi_1(\vec{r}) \pm \psi_2(\vec{r})] \quad (2.6)$$

$$|\pm\rangle = \frac{1}{\sqrt{2}} [|1_1 0_2\rangle \pm |0_1 1_2\rangle] \quad (2.7)$$

Now we can rewrite (2.5) as

$$\psi(\vec{r}) = \frac{1}{\sqrt{2}} [\psi_+(\vec{r})|+\rangle + \psi_-(\vec{r})|-\rangle] |b\rangle |d\rangle. \quad (2.8)$$

Therefore, we now consider the interaction between the radiation field in the cavities and the detector wall, which corresponds to an atom with a lower state  $|d\rangle$  and an excited state  $|e\rangle$ . Here we have to consider that the Hamiltonian between the radiation and the detector wall depends on the symmetric combinations of the field variables, and thus only  $|+\rangle$  will couple to the fields.

As a consequence, if the shutters are opened, the state of the system after the radiation-detector interaction can be written as

$$\psi(\vec{r}) = \frac{1}{\sqrt{2}} [\psi_+(\vec{r})|0_1 0_2\rangle|e\rangle + \psi_-(\vec{r})|-\rangle|d\rangle]|b\rangle, \quad (2.9)$$

and the probability density corresponds to

$$P(\vec{R}) = \frac{1}{2} [\psi_+^*(\vec{R})\psi_+(\vec{R}) + \psi_-^*(\vec{R})\psi_-(\vec{R})] = \frac{1}{2} [\psi_1^*(\vec{R})\psi_1(\vec{R}) + \psi_2^*(\vec{R})\psi_2(\vec{R})], \quad (2.10)$$

From (2.10) we now can obtain the probability density  $P_e(\vec{R})$  [ $P_d(\vec{R})$ ] for finding the detector excited[deexcited] and the atom in a position  $\vec{R}$  on the screen, which are given as

$$P_e(\vec{R}) = |\psi_+(\vec{R})|^2 = \frac{1}{2} [|\psi_1(\vec{R})|^2 + |\psi_2(\vec{R})|^2] + Re[\psi_1^*(\vec{R})\psi_2(\vec{R})], \quad (2.11)$$

$$P_d(\vec{R}) = |\psi_-(\vec{R})|^2 = \frac{1}{2} [|\psi_1(\vec{R})|^2 + |\psi_2(\vec{R})|^2] - Re[\psi_1^*(\vec{R})\psi_2(\vec{R})]. \quad (2.12)$$

The terms in red show fringes and antifringes for  $P_e(\vec{R})$  and  $P_d(\vec{R})$ , respectively. These patterns are obtained considering that once the atom has travelled from the source to the screen, crossing the micromaser, we can measure the state of the detector wall detector. If we observe a photocount, the path-information is erased and we observe fringes on the screen. After that, other atom crosses the setup and we perform a measurement upon the detector wall again. If this time we observe no photocount, we obtain antifringes since no path-information has been revealed. This sequence must be repeated many times to form the whole patterns. On the other hand, if the eraser photon signal is disregarded, we obtain no fringe visibility, due to the superposition of fringes and antifringes, which can be represented by the equation (2.13). This is, no measurement on the detector wall implies that the path-information is still available in the radiation and it can be extracted with a proper measurement of the number of photons in the cavities.

$$P(\vec{R}) = \frac{1}{2} (P_e(\vec{R}) + P_d(\vec{R})) \quad (2.13)$$

In order to clarify the concepts of quantum eraser and delay choice, now we will qualitatively discuss a particular model in which, instead of slits, two atom are located in specific positions [4]. We will consider the scattering of light from the atoms, whose position are defined as 1 and 2. First, we analyze the case in which resonant light impinges from the left on two-level atoms, thus an atom can be excited from the level  $b$  to  $a$  and then emit a  $\gamma$  photon. Since both atoms are finally in the state  $b$ , it is not possible to determine from which atom the photon  $\gamma$  came. Therefore, the resulting pattern obtained upon the screen shows fringe visibility after repeating the process many times. As a consequence, there is no path-information (see figure [2.4]).

Analogously to the model of micromasers, we can modify the system in order to obtain path-information at the expense of losing wave properties. In this case, we consider three-level atoms and a field  $I_1$ . One of the atoms can be excited from the state  $c$  to the state  $a$ , and then emit a photon  $\gamma$ . As a consequence, that atom ends up in the state  $b$  while the other atom remains

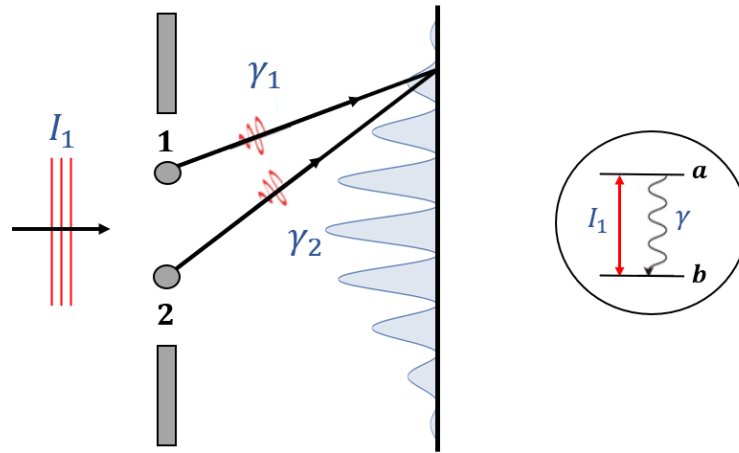


Figure 2.4: Two-level atoms are located in the position 1 and 2. An incident pulse  $I_1$  excites one of the atoms to the level  $a$  to later emit a  $\gamma$  photon. Since the final state of both atoms is the same, no path information can be extracted from them, and total interference is obtained.

in  $c$ . Therefore, in this case it is possible to determine which atom the photon came from by performing a measurement of the internal state of both atoms. Consequently, no fringe visibility is observed upon the screen (see figure 2.5).

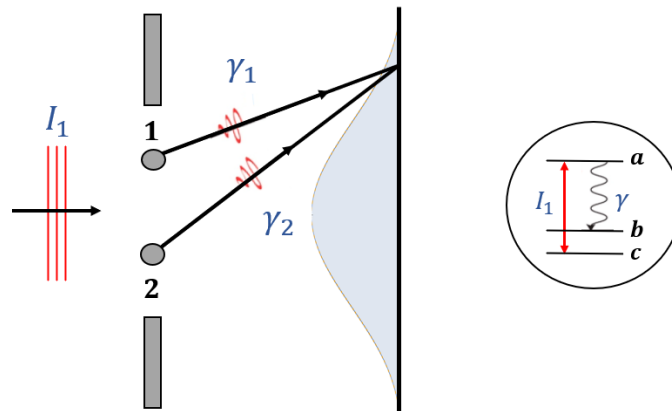


Figure 2.5: Three-level atoms are located in the position 1 and 2. An incident pulse  $I_1$  excites one of the two atoms from the level  $c$  to the level  $a$ , then it emits a  $\gamma$  photon and ends up in the state  $b$ . In this case the internal atomic state can reveal which-path information.

Finally, we show the case in which the atoms located in 1 and 2 have four levels and a pair of photons can be emitted by one of them due to the radiations  $I_1$  and  $I_2$ , which excite the atom as shown in the figure 2.6. When the atom decays from  $a$  to  $b$ , the  $\gamma$  photon proceeds to the screen in the right where is registered by a detector  $D$  at a location  $x_0$ . On other hand, when the atom decays from  $b'$  to  $c$ , a  $\phi$  photon is emitted. As a consequence, the final state of both atoms is the same, and no path-information can be obtained via an atomic measurement which implies that

total interference is obtained. However, if we perform a position measurement of the  $\phi$  photon, we could obtain path-information of the  $\gamma$  photon.

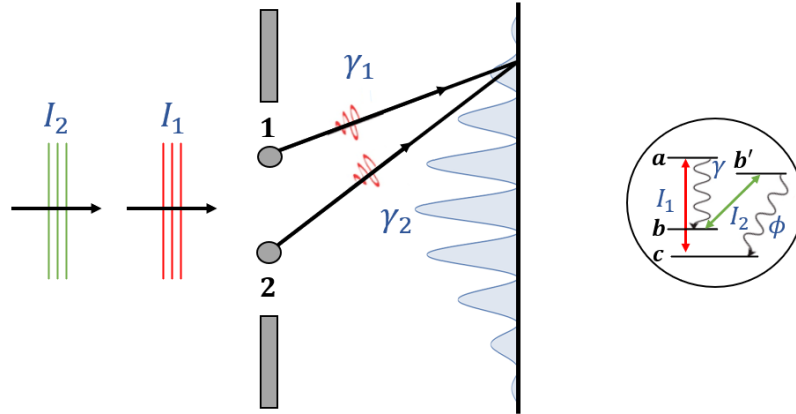


Figure 2.6: Four-level atoms are located in the position 1 and 2. Two incident pulse,  $I_1$  and  $I_2$ , excite one of the atoms from the level  $c$  to the level  $a$  and from  $b$  to  $b'$ , which allows the emission of the photons  $\gamma$  and  $\phi$ , respectively. As a consequence, the final atomic state is the same and there is no path-information.

In order to study the effects of the measurement of the  $\phi$  photon, we consider the scheme shown in the figure 2.7. We consider only those cases where the  $\phi$  photons scattered from the atom located at 1[2] proceeds to the 50/50 beam splitter  $B_1$ [ $B_2$ ]. Therefore, the  $\phi$  photon can be detected by the detectors  $D_3$  or  $D_4$ , which gives information about which atom it came from, since when  $D_3$ [ $D_4$ ] clicks, necessarily the  $\phi$  photon came from the atom in 1[2]. As a consequence, we conclude that the corresponding  $\gamma$  photon was also scattered from the same atom. On other hand, if after crossing the 50/50 beam splitter  $B$ , the  $\phi$  photon is detected in  $D_1$  or  $D_2$ , there is equal probability that it may have come from the atom in the position 1 or 2. In this case, the path-information of  $\phi$  is erased, and thus there is no path-information for  $\gamma$  photon either.

Therefore, we can consider that the protocol for this model works by following the next steps

- We separately identify the events where photons  $\phi$  are detected at ports  $D_1$ ,  $D_2$ ,  $D_3$  and  $D_4$ .
- For each of these events we locate the positions of the detected photons  $\gamma$  on screen D.
- For detection at  $D_3$  and  $D_4$ , the pattern formed by the photons  $\gamma$  does not show interference fringes on screen D.
- For detection at  $D_1$  and  $D_2$ , the pattern formed by the photons  $\gamma$  shows interference fringes.

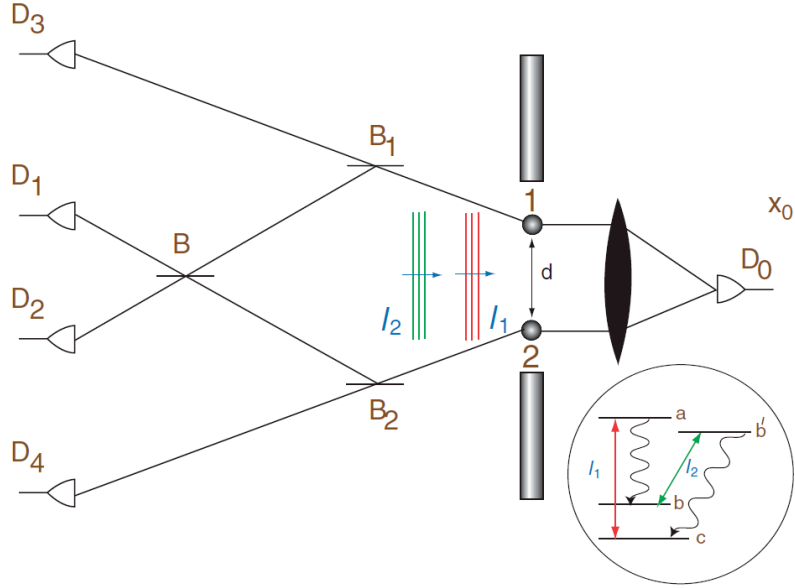


Figure 2.7: Theoretical delayed choice quantum eraser scheme.

The paradoxical character of this situation is that we can consider that the  $\phi$  photon detectors are located far away from the atoms, in comparison with the distance between atoms and the  $\gamma$  photon detector. Therefore, the measurement of the  $\phi$  photons (measured later) would have an influence on the behavior of the  $\gamma$  photons (measured before), which suggests that a future event could have consequences on a previously occurring event. For this reason, this and other delayed choice quantum eraser models have been a source of controversy to this day. In Chapter 5 we will return to this topic in order to implement a theoretical model based on the atom-field interaction.

### 2.1.3 Balance among visibility, distinguishability and concurrence

In the previous sections, we have seen that the wave-like and particle-like properties can be obtained depending on the setup of the model under study. The wave-like and particle-like behaviour have been defined based on the fringe visibility ( $V$ ) and which-path information or distinguishability ( $D$ ), respectively. Typically, double-slit Young-type schemes are considered in the realization of different theoretical and experimental models which study the duality [31, 35]. In that case, which-path information and visibility can be controlled by the probabilities  $c_{\uparrow}$  and  $c_{\downarrow}$  that a particle crosses the upper or bottom slit. When  $c_{\uparrow} = c_{\downarrow}$  we obtain total interference and null distinguishability. However, different devices can be used in order to detect the pass of the particle through one of the slits and which-path information can be obtained at the expense of losing interference [57, 58]. Considering this, the relation between  $V$  and  $D$  can be represented by the inequality [17]

$$V^2 + D^2 \leq 1. \quad (2.14)$$

This relation has also been studied considering a degree of entanglement between some intrinsic property of the particle and the paths of the schemes. This correlation has been quantified through the concurrence ( $C$ ), included as an additional parameter in the balance between distin-

guishability and visibility [31, 34, 35, 53, 67], resulting in the equality

$$V^2 + D^2 + C^2 = 1. \quad (2.15)$$

For instance, in case we send atoms through the double-slit, we can correlate the upper and bottom paths with two different internal states of the atom. In a similar way, if the scheme is crossed by photons, we can consider the same kind of correlation, but this time using the polarization of the photons as intrinsic property.

To study how the equality (2.15) is obtained and how the concurrence can control this balance, we consider a double-slit scheme crossed by photons, whose polarizations are correlated with the possible paths of the scheme [53]. Each hole of the double-slit is defined as  $a$  and  $b$  (see figure 2.8), with which we can identify the field corresponding to the pass of the photons through the holes as:

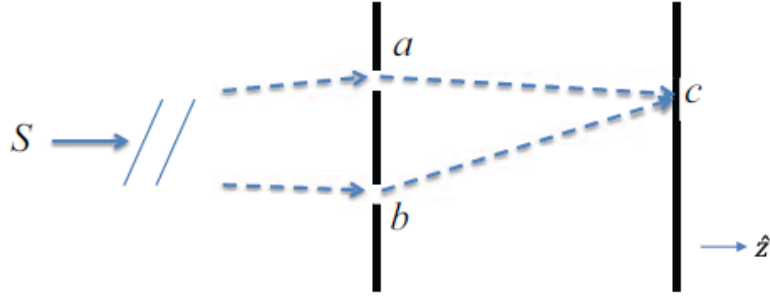


Figure 2.8: Young's two-slit scheme used to study the balance among wave, particle and concurrence

$$\begin{aligned} \hat{E}_a &= \hat{E}_a^{(+)} + \hat{E}_a^{(-)} \simeq \hat{a}_a e^{i\varphi_a} + \hat{a}_a^\dagger e^{-i\varphi_a} \\ \hat{E}_b &= \hat{E}_b^{(+)} + \hat{E}_b^{(-)} \simeq \hat{a}_b e^{i\varphi_b} + \hat{a}_b^\dagger e^{-i\varphi_b} \end{aligned} \quad (2.16)$$

where  $\hat{a}$  and  $\hat{a}^\dagger$  correspond to the annihilation and creation operators, respectively, while  $\varphi_{a,b}$  represent the phases associated to each field. After crossing the double-slit, the quantum state of the photon can be described as

$$|\Psi\rangle = c_a |\mathbb{1}_a\rangle \otimes |\phi_a\rangle + c_b |\mathbb{1}_b\rangle \otimes |\phi_b\rangle = c_a |\mathbb{1}_a, \phi_a\rangle + c_b |\mathbb{1}_b, \phi_b\rangle, \quad (2.17)$$

with  $c_a$  and  $c_b$  normalized coefficients such that  $|c_a|^2 + |c_b|^2 = 1$ . On other hand,  $|\mathbb{1}_a\rangle$  and  $|\mathbb{1}_b\rangle$  represent a photon in the modes  $a$  and  $b$ , respectively, while  $|\phi_a\rangle$  and  $|\phi_b\rangle$  correspond to normalized states of an intrinsic property of the photon, in this case the polarization, with  $|\langle\phi_a|\phi_b\rangle| \equiv |\gamma| \leq 1$ .

Once defined the state of the photon after it crosses the double-slit, we analyze the wave-particle duality consider the definitions of path distinguishability ( $D$ ) and fringe visibility ( $V$ )

as [25, 31, 32]

$$D = \left| \frac{p_a - p_b}{p_a + p_b} \right| \quad (2.18)$$

and

$$V = \frac{p_c^{max} - p_c^{min}}{p_c^{max} + p_c^{min}}. \quad (2.19)$$

where

$p_a \propto \langle \hat{E}_a^{(-)} \hat{E}_a^{(+)} \rangle$ : Detected probability of photon passing through the slit  $a$ .  
 $p_b \propto \langle \hat{E}_b^{(-)} \hat{E}_b^{(+)} \rangle$ : detected probability of photon passing through the slit  $b$ .  
 $p_c \propto \langle \hat{E}^{(-)} \hat{E}^{(+)} \rangle$ : Detected probability of photon registered at the screen  $c$ .

Therefore, using (2.16) and (2.17) we obtain (see Appendix)

$$\langle \hat{E}_a^{(-)} \hat{E}_a^{(+)} \rangle = |c_a|^2 \quad (2.20)$$

$$\langle \hat{E}_b^{(-)} \hat{E}_b^{(+)} \rangle = |c_b|^2 \quad (2.21)$$

$$\langle \hat{E}^{(-)} \hat{E}^{(+)} \rangle = |c_a|^2 + c_a^* c_b \gamma e^{i(\varphi_a - \varphi_b)} + c_b^* c_a \gamma^* e^{-i(\varphi_a - \varphi_b)} + |c_b|^2 \quad (2.22)$$

Then,  $D$  y  $V$  can be written as

$$D = \left| |c_a|^2 - |c_b|^2 \right| \quad (2.23)$$

$$V = 2|c_a c_b \gamma|. \quad (2.24)$$

On other hand, the concurrence ( $C$ ) can be defined as [67]

$$C = 2|c_a c_b| \sqrt{1 - |\gamma|^2}, \quad (2.25)$$

with which it is fulfilled that

$$\begin{aligned} V^2 + D^2 + C^2 &= 4|c_a c_b \gamma|^2 + |c_a|^4 - 2|c_a|^2 |c_b|^2 + |c_b|^4 + 4|c_a c_b|^2 (1 - |\gamma|^2) \\ &= |c_a|^4 + 2|c_a|^2 |c_b|^2 + |c_b|^4 \\ &= (|c_a|^2 + |c_b|^2)^2 \\ &= 1. \end{aligned} \quad (2.26)$$

Therefore, the concurrence can be considered as third parameter which can contribute to the balance between the wave-like and particle-like behaviour. In fact, we can choose certain values of the parameters that define  $C$  in order to obtain  $C = 1$  and thus  $V = D = 0$ . This leads us to the question: can be the wave-particle duality turned off? We will discuss this question in the chapter 3 based in our atom-field interaction model.

## 2.2 Atom-field interaction

In a typical configuration of a double-slit Young's experiment, the interference patterns are observed due to the incidence of a electromagnetic radiation on both slits. As a consequence, these act as point sources of waves, which interfere constructively or destructively depending on the difference in their phases. This allows obtaining a certain interference pattern at a certain distance from the slits, which proves the wave-like behavior of light. Therefore, we can describe this phenomenon as the result of the interaction between the light emitted by some particular source and the slits, that is, as the interaction between electromagnetic radiation and matter.

In this section, we consider a model analogous to the one used in Young's experiment, in which instead of a beam of photons crossing a double-slit, we will consider a beam of atoms crossing a cavity with an electromagnetic field. This will allow us to study the interaction between traveling atoms and field cavities, which, due to the wave-like behavior of matter, will lead us to implement this interaction in a double-slit model that allows us to use quantum fields as which-path detectors.

### 2.2.1 Quantum description

To analyze the proposed model with atom-field interaction, we consider the coupling between an atom, considered as a two-level system, and a quantum field in a cavity with only one radiation mode, which corresponds to a model presented by Walls et al. [62]. The Hamiltonians are given respectively by the expressions (2.27) and (2.28), while the Hamiltonian that models the interaction between both is given by (2.29).

$$\hat{H}_{atom} = \frac{\hbar\omega_0\hat{\sigma}_z}{2} + \frac{\hat{p}^2}{2m} \quad (2.27)$$

$$\hat{H}_{field} = \hbar\omega_a(\hat{a}^\dagger\hat{a} + \frac{1}{2}). \quad (2.28)$$

$$\hat{H}_{int} = \hbar \cos(kx + \xi)(g^*\hat{\sigma}_-\hat{a}^\dagger + g\hat{\sigma}_+\hat{a}). \quad (2.29)$$

Where

$\hat{a}, \hat{a}^\dagger$  : annihilation and creation operators

$\sigma_z = \begin{bmatrix} 1 & 0 \\ 0 & -1 \end{bmatrix}, \sigma_+ = \begin{bmatrix} 0 & 1 \\ 0 & 0 \end{bmatrix}, \sigma_- = \begin{bmatrix} 0 & 0 \\ 1 & 0 \end{bmatrix}$  : internal atomic operators

$\omega_a$  : mode frequency in cavity (field)

$\omega_0$  : atomic transition frequency

$k$  : Wavenumber of the standing wave in the cavity (field)

$\Delta = \omega_0 - \omega_a$  : Detuning

$|g|$  : coupling constant

(2.30)

Therefore, the total system is described by the sum of the three Hamiltonians shown above, such that

$$\hat{H}_{system} = \hat{H}_{field} + \hat{H}_{atom} + \hat{H}_{int}. \quad (2.31)$$

In the regime of a high detuning we can obtain the effective Hamiltonian considering

$$\hat{H} = \hat{H}_0 + \hat{H}_I, \quad (2.32)$$

where

$$\hat{H}_0 = \hbar\omega_a \hat{a}^\dagger \hat{a} + \frac{\hbar\omega_o \hat{\sigma}_z}{2} \quad (2.33)$$

and  $\hat{H}_I = \hat{H}_{int}$  defined in (2.29). Therefore, the Schrodinger equation that describes the evolution of the system corresponds to

$$i\hbar \frac{d}{dt} |\psi_S(t)\rangle = (\hat{H}_0 + \hat{H}_I) |\psi_S(t)\rangle. \quad (2.34)$$

If we consider the interaction picture using the free Hamiltonian and the operator  $\hat{U}_0 = e^{-\frac{i\hat{H}_0 t}{\hbar}}$ , we have

$$|\psi_I(t)\rangle = e^{\frac{i\hat{H}_0 t}{\hbar}} |\psi_S(t)\rangle = \hat{U}_0^{-1} |\psi_S(t)\rangle, \quad (2.35)$$

and thus (see Appendix)

$$\begin{aligned} i\hbar \frac{d}{dt} |\psi_I(t)\rangle &= i\hbar \frac{d}{dt} [\hat{U}_0^{-1} |\psi_S(t)\rangle] \\ &= [-i\hbar \hat{U}_0^{-1} \frac{d}{dt} \hat{U}_0 + \hat{U}_0^{-1} \hat{H} \hat{U}_0] |\psi_I(t)\rangle \\ &= \hat{W}_I(t) |\psi_I(t)\rangle, \end{aligned} \quad (2.36)$$

where  $\hat{W}_I(t)$  corresponds to the perturbative term in the interaction picture, which can be rewritten as

$$\begin{aligned} \hat{W}_I(t) &= -i\hbar \hat{U}_0^{-1} \frac{d}{dt} \hat{U}_0 + \hat{U}_0^{-1} \hat{H} \hat{U}_0 \\ &= -i\hbar e^{\frac{i\hat{H}_0 t}{\hbar}} \frac{d}{dt} e^{-\frac{i\hat{H}_0 t}{\hbar}} + e^{\frac{i\hat{H}_0 t}{\hbar}} \hat{H} e^{-\frac{i\hat{H}_0 t}{\hbar}} \\ &= \hbar \cos(kx + \xi) [g^* e^{\frac{i\hat{H}_0 t}{\hbar}} \hat{\sigma}_- \hat{a}^\dagger e^{-\frac{i\hat{H}_0 t}{\hbar}} + g e^{\frac{i\hat{H}_0 t}{\hbar}} \hat{\sigma}_+ \hat{a} e^{-\frac{i\hat{H}_0 t}{\hbar}}] \\ &= \hbar \cos(kx + \xi) [g^* \hat{\sigma}_- \hat{a}^\dagger e^{-i\Delta t} + g \hat{\sigma}_+ \hat{a} e^{i\Delta t}], \end{aligned} \quad (2.37)$$

where we have use  $e^{\hat{A}} \hat{B} e^{-\hat{A}} = \hat{B} + [\hat{A}, \hat{B}] + \frac{1}{2!} [\hat{A}, [\hat{A}, \hat{B}]] + \dots$  and (2.33) to obtain (see Appendix)

$$e^{\frac{i\hat{H}_0 t}{\hbar}} \hat{\sigma}_- \hat{a}^\dagger e^{-\frac{i\hat{H}_0 t}{\hbar}} = \hat{\sigma}_- \hat{a}^\dagger e^{-i\Delta t}, \quad (2.38)$$

and analogously

$$e^{\frac{i\hat{H}_0 t}{\hbar}} \hat{\sigma}_+ \hat{a} e^{-\frac{i\hat{H}_0 t}{\hbar}} = \hat{\sigma}_+ \hat{a} e^{i\Delta t}. \quad (2.39)$$

Now we can study the evolution of the system considering the perturbative term  $\hat{W}_I(t)$  and the evolution equation  $i\hbar \frac{d}{dt} |\psi_I(t)\rangle = \hat{W}_I(t) |\psi_I(t)\rangle$  to show that (see Appendix)

$$e^{-\frac{i}{\hbar} \int_0^t \hat{W}_I(t') dt'} = 1 - \frac{it}{\hbar} \left[ \frac{\hbar |g|^2 \cos^2(kx + \xi)}{\Delta} [\hat{\sigma}_+ \hat{a}, \hat{\sigma}_- \hat{a}^\dagger] \right] + \dots \quad (2.40)$$

and thus

$$\begin{aligned}
\hat{W}_I &= \frac{\hbar|g|^2 \cos^2(kx + \xi)}{\Delta} [\hat{\sigma}_+ \hat{a}, \hat{\sigma}_- \hat{a}^\dagger] \\
&= \frac{\hbar|g|^2 \cos^2(kx + \xi)}{\Delta} (\hat{\sigma}_+ \hat{\sigma}_- \hat{a} \hat{a}^\dagger - \hat{\sigma}_- \hat{\sigma}_+ \hat{a}^\dagger \hat{a}) \\
&= \frac{\hbar|g|^2 \cos^2(kx + \xi)}{\Delta} (\hat{\sigma}_+ \hat{\sigma}_- (1 + \hat{a}^\dagger \hat{a}) - \hat{\sigma}_- \hat{\sigma}_+ \hat{a}^\dagger \hat{a}) \\
&= \frac{\hbar|g|^2 \cos^2(kx + \xi)}{\Delta} (\hat{\sigma}_+ \hat{\sigma}_- + \hat{\sigma}_+ \hat{\sigma}_- \hat{a}^\dagger \hat{a} - \hat{\sigma}_- \hat{\sigma}_+ \hat{a}^\dagger \hat{a}) \\
&= \frac{\hbar|g|^2 \cos^2(kx + \xi)}{\Delta} (\hat{\sigma}_+ \hat{\sigma}_- + \hat{\sigma}_z \hat{a}^\dagger \hat{a}) \\
&= \frac{\hbar|g|^2 \cos^2(kx + \xi)}{\Delta} \hat{\sigma}_+ \hat{\sigma}_- + \frac{\hbar|g|^2 \cos^2(kx + \xi)}{\Delta} \hat{\sigma}_z \hat{a}^\dagger \hat{a}. \\
&\equiv \hat{W}_I^{eff}
\end{aligned} \tag{2.41}$$

Once an expression for  $\hat{W}_I^{eff}$  is found, we obtain the total effective Hamiltonian that describes the atom-field interaction, which corresponds to:

$$\hat{H}_{eff} = \hbar\omega_0 \hat{\sigma}_z + \hbar\omega_a \hat{a}^\dagger \hat{a} + \frac{\hbar|g|^2 \cos^2(kx + \xi)}{\Delta} \hat{\sigma}_+ \hat{\sigma}_- + \frac{\hbar|g|^2 \cos^2(kx + \xi)}{\Delta} \hat{\sigma}_z \hat{a}^\dagger \hat{a} \tag{2.42}$$

The third term, which is present even in the absence of photons, is a kind of atomic Kerr effect induced in the cavity field [21]. Therefore, we consider the final  $\hat{H}_{eff}$  simply as:

$$\begin{aligned}
\hat{H}_{eff} &= \hbar\omega_0 \hat{\sigma}_z + \hbar\omega_a \hat{a}^\dagger \hat{a} + \frac{\hbar|g|^2 \cos^2(kx + \xi)}{\Delta} \hat{\sigma}_z \hat{a}^\dagger \hat{a} \\
&= \hbar\omega_0 \hat{\sigma}_z + \hbar\omega_a \hat{a}^\dagger \hat{a} + \frac{\hbar|g|^2 \cos^2(kx + \xi)}{\Delta} \hat{\sigma}_z \hat{a}^\dagger \hat{a} + \hbar\omega_a \hat{\sigma}_z - \hbar\omega_a \hat{\sigma}_z \\
&= \hbar\omega_a \hat{\sigma}_z + \hbar\omega_a \hat{a}^\dagger \hat{a} + \frac{\hbar|g|^2 \cos^2(kx + \xi)}{\Delta} \hat{\sigma}_z \hat{a}^\dagger \hat{a} + \hbar\Delta \hat{\sigma}_z,
\end{aligned} \tag{2.43}$$

From the previous expression, we can observe that the potential experienced by the atom as it passes through the standing wave (field) is

$$V = \frac{\hbar|g|^2 \cos^2(kx + \xi)}{\Delta} \hat{\sigma}_z \hat{a}^\dagger \hat{a} + \hbar\Delta \hat{\sigma}_z. \tag{2.44}$$

Therefore, in the next section we consider (2.44) to study the interaction between atoms and field cavities, in order to implement a model in which this interaction can be used to control the wave-particle duality.

### 2.2.2 Atomic location based on atom-field interaction

Once the effective Hamiltonian that governs the atom-field interaction is found, we can study the possibilities that it can offers us if we want to consider a double-slit scheme crossed by

atoms. In this section, we discuss a Young-type double-slit model in which, after crossing the slits, the atom passes through a standing wave, whose quantum state is modified depending on the relative position of the atom with respect to nodes and antinodes of the wave. Therefore, after atom leaves the setup, a field measurement could reveal the position that the atom passed through. For this purpose, we previously consider only the effects of the atom-field interaction on the quantum state of the field. After that, in the next chapter, we will explain how the standing wave must be located in order to meet the goal of locating the atom once it crossed the double-slit.

Before the atom-field interaction, the quantum field is described as coherent state of amplitude  $\alpha$  given by

$$|\psi(0)\rangle_{field} = |\alpha\rangle = e^{-\frac{|\alpha|^2}{2}} \sum_{n=0}^{\infty} \frac{\alpha^n}{\sqrt{n!}} |n\rangle \equiv \hat{D}(\alpha)|0\rangle, \quad (2.45)$$

with  $\hat{D}$  being the displacement operator

$$\hat{D}(\alpha) = e^{\alpha\hat{a}^\dagger - \alpha^*\hat{a}}. \quad (2.46)$$

On other hand, we assume that the atom enters in the cavity in the groundstate  $|g\rangle$  with a probability function of the transverse position to its trajectory given by  $\kappa(x)$ . Therefore, we can describe its state before the interaction as

$$|\psi(0)\rangle_{atom} = \int dx |x, g\rangle \langle x, g | \psi(0)\rangle_{atom} = \int dx \kappa(x) |x, g\rangle. \quad (2.47)$$

Therefore, the total initial state of the system corresponds to

$$|\psi(0)\rangle = |\alpha\rangle \otimes |\psi(0)\rangle_{atom} = \int dx \kappa(x) |\alpha\rangle \otimes |x, g\rangle, \quad (2.48)$$

whose evolution, using (2.44), is given by (see appendix 2.3.2)

$$\begin{aligned} |\psi(t)\rangle &= \int dx \kappa(x) e^{-\frac{iVt}{\hbar}} |\alpha\rangle \otimes |x, g\rangle \\ &= \int dx \kappa(x) e^{it\Delta} e^{i\eta(x)\hat{a}^\dagger\hat{a}} |\alpha\rangle \otimes |x, g\rangle \quad \text{with} \quad \eta(x) = \frac{t|g|^2 \cos^2(kx + \xi)}{\Delta} \\ &= e^{it\Delta} \int dx \kappa(x) |\alpha e^{i\eta(x)}\rangle \otimes |x, g\rangle. \end{aligned} \quad (2.49)$$

Therefore, since the position of the atom  $x$  is contained in  $\eta(x)$ , it is recorded in the final state of the field, due to the entanglement between them. As a consequence, since the final state of the field depends on the position of the atom during the interaction, we can perform a quadrature measurement on the field to determine the position of the atom when it crossed the wave.

To perform the quadrature measurement of the field, we consider the projection of the eigenstate  $|\chi_\theta\rangle$  of the quadrature operator  $X_\theta = \frac{ae^{-i\theta} + a^\dagger e^{i\theta}}{2}$  on (2.49), such that

$$|\psi(t)\rangle_{atom} = N \int dx \kappa(x) \langle \chi_\theta | \alpha e^{i\frac{|g|^2 t}{\Delta} \cos^2(kx + \xi)} \rangle |x, g\rangle. \quad (2.50)$$

Here  $X_{\theta=0} \equiv X$  ( $X_{\theta=\pi/2} \equiv Y$ ) represents an amplitude (phase) quadrature measurement of the field and  $\chi_\theta$  the resulting value. To obtain an expression for the atom state after the quadrature measurement, we consider that  $|\chi_\theta\rangle$ , corresponds to a maximally squeezed state defined as (see appendix 2.3.2):

$$\begin{aligned} |\chi_\theta\rangle &= \frac{1}{\sqrt[4]{2\pi}} \exp\left[-\frac{1}{2}(a^\dagger e^{i\theta} - \chi_\theta)^2 + \frac{1}{4}\chi_\theta^2\right] |0\rangle \\ &= \frac{1}{\sqrt[4]{2\pi}} e^{-\frac{1}{4}\chi_\theta^2} \left[ \sum_{n=0}^{\infty} \frac{e^{in\theta} \chi_\theta^n}{\sqrt{n!}} |n\rangle - \frac{1}{2} \sum_{n=0}^{\infty} \sqrt{(n+2)!} \frac{e^{i(n+2)\theta} \chi_\theta^n}{n!} |n+2\rangle \right. \\ &\quad \left. + \frac{1}{2!} \frac{1}{4} \sum_{n=0}^{\infty} \sqrt{(n+4)!} \frac{e^{i(n+4)\theta} \chi_\theta^n}{n!} |n+4\rangle - \frac{1}{3!} \frac{1}{8} \sum_{n=0}^{\infty} \sqrt{(n+6)!} \frac{e^{i(n+6)\theta} \chi_\theta^n}{n!} |n+6\rangle + \dots \right], \end{aligned} \quad (2.51)$$

moreover, we recall that the state of the quantum field after the interaction can be written as

$$|\alpha e^{i\frac{|g|^2 t}{\Delta} \cos^2(kx+\xi)}\rangle = |\alpha e^{i\eta}\rangle = e^{-\frac{|\alpha e^{i\eta}|^2}{2}} \sum_{n=0}^{\infty} \frac{(\alpha e^{i\eta})^n}{\sqrt{n!}} |n\rangle. \quad (2.52)$$

Therefore (see Appendix)

$$\langle \chi_\theta | \alpha e^{i\eta} \rangle = \frac{1}{\sqrt[4]{2\pi}} e^{-[(\alpha_1 - \frac{\chi_\theta}{2})^2 + i\alpha_2(\alpha_1 - \chi_\theta)]} \quad (2.53)$$

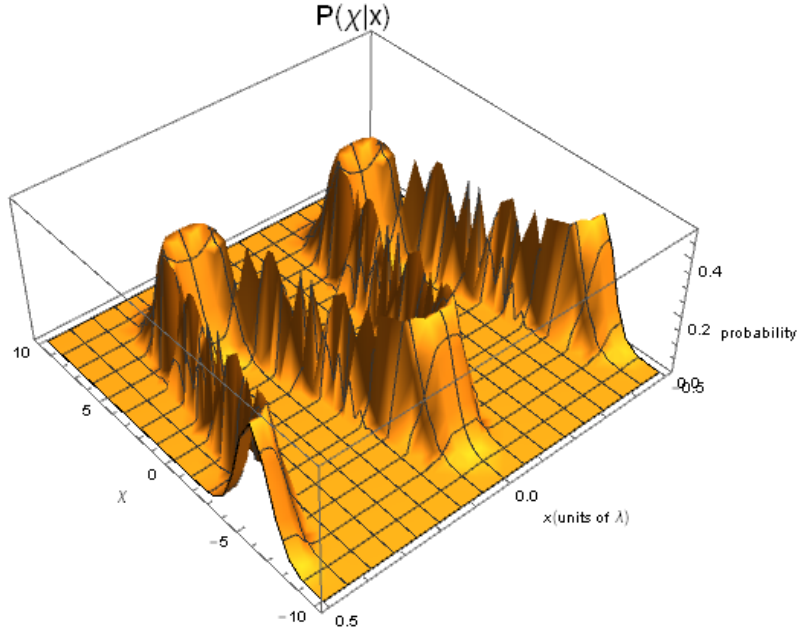
with  $\alpha_1 + i\alpha_2 \equiv \alpha e^{i[(|g|^2 t/\Delta) \cos^2(kx+\xi) - \theta]} = \alpha e^{i(\eta - \theta)}$ , which allows us to obtain the final state of the atom given by

$$|\psi(t)\rangle_{atom} = N \int dx \kappa(x) \frac{1}{\sqrt[4]{2\pi}} e^{-[(\alpha_1 - \frac{\chi_\theta}{2})^2 + i\alpha_2(\alpha_1 - \chi_\theta)]} |x, g\rangle. \quad (2.54)$$

Otherwise, considering (2.50), we can obtain the position probability distribution  $P(x|\chi_\theta)$  of the atom given that the value  $\chi_\theta$  has been measured for the field when the quadrature measurement is performed

$$\begin{aligned} P(\chi_\theta|x) &= \left| \left\langle \chi_\theta \left| \alpha e^{i\frac{|g|^2 t}{\Delta} \cos^2(kx+\xi)} \right. \right\rangle \right|^2 = \left| \frac{1}{\sqrt[4]{2\pi}} e^{-[(\alpha_1 - \frac{\chi_\theta}{2})^2 + i\alpha_2(\alpha_1 - \chi_\theta)]} \right|^2 \\ &= \frac{1}{\sqrt{2\pi}} e^{-2[\alpha_1(x) - \frac{\chi_\theta}{2}]^2} = \frac{1}{\sqrt{2\pi}} e^{-\frac{[2\alpha_1(x) - \chi_\theta]^2}{2}}, \end{aligned} \quad (2.55)$$

with  $\alpha_1(x) = \alpha \cos \left[ \frac{|g|^2 t}{\Delta} \cos^2(kx + \xi) - \theta \right]$ , which implies that for a specific position  $x$ , the probability of measuring  $\chi_\theta$  has a Gaussian dependence, which can be observed in the figure (2.9), where we have considered the amplitude of the field  $\alpha = \sqrt{8}$ . For a certain results of the quadrature measurement, we can obtain a specific position probability distribution. For instance, if the result of the measurement is  $\chi_0 = \alpha$  or  $\chi_0 = -\alpha$ , the probability distribution is the one shown in the figure (2.10) by the red and blue lines, respectively. For  $X = 0$ , the probability distribution is shown in figure (2.11).

Figure 2.9: Conditional probability  $P(\chi|x)$ .

Therefore, if a field measurement is performed, we can express the atom state as the density matrix

$$\rho_{atom}(t) = |\psi(t)\rangle_{atom}\langle\psi(t)| \quad (2.56)$$

with

$$|\psi(t)\rangle_{atom} = N \int dx \kappa(x) \frac{1}{\sqrt[4]{2\pi}} e^{-[(\alpha_1 - \frac{x\theta}{2})^2 + i\alpha_2(\alpha_1 - \chi\theta)]} |x, g\rangle, \quad (2.57)$$

where  $N$  is obtained from the normalization condition  $\langle\psi(t)|\psi(t)\rangle = 1$ :

On other hand, if any measurement is performed on the system, we obtain  $\rho_{atom}(t)$  through the partial trace over field

$$\rho_{atom}(t) = Tr_{field}\{|\psi(t)\rangle\langle\psi(t)|\}, \quad (2.58)$$

where

$$|\psi(t)\rangle = \int dx \kappa(x) \left| \alpha e^{i\frac{|g|^2 t}{\Delta} \cos^2(kx + \xi)} \right\rangle |x, g\rangle. \quad (2.59)$$

If the atom leaves the cavity and it propagates freely, its final state at a time  $t'$  after crossing the cavity will correspond to

$$\hat{\rho}_{atom}(t') = \hat{U}(t') \hat{\rho}_{atom}(0) \hat{U}^\dagger(t') \quad (2.60)$$

with

$$\hat{U}(t') = \exp\left(-\frac{it'}{\hbar} \frac{\hat{p}^2}{2m}\right), \quad (2.61)$$

and

$$\hat{\rho}_{atom}(0) = |\psi(t)\rangle_{atom}\langle\psi(t)|. \quad (2.62)$$

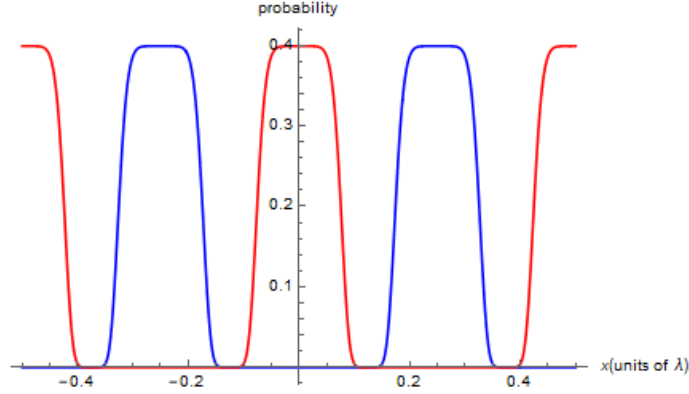


Figure 2.10: Probability distribution of the atom after an  $X$  quadrature measurement of the field with values  $\chi_0 = \alpha$  (red) and  $\chi_0 = -\alpha$  (blue).

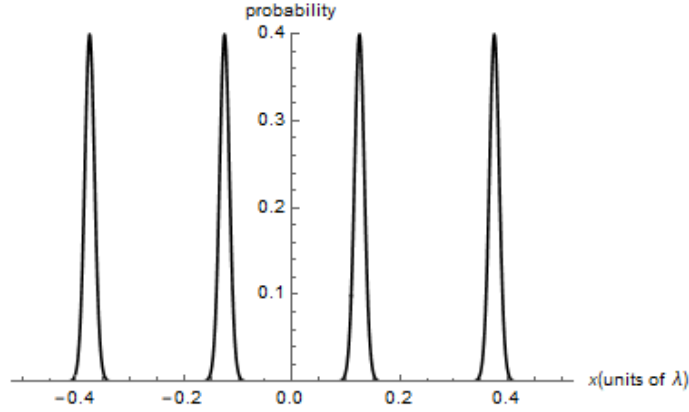


Figure 2.11: Probability distribution of the atom after the  $X$  quadrature measurement of the field with value  $\chi_0 = 0$ .

In order to observe the way in which the atom propagates after it leaves the cavity, we show a case in which we assume that the specific value  $\chi_0 = 0$  is obtained when an  $X_0$  quadrature measurement is performed over the field. Thus, from (2.57) we obtain

$$\begin{aligned}
 |\psi(t')\rangle_{atom} &= e^{-\frac{it'}{\hbar} \frac{\hat{p}^2}{2m}} |\psi(t)\rangle_{atom} \\
 &= e^{-\frac{it'}{\hbar} \frac{\hat{p}^2}{2m}} \left[ N \int dx \kappa(x) \frac{1}{\sqrt[4]{2\pi}} e^{-[\alpha_1^2(x) + i\alpha_2(x)\alpha_1(x)]} |x, g\rangle \right] \\
 &= e^{-\frac{it'}{\hbar} \frac{\hat{p}^2}{2m}} \int dx |x, g\rangle \langle x, g | \psi(t)\rangle_{atom}.
 \end{aligned} \tag{2.63}$$

Projecting  $\langle x', g |$  on the state  $|\psi(t')\rangle$  we can obtain an expression of the wavefunction  $\psi(x', t')$  of the atom in terms of the time  $t'$  and the position  $x'$ , which describes the system after the atom leaves the cavity (see appendix 2.3.2).

$$\langle x', g | \psi(t')\rangle = \int dx \langle x', g | e^{-\frac{it'}{\hbar} \frac{\hat{p}^2}{2m}} |x, g\rangle \langle x, g | \psi(t)\rangle \equiv \psi(x', t'). \tag{2.64}$$

Therefore, the probability of finding the atom in a position  $x'$  in a time  $t'$  after the atom-field interaction is given by  $|\psi(x', t')|^2$ , which is plotted in the figure 2.12. In the image we

can observe how the peaks of probability propagate causing interference in certain value of  $t'$ . For instance, if we take  $t' = 0.015$ , the interference pattern is shown in the figure 2.13. On the other hand, for  $t' = 3$ , the pattern in the figure 2.14 shows that peaks of probability are spatially separated due to the temporal evolution of the system, and thus there is no interference.

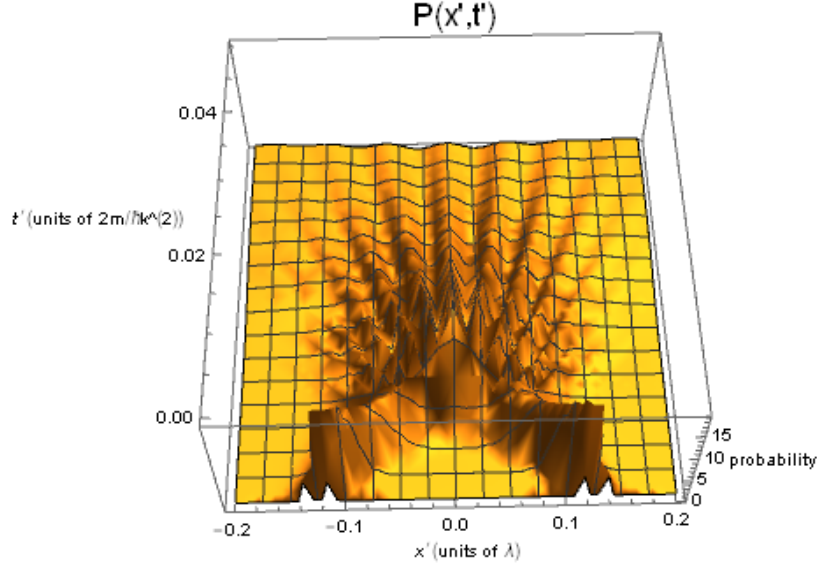


Figure 2.12: Probability distribution in function of  $x'$  y  $t'$ .

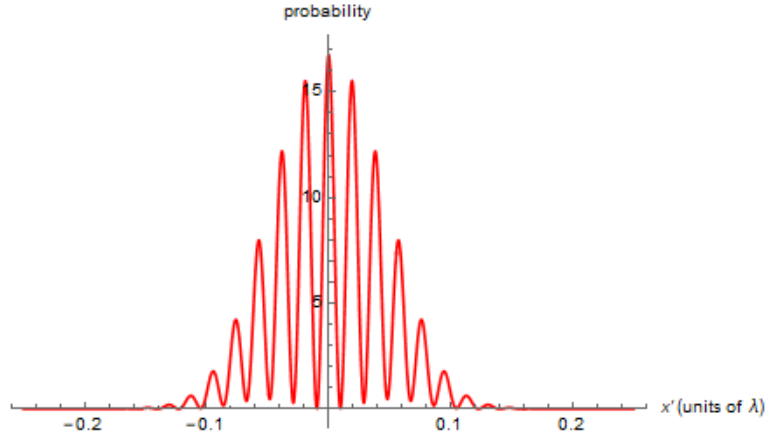


Figure 2.13: Postion probability distribution for  $t' = 0.015$ .

So far we have considered that the initial atomic distribution extends in a width equal to  $\lambda/2$  and  $\xi = 0$ . Thus, it is only possible to obtain the two central peaks of the figure 2.11 and their time evolution shown in 2.13. In order to exemplify another case, we consider that the initial atomic distribution previous to the entry of the atom in the cavity spans  $3\lambda/4$  and  $\xi = 1/8$ . This implies to obtain a new normalization constant, which is shown in the appendix (2.3.2), and a new probability distribution after performing the quadrature measurement figure 2.15.

In this case, the central peak scrolls left during a time  $t'$  after the atom-field interaction, while the rest of peaks scroll right, as the figure 2.16 shows.

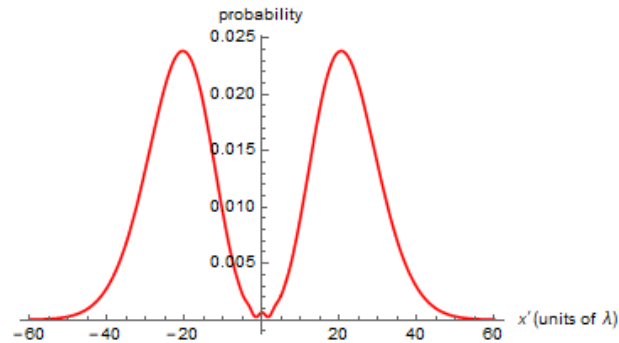


Figure 2.14: Position probability distribution for  $t' = 3$ .

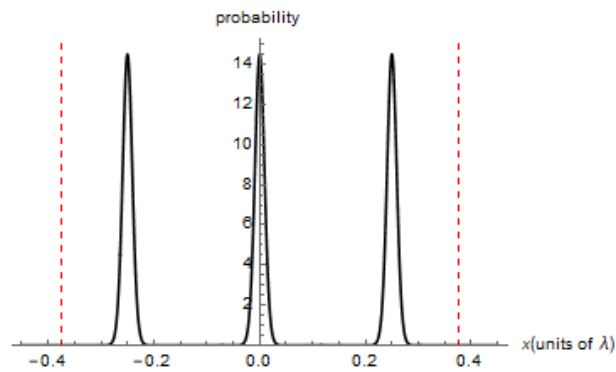


Figure 2.15: Atomic probability distribution when the value  $\chi_0 = 0$  is obtained after to perform an  $X_0$  quadrature measurement. The initial atomic distribution is taken  $\kappa(x) = 3\lambda/4$ .

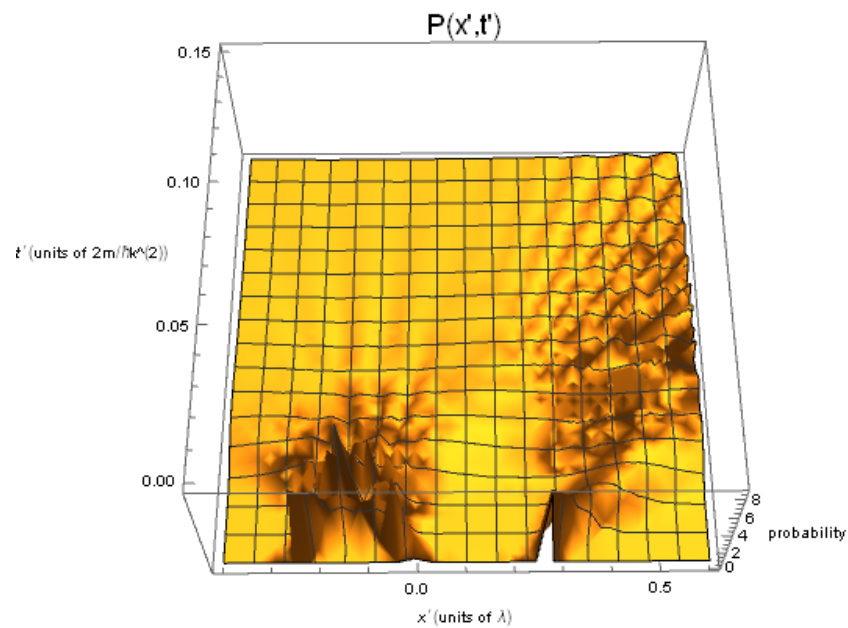


Figure 2.16: Atomic probability distribution in function of  $x'$  y  $t'$  after field measurement when  $\kappa(x) = 3\lambda/4$ .

Finally, to visualize the interference effects we take some values  $t'$  which show different pattern as the atom moves away from the cavity field.

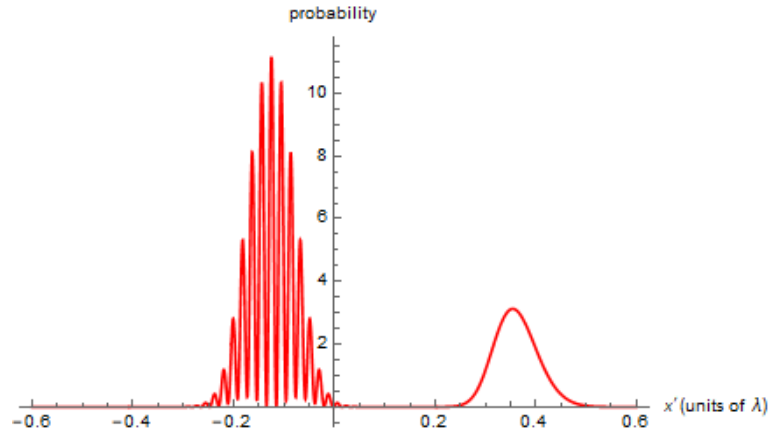


Figure 2.17: Atomic probability distribution in function of  $x'$  for  $t' = 0.015$ .

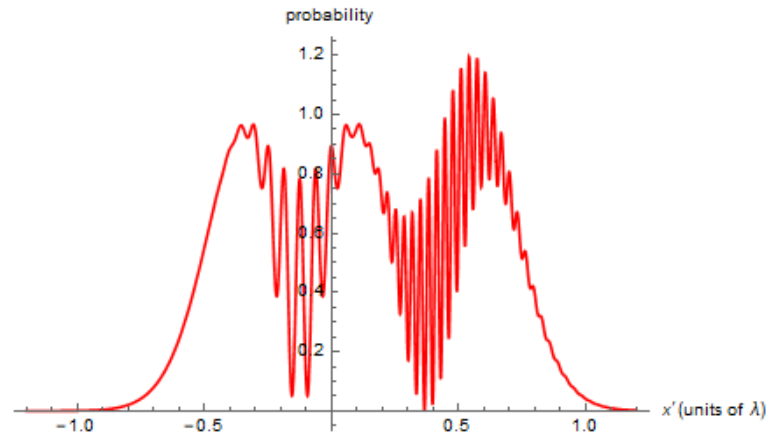


Figure 2.18: Atomic probability distribution in function of  $x'$  for  $t' = 0.05$ .

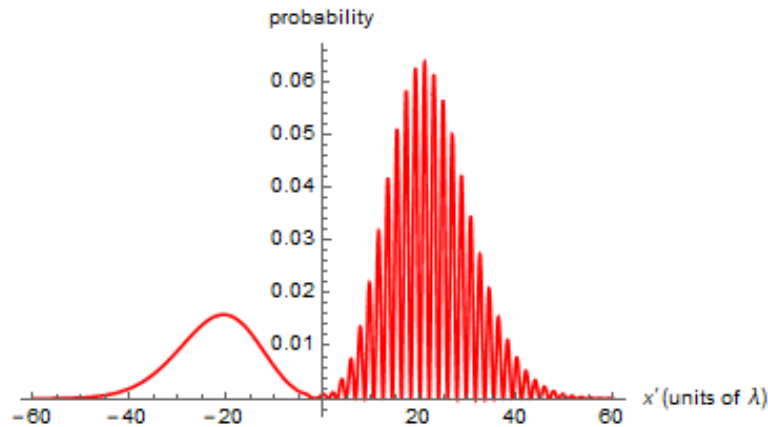


Figure 2.19: Atomic probability distribution in function of  $x'$  for  $t' = 3$ .

Up to this point, we can notice that the atom-field interaction allows us to measure the state of the quantum field by performing a quadrature measurement, and from the obtained results one may study the behavior of the atom after it crosses the cavity field. Therefore, this offers us the possibility of implementing a model based on the atom-field interaction, by which to study the wave-particle duality in a double-slit scheme. In the next chapters, we present the models that we have proposed in order to analyze how the duality can be controlled by different atomic and field parameters, depending of the behaviour that we want to obtain, wave-like or particle-like, once the atom crosses the scheme. Also, we give all the details about the preparation of the atomic and field states, as well as the measurement processes.

## Chapter 3

# Controlling the wave-particle duality with quantum fields

As we have seen previously, quantum fields can be used to determine atomic positions depending on the amplitude of the field and the quadrature measurements performed. This is because the interaction atom-field interaction depends on the position in which the standing wave is crossed by the atom. Therefore, by locating the slits of Young-type scheme in front of specific positions of the quantum field, we could detect unambiguously the path followed by the atom. As a consequence, the wave-like properties of the system are lost.

In this section, we consider a two-level atom crossing a double-slit scheme, which is located immediately before a cavity with a standing wave represented by a quantum field. This allows us to establish only two possible paths on which the atom passes through the cavity. The slits are located in front of a node and an antinode of the wave, in such a way that the interaction is maximum when the atom crosses the antinode and null when it crosses a node, causing a maximum or null shift of the phase of the field, respectively. Therefore, an adequate measurement of the quadratures of the quantum field offers us the possibility of detecting the position of the atom during the interaction and thus, its trajectory.

For a coherent state, it is known that the path information can be controlled by the amplitude of the quantum field, causing partial interference as its value decreases [62]. In this section we consider in addition to the coherent states, different quantum states such as squeezed states, cat states and thermal states, in order to analyze how the parameters present in each one can help to control the visibility of fringes and the path information. In addition, we correlate the internal states of the two-level atoms with the paths of the scheme, which allows us to have a certain level of concurrence in the system, in order to study its relation with visibility and distinguishability. This configuration also offers us the possibility of having two path detectors, the quantum field and the internal state of the atom.

### 3.1 Model

A two-level atom crosses a cavity with a quantum field with wave number  $k = 2\pi/\lambda$ . A double-slit is placed immediately before the field with top slit located in front of an antinode and the bottom slit in front of a node with a separation distance of  $0.25\lambda$  between slits (figure 3.1) [45, 62]. This allows to establish only two possible paths for the atom, which results in maximum or null interaction with the quantum field. Therefore, if the interaction produces some effect on the field, it could be used to reveal which-path information. Furthermore, we consider a highly localized atomic spatial distribution due to the position of the slits, and a negligible change in the transverse distance traveled by the atom during the interaction. Thus  $\Delta x \ll \lambda$ , which implies that the atomic distribution spreads once the atom leaves the cavity [62]. Initially the atom is in the ground state and it can be reflected or transmitted by the atomic beam splitter (ABS) [22, 24] with reflection and transmission coefficients  $c_\uparrow$  and  $c_\downarrow$ , satisfying  $|c_\uparrow|^2 + |c_\downarrow|^2 = 1$ . If the atom is transmitted, it flies in the ground state along the bottom path and crosses the slit at the node of the standing wave ( $x = 0.25\lambda$ ). On other hand, if the atom is reflected, it goes through the top slit passing by an atomic mirror (AM) [5, 43] and a Ramsey field (RF) [54]. This allows to prepare a superposition of the states  $|b\rangle$  and  $|a\rangle$ , which remains during the time of interaction of the atom with the quantum field. This requires the use of long lived atoms in order to avoid the spontaneous emission in the cavity [26]. The probability coefficients of exciting the state  $|a\rangle$  and remaining in the state  $|b\rangle$  are  $\sin^2 \phi$  and  $\cos^2 \phi$ , respectively. In this case, the atom crosses the top slit and the antinode of the field ( $x = 0$ ). Therefore, the top path is correlated with the internal atomic state  $|\Phi_\uparrow\rangle = \cos \phi |b\rangle + \sin \phi |a\rangle$ , while the bottom path is correlated with the state  $|\Phi_\downarrow\rangle = |b\rangle$ .

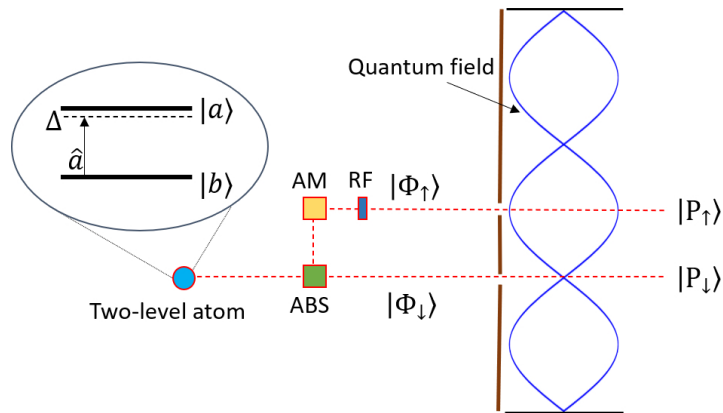


Figure 3.1: Double-slit scheme. A two-level atom passes through the atomic beam splitter (ABS) in the ground state. In the upper path  $|P_\uparrow\rangle$ , the atomic mirror (AM) and Ramsey field (RF) generate the internal atomic state  $|\Phi_\uparrow\rangle$ , while in the bottom path  $|P_\downarrow\rangle$  the initial atomic state remains the same. Finally, the atom crosses a node or antinode of the quantum field.

### 3.1.1 Initial state

Once the atom passes through the ABS, its state can be described as

$$|\psi(0)\rangle_{atom} = c_{\uparrow}|P_{\uparrow}\rangle \otimes |\Phi_{\uparrow}\rangle + c_{\downarrow}|P_{\downarrow}\rangle \otimes |\Phi_{\downarrow}\rangle = c_{\uparrow}|P_{\uparrow}\rangle \otimes [\cos \phi|b\rangle + \sin \phi|a\rangle] + c_{\downarrow}|P_{\downarrow}\rangle \otimes |b\rangle, \quad (3.1)$$

where the states  $|P_{\uparrow}\rangle$  and  $|P_{\downarrow}\rangle$  represent the top and bottom path of the scheme, respectively.

Immediately to the right of the double slit, the cavity with the quantum field is located. We consider different states of the field in order to analyse different ways of controlling the wave-particle duality. Before the interaction the state of the field is represented by a squeezed coherent state, a cat state and a thermal state, respectively.

#### 3.1.1.1 Squeezed coherent state

The first state of the field corresponds to a squeezed coherent state defined as

$$|\psi(0)\rangle_{field} = |\alpha, \xi\rangle = \hat{D}(\alpha)\hat{S}(\xi)|0\rangle = \hat{S}(\xi)\hat{D}(\beta)|0\rangle = \sum_{n=0} c_n |n\rangle, \quad (3.2)$$

where

$$\beta = \alpha \cosh(r) + \alpha^* e^{i\vartheta} \sinh(r) \quad (3.3)$$

The squeeze and displacement operators are given respectively by [50]

$$\hat{S}(\xi) = e^{\frac{1}{2}\xi^* \hat{a}^2 - \frac{1}{2}\xi(\hat{a}^\dagger)^2}, \quad (3.4)$$

with  $\xi = r e^{i\vartheta}$  and

$$\hat{D}(\alpha) = e^{\alpha \hat{a}^\dagger - \alpha^* \hat{a}} \quad (3.5)$$

with  $\alpha = \alpha' e^{i\varphi}$ . The coefficients  $c_n$  are defined as [23]

$$c_n = e^{-\frac{1}{2}|\beta|^2 + \frac{1}{2}\beta^2 e^{-i\vartheta} \tanh(r)} \frac{\left(\frac{1}{2}e^{i\vartheta} \tanh(r)\right)^{n/2}}{\sqrt{n! \cosh(r)}} H_n(\beta[e^{i\vartheta} \sinh(2r)]^{-1/2}). \quad (3.6)$$

Therefore, the state of the total initial system is given as

$$|\psi(0)\rangle_{system} = |\psi(0)\rangle_{atom} \otimes |\psi(0)\rangle_{field} = \left( c_{\uparrow}|P_{\uparrow}\rangle \otimes [\cos \phi|b\rangle + \sin \phi|a\rangle] + c_{\downarrow}|P_{\downarrow}\rangle \otimes |b\rangle \right) \otimes |\alpha, \xi\rangle. \quad (3.7)$$

#### 3.1.1.2 Cat state

As a second case, we consider that the quantum field is represented by a cat state, which corresponds to a superposition of two coherent states  $|\pm \alpha\rangle$ . The even or odd cat states are defined respectively by

$$|cat\rangle_{even} = \frac{|\alpha\rangle + |-\alpha\rangle}{\sqrt{2(1 + e^{-2|\alpha|^2})}} \quad (3.8)$$

and

$$|cat\rangle_{odd} = \frac{|\alpha\rangle - |-\alpha\rangle}{\sqrt{2(1 + e^{-2|\alpha|^2})}}, \quad (3.9)$$

where

$$|\pm\alpha\rangle = e^{\frac{\pm\alpha}{2}} \sum_{n=0}^{\infty} \frac{(\pm\alpha)^n}{\sqrt{n!}} |n\rangle. \quad (3.10)$$

In this case, the state of the total initial system corresponds to

$$|\psi(0)\rangle_{system} = |\psi(0)\rangle_{atom} \otimes |\psi(0)\rangle_{field} = \left( c_{\uparrow}|P_{\uparrow}\rangle \otimes [\cos\phi|b\rangle + \sin\phi|a\rangle] + c_{\downarrow}|P_{\downarrow}\rangle \otimes |b\rangle \right) \otimes |cat\rangle_{e,o}. \quad (3.11)$$

### 3.1.1.3 Thermal state

Finally, we consider a thermal state in order to analyse how it can be used to control the wave-particle duality. The density operator for a one-mode thermal state is given by [50]

$$\rho_{thermal} = \sum_n \frac{\langle n \rangle_{th}^n}{(1 + \langle n \rangle_{th})^{n+1}} |n\rangle\langle n|, \quad (3.12)$$

where  $\langle n \rangle_{th}$  corresponds to the average photon number. Therefore, the initial state of the system is given as

$$\rho(0)_{system} = \rho_{atom} \otimes \rho_{thermal}, \quad (3.13)$$

where  $\rho_{atom} = |\psi(0)\rangle_{atom}\langle\psi(0)|$ .

### 3.1.2 Time evolution

After the interaction the total initial system will evolve to the state

$$|\psi(t)\rangle_{system} = \hat{U}|\psi(0)\rangle_{system} = e^{-\frac{i\hat{V}t}{\hbar}}|\psi(0)\rangle_{system}, \quad (3.14)$$

where  $\hat{V}$  is the Hamiltonian in the interaction framework considering a rotating wave approximation and a large detuning  $\Delta$  in order to avoid photon emission (figure 3.1).  $x$  corresponds to the transverse position of the atom during the interaction. This is expressed in units of the wavelength of the quantum field and it is measured with respect to the antinode in front of the upper slit ( $x = 0$ ) [63].

$$\hat{V} = \frac{\hbar|g|^2 \cos^2(kx)}{\Delta} \hat{\sigma}_z \hat{a}^\dagger \hat{a} + \hbar\Delta \hat{\sigma}_z. \quad (3.15)$$

If the quantum field is represented by a squeezed coherent state  $|\alpha, \xi\rangle$ , the state of the system after a time of interaction  $t$  can be written as [see eq (7.24) in Appendix chapter 3]

$$\begin{aligned} |\psi(t)\rangle &= e^{-\frac{i\hat{V}t}{\hbar}} (|\psi(0)\rangle_{atom} \otimes |\psi(0)\rangle_{field}) \\ &= e^{it\Delta} c_{\uparrow}|P_{\uparrow}\rangle \otimes \cos\phi|b\rangle \otimes |e^{in(x)}\alpha, \xi\rangle \\ &\quad + e^{-it\Delta} c_{\uparrow}|P_{\uparrow}\rangle \otimes \sin\phi|a\rangle \otimes |e^{-in(x)}\alpha, \xi\rangle \\ &\quad + e^{it\Delta} c_{\downarrow}|P_{\downarrow}\rangle \otimes |b\rangle \otimes |\alpha, \xi\rangle, \end{aligned} \quad (3.16)$$

with  $\eta(x) = \frac{t|g|^2 \cos^2(kx)}{\Delta}$  and where we have defined  $\sum_n e^{\pm i\eta(x)n} c_n |n\rangle \equiv |e^{\pm i\eta(x)}\alpha, \xi\rangle$ . We take  $\frac{t|g|^2}{\Delta} = \pi$ . Therefore, if the atom takes the upper path, the final phase is the same for both internal atomic states,  $|a\rangle$  (clockwise phase-shift) or  $|b\rangle$  (counter-clockwise phase-shift), due to  $e^{\pm i\eta(x)n} = e^{\pm i\pi \cos^2(kx)n}$ . However, if the value of  $\frac{t|g|^2}{\Delta}$  is different from  $m\pi$  with  $m = 1, 2, 3, \dots$ , the final phase produced by the atom in the state  $|a\rangle$  is different from the final phase produced by the atom in the state  $|b\rangle$ . On the contrary, if the atom takes the bottom path, the initial phase remains unaffected.

On other hand, when the quantum field corresponds to a cat state, the total system will evolve as [see eq (7.25) in Appendix chapter 3]

$$\begin{aligned}
 |\psi(t)\rangle &= e^{-\frac{i\hat{V}t}{\hbar}} (|\psi(0)\rangle_{atom} \otimes |\psi(0)\rangle_{field}) \\
 &= e^{it\Delta} c_{\uparrow} |P_{\uparrow}\rangle \otimes \cos \phi |b\rangle \otimes \left( \frac{|e^{i\eta(x)}\alpha\rangle \pm |-e^{i\eta(x)}\alpha\rangle}{\sqrt{2(1 + e^{-2|\alpha|^2})}} \right) \\
 &+ e^{-it\Delta} c_{\uparrow} |P_{\uparrow}\rangle \otimes \sin \phi |a\rangle \otimes \left( \frac{|e^{-i\eta(x)}\alpha\rangle \pm |-e^{-i\eta(x)}\alpha\rangle}{\sqrt{2(1 + e^{-2|\alpha|^2})}} \right) \\
 &+ e^{it\Delta} c_{\downarrow} |P_{\downarrow}\rangle \otimes |b\rangle \otimes \left( \frac{|\alpha\rangle \pm |-\alpha\rangle}{\sqrt{2(1 + e^{-2|\alpha|^2})}} \right).
 \end{aligned} \tag{3.17}$$

Finally, if we consider a thermal state, the evolution of the systems will be given as

$$\rho(t) = e^{-\frac{i\hat{V}t}{\hbar}} (\rho_{atom} \otimes \rho_{thermal}) e^{\frac{i\hat{V}t}{\hbar}} = e^{-i\eta(x)\hat{\sigma}_z \hat{a}^\dagger \hat{a}} e^{-it\Delta \hat{\sigma}_z} (\rho_{atom} \otimes \rho_{thermal}) e^{i\eta(x)\hat{\sigma}_z \hat{a}^\dagger \hat{a}} e^{it\Delta \hat{\sigma}_z}. \tag{3.18}$$

### 3.1.3 Which-path information and fringe visibility

The phase-shift of the quantum field is a consequence of the atom's position during the interaction time. Therefore, a proper quadrature measurement can reveal which-path information. If the quadrature

$$X_\theta = \frac{ae^{-i\theta} + a^\dagger e^{i\theta}}{2} \tag{3.19}$$

is measured with an eigenvalue  $\chi_\theta$ , the corresponding eigenstate  $|\chi_\theta\rangle$  is an infinitely squeezed state given by [51, 62]

$$|\chi_\theta\rangle = \frac{1}{\sqrt[4]{2\pi}} \exp\left[-\frac{1}{2}(a^\dagger e^{i\theta} - \chi_\theta)^2 + \frac{1}{4}\chi_\theta^2\right] |0\rangle = \sum_n b_n |n\rangle, \tag{3.20}$$

where

$$b_n = \frac{N}{\sqrt{n!}} \left(\frac{1}{2}e^{i\theta}\right)^{n/2} H_n(z), \tag{3.21}$$

with  $N$  being a normalization constant and  $H_n(z)$  the Hermite polynomials with  $z = (\alpha e^{-i\theta} + \alpha^* e^{i\theta})/2$ .

In absence of the quantum field, we define the distinguishability, visibility and concurrence as  $D_0$ ,  $V_0$  and  $C_0$ , respectively. The relation among these quantities in a typical double-slit scheme, in which some intrinsic property of the particle is correlated with the paths, can be written as the equality (2.15) [53] with

$$\begin{aligned} D_0 &= ||c_\uparrow|^2 - |c_\downarrow|^2| \\ V_0 &= 2|c_\uparrow c_\downarrow \gamma| \\ C_0 &= 2|c_\uparrow c_\downarrow| \sqrt{1 - |\gamma|^2}, \end{aligned} \quad (3.22)$$

[25, 31, 32, 68] where the coefficients  $c_\uparrow$  and  $c_\downarrow$  define the probabilities for the atom of taking the top or bottom path and  $\gamma \equiv \langle \Phi_\uparrow | \Phi_\downarrow \rangle = \cos \phi$ , where the normalized states  $|\Phi_{\uparrow,\downarrow}\rangle$  correspond to intrinsic degrees of freedom of the particle. In our scheme, we establish correlations between the internal atomic states and the paths in order to analyze cases with different degrees of concurrence. In this case, in addition to phase-shift of the quantum field, the which-path information can also be controlled through the coefficients  $c_\uparrow$  and  $c_\downarrow$ , which define the atomic state according to the equation (3.1). Therefore, we consider  $c_\uparrow = c_\downarrow$  in order to study the points shown in the plane CV of the sphere VDC (figure 3.2). This choice allows to control the fringe visibility through the parameter  $\phi$  in the atomic state, and the parameters which define each quantum field.

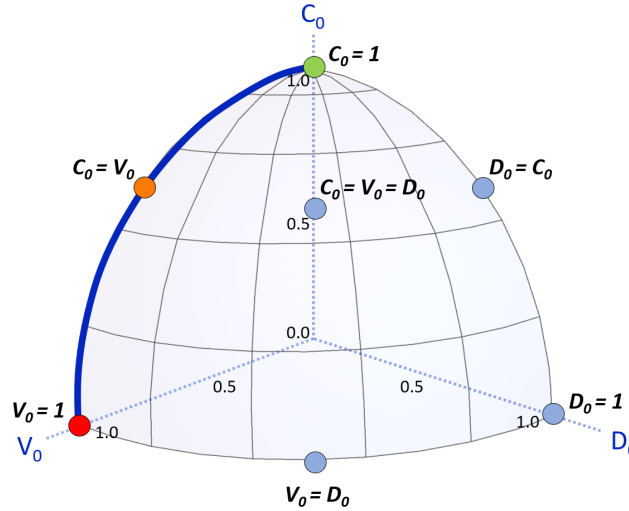


Figure 3.2: Unit sphere  $D_0^2 + V_0^2 + C_0^2 = 1$ . The cases studied in this article are  $C_0 = 1$  (green dot),  $C_0 = V_0$  (orange dot) and  $V_0 = 1$  (red dot).

## 3.2 Results

In this section we present different cases in which different parameters of both, atom and field, control the wave-particle duality. First, we consider the simpler case in which the quantum field corresponds to a coherent state and we show how the which-path information is controlled by the amplitude  $\alpha'$  and the phase  $\varphi$ . Subsequently, we consider the squeeze parameters  $r$  and  $\vartheta$ , in

order to analyse their effects on the observed pattern. As a third case, we consider the cat states and we vary the interaction time to control the which-path information and visibility. Finally, we study the effects of the average photon number on the wave-particle duality in the case in which the quantum field corresponds to a thermal state. In each case, after atom-field interaction, we trace over the field in order to obtain information about the wavelike or particlelike behaviour of the atom [eq. (3.23)]. We suppose that the possible states of the quantum field after interaction are determined by the possible outcomes of each quadrature measurement [eq. (3.20)], which correspond to one of the most probable values.

We consider that the initial atomic distribution once the atom merges from the double-slit corresponds to two Gaussian profiles with standard deviation  $\sigma = 0.05\lambda/2\pi$ . Each Gaussian profiles is centered in the position  $x = 0$  and  $x = 0.25\lambda$ , respectively. Therefore, these define the states of the paths  $|P_{\uparrow,\downarrow}\rangle$  of the scheme. Once the atom leaves the cavity, it freely evolves during a time  $t'$  (in units of  $2m/\hbar k^2$ ) and we obtain the atomic probability distribution for a specific flight time  $t' = 3$ , as a function of the position  $x'$  expressed in units of  $\lambda$  (figure 3.3). Therefore, the atomic state evolves as

$$\rho_{atom}(t') = \hat{U} Tr_{field} [\rho(t)] \hat{U}^\dagger = e^{-\frac{i\hat{H}t'}{\hbar}} \rho_{atom}(t) e^{\frac{i\hat{H}t'}{\hbar}}, \quad (3.23)$$

where  $\hat{H} = \frac{\hat{p}^2}{2m}$  is the free particle Hamiltonian and  $\rho(t) = |\psi(t)\rangle\langle\psi(t)|$ , with  $|\psi(t)\rangle$  given by (5.7) and (3.17) for a squeezed coherent state and a cat state, respectively. For a thermal state  $\rho(t)$  is given by (3.18). We study the cases in the plane CV of the sphere VCD (figure 3.2), thus in addition to  $c_\uparrow = c_\downarrow = \frac{1}{\sqrt{2}}$ , we take  $0 \leq \gamma \leq 1$  ( $\frac{\pi}{2} \geq \phi \geq 0$ ). The values of  $V_0$  and  $C_0$  represent the choice of the parameters  $c_\uparrow, c_\downarrow$  and  $\gamma$  according to the definitions shown in (3.22). Therefore, these do not define by themselves the patterns observed in each case in presence of the quantum field.

### 3.2.1 Coherent state

In a typical double-slit scheme (without field) the atomic probability distributions show total, partial and null interference for the cases  $V_0 = 1$ ,  $V_0 = C_0$  and  $C_0 = 1$ , respectively (figure 3.3). However, in presence of a quantum field the which-path information can be recorded in the phase of it, which modifies the patterns observed on the screen. In this section, we consider three combinations of the parameters  $\alpha'$ ,  $\varphi$  and we take  $r = \vartheta = 0$  in order to show how a coherent state can alter the balance between path-information and visibility.

#### 3.2.1.1 Wave-particle duality controlled by the coherent amplitude $\alpha'$

If we consider  $t|g|^2/\Delta = \pi$ , for  $\alpha' = 3$  the phases before and after of the atom-field interaction are different and these are separated in the phase space represented by the plane  $XY$ , where  $X$  and  $Y$  correspond to the amplitude and phase quadrature, respectively (figure 3.4). Therefore, no interference appears on the screen when an  $X$  quadrature measurement is performed and one of the most probable result is obtained, independently of the degree of concurrence established between the internal atomic states and the paths of the double-slit scheme [see a) - c) in figure 3.7]. In this case, the fringe visibility can not be controlled by the atomic parameters, since that the path information is completely stored in the quantum phase of the field. However, as

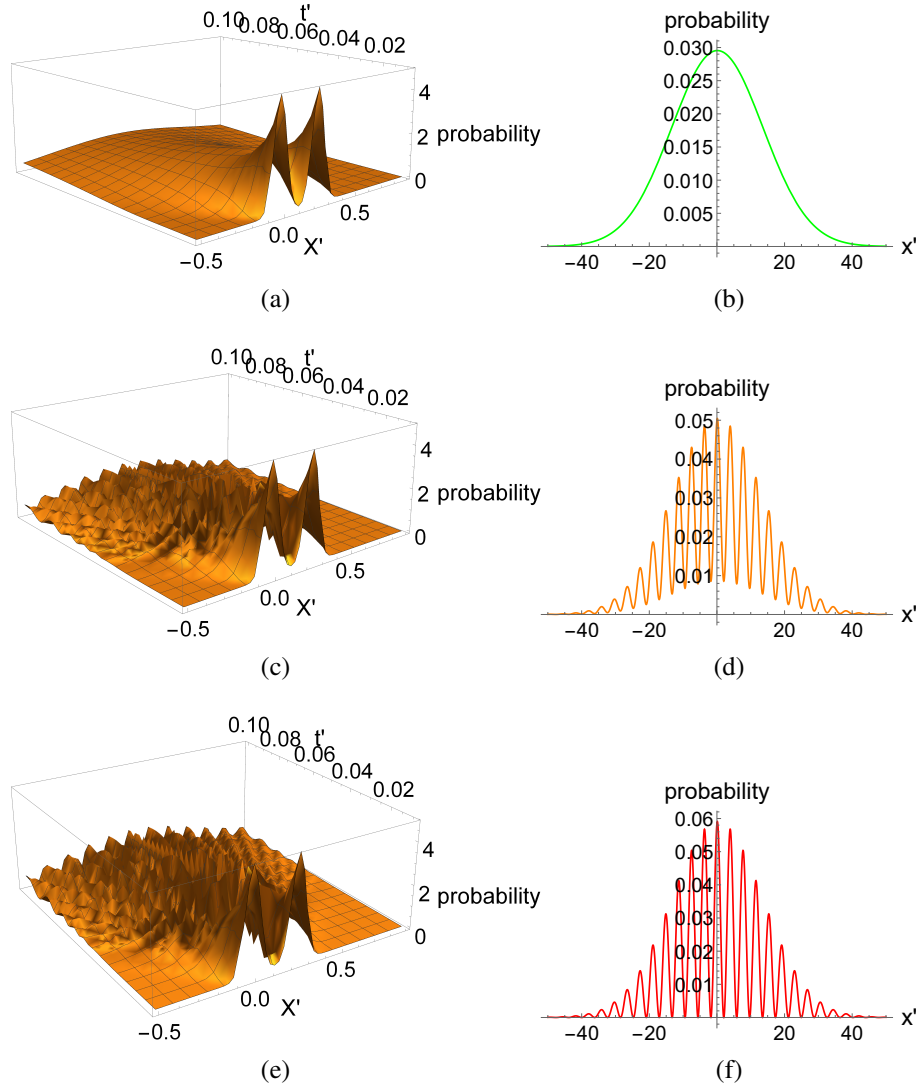


Figure 3.3: Spread of the atomic distribution once the atom crosses a typical double-slit scheme. In this case, we consider the evolution of the distribution in absence of the quantum field. Therefore, the images (a) – (b), (c) – (d) and (e) – (f) correspond to the cases  $C_0 = 1(\phi = \pi/2)$ ,  $V_0 = C_0(\phi = \pi/4)$  and  $V_0 = 1(\phi = 0)$ , respectively. On the left are shown the atomic probability distributions as a function of both, time  $t'$  and distance  $x'$ , on the right are shown the patterns obtained for a flight time  $t' = 3$ .

the amplitude  $\alpha'$  decreases both, initial and final phases get closer (figure 3.5) and interference is partially recovered due to the  $X$  quadrature measurement becomes ambiguous [see d) - f) in figure 3.7]. Therefore, in this case the interference can be varied through the choice of  $\phi$ , which defines the concurrence and the initial atomic state. For  $\phi = \pi/2$  the concurrence is maximum and there is no visibility, since the paths of the double-slit scheme are correlated with different atomic states and thus a measurement on the atom once it crosses the cavity can reveal path-information.

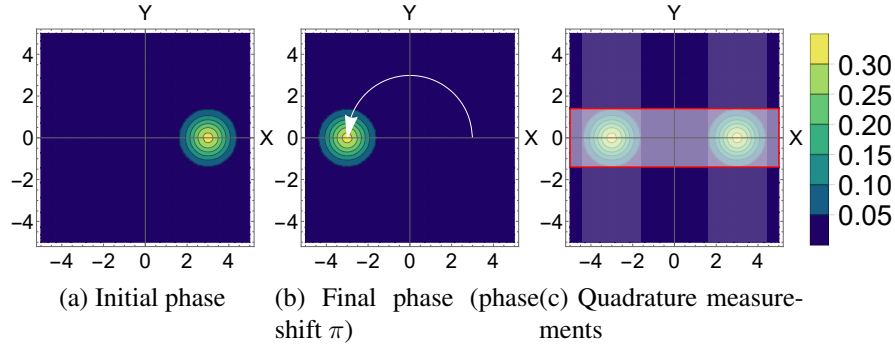


Figure 3.4: Phase-shift (counter-clock wise) produced by the interaction of an atom in the state  $|b\rangle$  ( $\phi = 0$ ) and a coherent state with  $\alpha' = 3$  and  $\varphi = 0$ . An  $X$  quadrature measurement [vertical shadows in (c)] can reveal which-path information and no interferences appears. A  $Y$  quadrature measurement [horizontal shadow with red edges in (c)] can not distinguish one phase from the other one and total interference is obtained.

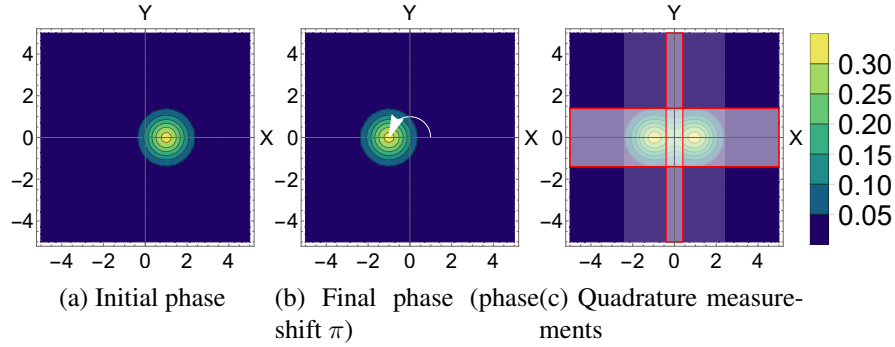


Figure 3.5: For a coherent state with  $\alpha' = 1$  and  $\varphi = 0$  there is overlap between both, initial and final phases [vertical shadow with red edges in (c)]. Therefore, an  $X$  quadrature measurement becomes ambiguous and partial interference appears. A  $Y$  quadrature measurement still shows total interference.

### 3.2.1.2 Wave-particle duality controlled by the coherent phase $\varphi$

In this case, we consider the phase of the coherent state as a variable parameter and we fix the amplitude of the field. We take  $\alpha' = 3$  and  $\varphi = \frac{15\pi}{32}$  (figure 3.6) in order to show that considering  $t|g|^2/\Delta = \pi$ , an  $X$  quadrature measurement becomes ambiguous and thus partial interference can be obtained [see g) - i) in figure 3.7], while a  $Y$  quadrature measurement can reveal the path followed by the atom, since the most probable results of the measurement can reveal the phase of the field. In this sense, the initial phase of the coherent state can also be considered a controller of fringe visibility and which-path information.

## 3.2.2 Squeezed coherent state

This time we consider two new combinations of the parameters  $\alpha'$ ,  $\varphi$ ,  $r$  and  $\vartheta$  to represent a squeezed coherent state, showing that the path-information and fringe visibility can also depend

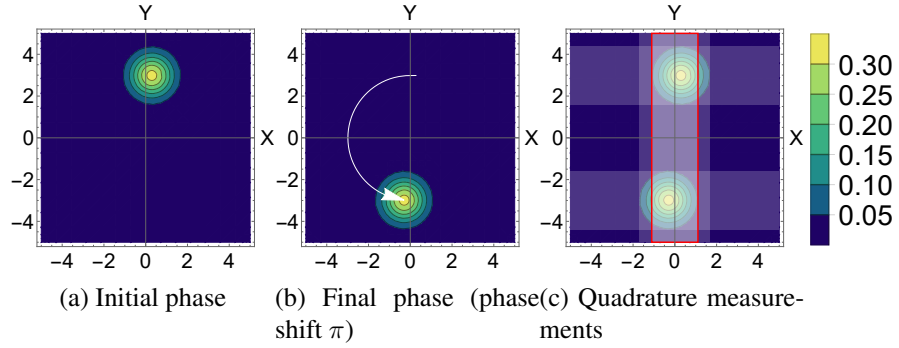


Figure 3.6: An atom in the state  $|b\rangle$  produces a counter-clockwise phase-shift in a coherent state with  $\alpha' = 3$  and  $\varphi = \frac{15\pi}{32}$ . The initial and final phases show overlap for an  $X$  quadrature measurement [vertical shadows with red edges in (c)] and thus partial interference can be observed. On the contrary, a  $Y$  quadrature measurement [horizontal shadows in (c)] can reveal which-path information (no overlap).

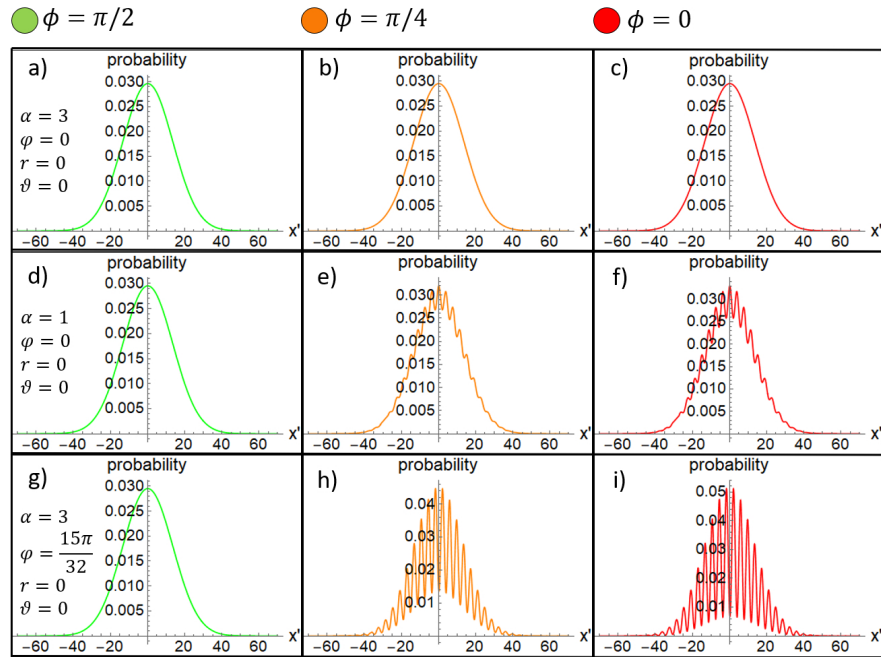


Figure 3.7: Atomic probability distribution obtained for an  $X$  quadrature measurement after atom-field interaction, considering a quantum field represented by a coherent state. The field and atomic parameters are varied in the vertical and horizontal directions, respectively.

on the squeeze amplitude and phase.

### 3.2.2.1 Wave-particle duality controlled by the squeeze amplitude $r$

In this stage, we consider the coherent parameters  $\alpha' = 3$ ,  $\varphi = 0$  and the squeeze parameter  $\xi = 2e^{i\pi}$  ( $r = 2$ ,  $\vartheta = \pi$ ). This set of parameters allows to obtain fringe visibility due to the

overlap between the initial and the final phases of the quantum field (figure 3.8). The bigger the value of  $r$ , the more overlap and interference. On the other hand, the fringes observed on the screen can be controlled, in addition to the squeeze parameters, by the atomic parameter  $\phi$  which can be varied from 0 to  $\pi/2$  in order to erase gradually the interference pattern [see a) - c) in figure 3.10]. In the case  $\phi = \pi/2$ , the change in the phase of the quantum field is produced by the atom in the internal state  $|a\rangle$ , and thus there is a clockwise phase-shift.

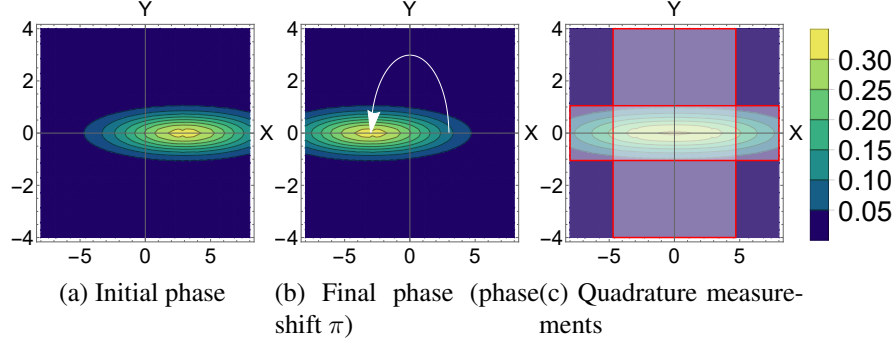


Figure 3.8: Phase-shift for a squeezed coherent state with  $\alpha' = 3$ ,  $\varphi = 0$ ,  $r = 2$  and  $\vartheta = \pi$ , considering interaction with an atom in the state  $|b\rangle$ . For these parameters there is a considerable overlap between the initial and final phases. As a consequence, an  $X$  quadrature measurement [vertical shadow in (c)] becomes ambiguous. On the other hand, total interference is obtained if a  $Y$  quadrature measurement [horizontal shadow in (c)] is performed.

### 3.2.2.2 Wave-particle duality controlled by the squeeze phase $\vartheta$

Finally, we rotate the phase of the squeeze parameter (figure 3.9). We take  $\vartheta = 3\pi/2$  in order to analyse the changes in the interference patterns. We observe that, without varying the atomic parameters, the interference decreases when this phase increases from  $\pi$  to higher values if we perform an  $X$  quadrature measurement [see d) - f) in figure 3.10]. On the other hand, for a  $Y$  quadrature measurement, the interference remains the same as compared to the case in which  $\vartheta = \pi$ , since in both cases the possible results of the measurement do not allow to differentiate the initial phase from the final one.

## 3.2.3 Cat states

Now that we have studied the possibilities that the squeezed coherent states offer to control the wave-particle duality, we will analyse the even cat states. In this case, we consider  $\alpha' = 3$  and  $\varphi = 0$ , and we take the interaction time between the atom and the field as controlling parameter of wave-particle duality .

### 3.2.3.1 Interaction time: $|g|^2 t / \Delta = \pi$

If the phase-shift after the interaction is taken as  $\eta(x) = (|g|^2 t / \Delta) \cos(kx)$  with  $|g|^2 t / \Delta = \pi$ , the final phase is practically the same as the initial one due to the symmetry of the distributions in the  $XY$  plane (figure 3.11). Therefore, an  $X$  or  $Y$  quadrature measurement will show

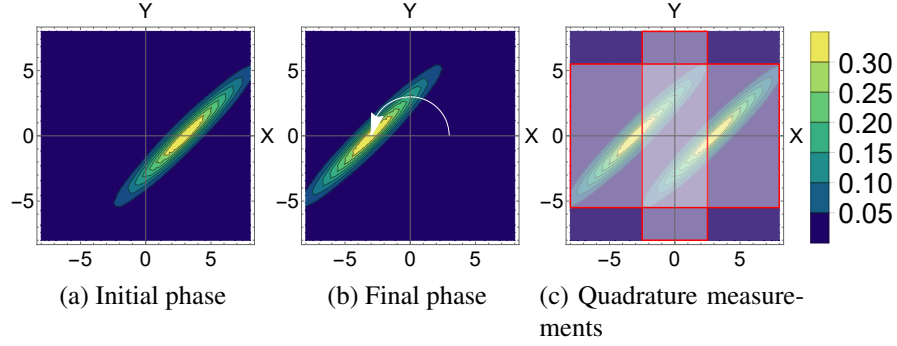


Figure 3.9: The changes in the phases of the field show that for an  $X$  quadrature measurement the overlap between the phases decreases when the squeeze phase increases [see (c)]. Therefore, there is more which-path information and less interference, as compared to the previous case.

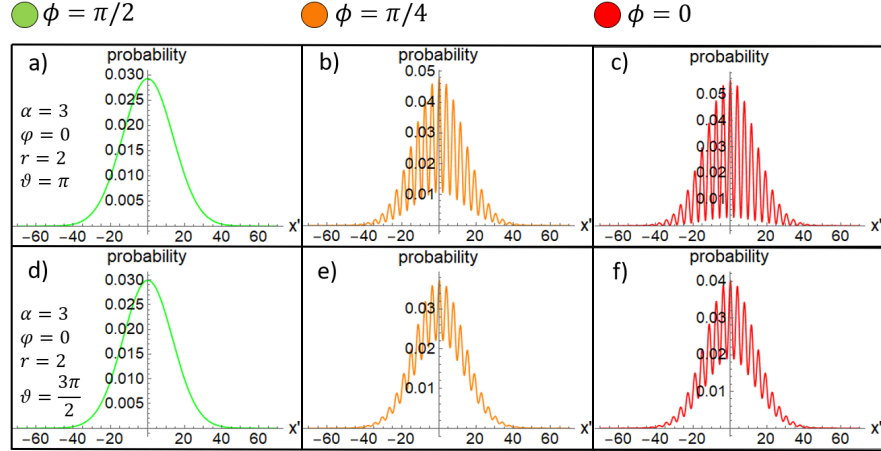


Figure 3.10: Atomic probability distribution obtained for an  $X$  quadrature measurement. In this case the quantum field corresponds to a squeezed coherent state. The field parameters are varied vertically while  $\phi$ , which defines the atomic state, is varied horizontally.

total interference, since it is not possible to obtain path-information from the results of the measurement. Therefore, in this case the presence of the field is irrelevant, since the interference patterns observed are the same as the ones obtained in absence of it [see a) - c) in figure 3.14]. In other words, the interference can be controlled only by the parameter  $\phi$  which defines  $\gamma$ , in an analogue way to a typical double-slit scheme with  $c_{\uparrow} = c_{\downarrow}$ .

### 3.2.3.2 Interaction time: $|g|^2 t / \Delta = 3\pi/4$

If we consider a lower interaction time, such as  $|g|^2 t / \Delta = 3\pi/4$ , the phase-shifts produced by the atomic states are different. In the state  $|b\rangle$ , the atom produces in the field a counterclockwise phase-shift equal to  $3\pi/4$ , which can not be detected completely by performing an  $X$  or  $Y$  quadrature measurement due to the overlap between the initial and final phases (figure 3.12). However, some possible results of the quadrature measurements can reveal path-information and thus partial interference is obtained. On the other hand, the state  $|a\rangle$  produces the same phase-

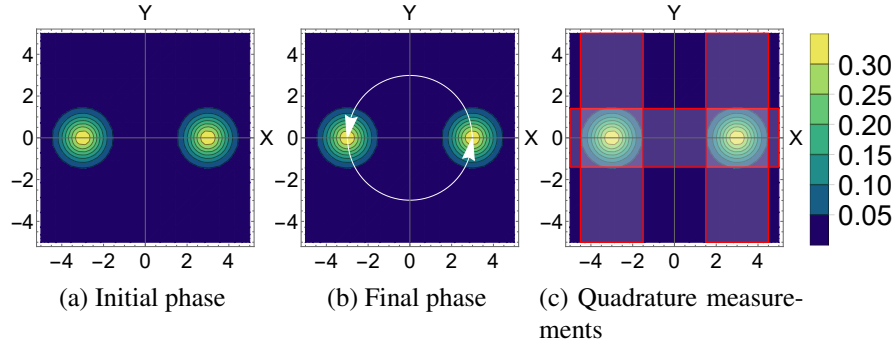


Figure 3.11: A phase-shift  $\pi$  just interchanges clockwise or counterclockwise the position of the distributions of the initial phase of the cat state, if the internal atomic state corresponds to  $|a\rangle$  or  $|b\rangle$  [see (b)], respectively. Therefore, it is not possible to obtain path-information if an  $X$  or  $Y$  quadrature measurement is performed [see (c)].

shift in the field but clockwise. In this case, both quadrature measurements can not distinguish completely the initial phase from the final one. However, no interference is obtained since total path information is stored in the internal state of the atom. Therefore, fringe visibility can be controlled by varying the degree of concurrence in the scheme through the parameter  $\phi$  [see d) - f) in figure 3.14].

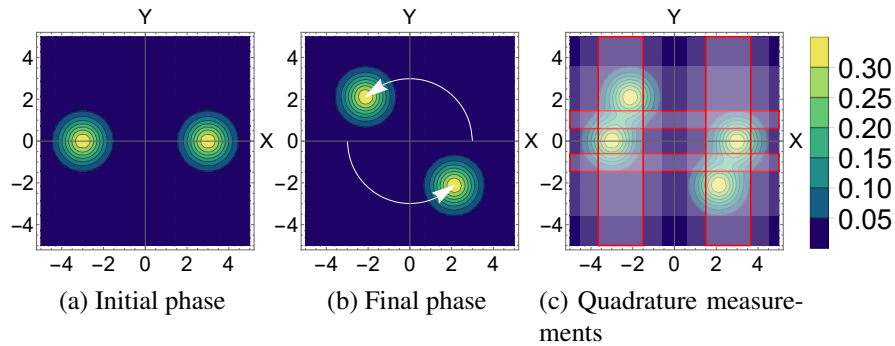


Figure 3.12: A phase-shift equal to  $3\pi/4$  allows to differentiate the initial phase from the final one for certain results of the quadrature measurements. Therefore, partial path-information can be obtained with an  $X$  or  $Y$  quadrature measurement [see (c)].

### 3.2.3.3 Interaction time: $|g|^2t/\Delta = \pi/2$

We consider a third case where  $|g|^2t/\Delta = \pi/2$ , in which the initial and final phases of the cat state can be almost completely differentiated (figure 3.13). For this interaction time the final phases produced by the states  $|b\rangle$  and  $|a\rangle$  are the same but with shifts in opposite directions. In this case, the fringe visibility is almost null for the amplitude  $\alpha' = 3$ , but it can still be slightly controlled by the atomic parameter  $\phi$  [see g) - i) in figure 3.14]. As a consequence, for most results path-information can be extracted when an  $X$  or  $Y$  quadrature measurement is performed.

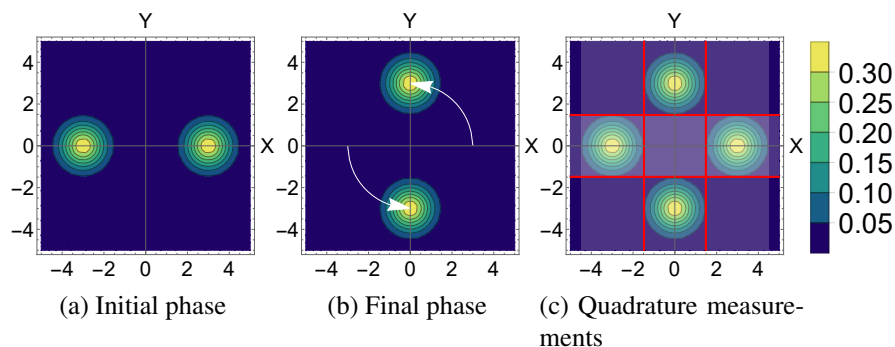


Figure 3.13: A phase-shift equal to  $\pi/2$  allows a better phase differentiation. In this case, path-information can be obtained for most results of an  $X$  or  $Y$  quadrature measurement. Red lines in (c) represent the possible results for which these measurements become ambiguous.

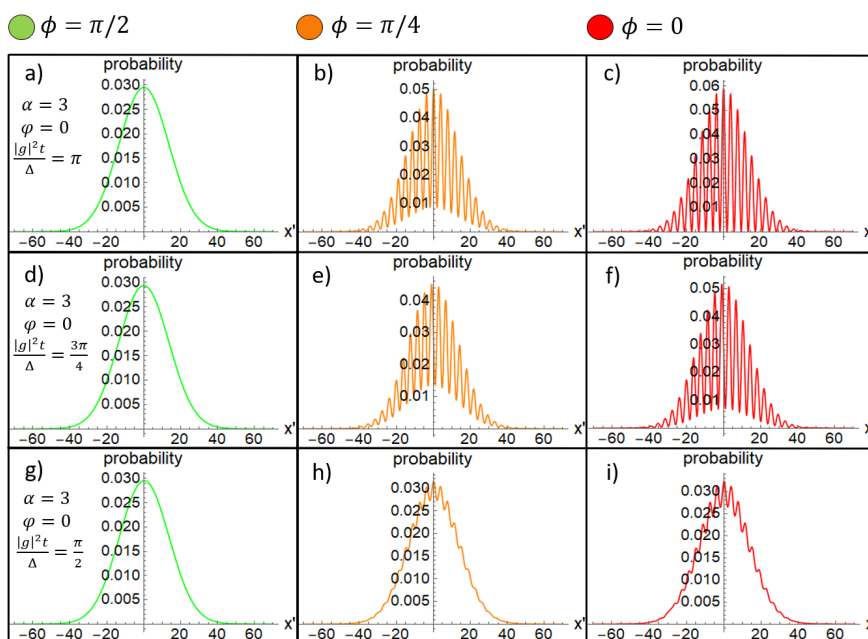


Figure 3.14: Atomic probability distribution obtained for an  $X$  quadrature measurement considering different interaction times between an atom and a cat state with  $\alpha' = 3$  and  $\varphi = 0$ . The atomic parameter  $\phi$  is varied horizontally and the interaction time vertically.

### 3.2.4 Thermal state

Finally, we present a brief analysis of the possible controlling parameters of the wave-particle duality in the thermal states. In this case, the only option is to vary the average photon number [see eq. (3.12)]. This variation just causes a change in the width of the distribution in the plane  $XY$ , whose center matches with the coordinates origin (figure 3.15). Therefore, the phase of the field stays in the same position against possible phase-shifts which could appear in the evolution operator that describes the atom-field interaction. As a consequence, we can not obtain path-information by performing a quadrature measurement after interaction, since the initial phase

remains unaffected.

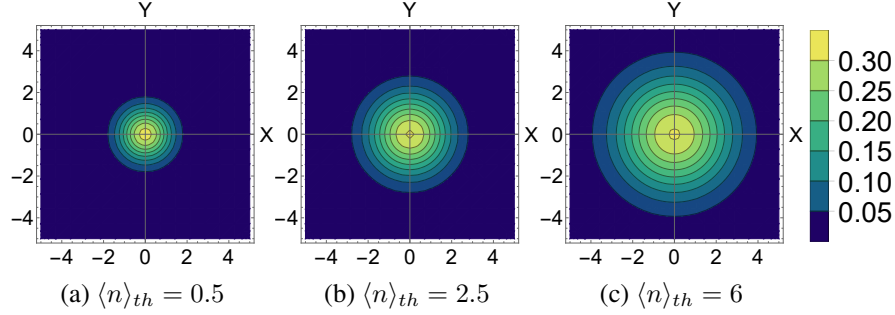


Figure 3.15: For different values of  $\langle n \rangle_{th}$  the phase of the thermal state remains in the center of the  $XY$  plane. Therefore, the possible phase-shifts in the evolution operator can not be detected after the interaction.

Nevertheless, the average photon number can be used as a controlling parameter of the wave-particle duality if we consider, for instance, a displaced squeezed thermal state given by [49]

$$\rho = D(\alpha)S(\xi)\rho_{thermal}S^\dagger(\xi)D^\dagger(\alpha). \quad (3.24)$$

In this case, and considering the results shown in the sections 3.A and 3.B, the average photon number  $\langle n \rangle_{th}$  can be modified in order to widen the distributions in the  $XY$  plane. This, in addition to the displace and squeeze parameters, could cause a larger or smaller overlap between the initial and final phases for a specific quadrature measurement, especially in cases in which both phases have close positions.

# Chapter 4

## Wave-particle duality controlled by a classical radiation

In this chapter, we study the effects of a classical parameter in the control of the wave-particle duality. A double cavity with a quantum mechanical and a classical field is located immediately behind of a double-slit in order to analyse the wave-particle duality. Both fields have common nodes and antinodes through which a three-level atom passes after crossing the double-slit. The atom-field interaction is maximum when the atom crosses a common antinode and path-information can be recorded on the phase of the quantum field. On other hand, if the atom crosses a common node, the interaction is null and no path-information is stored. A quadrature measurement on the quantum field can reveal the path followed by the atom, depending on its initial amplitude  $\alpha$  and the classical amplitude  $\varepsilon$ . We show that the classical radiation acts like a focusing element of the interference and diffraction patterns and how it alters the visibility and distinguishability. Furthermore, in this double-slit scheme also the two possible paths are correlated with the internal atomic states, which allows us to study the relationship between concurrence and wave-particle duality considering different cases.

### 4.1 Model

We consider a three-level atom crossing a double cavity with quantum and classical fields (figure 4.3). The fields have wave numbers  $k = 2\pi/\lambda_{\text{QF}} = 3k'$  and  $k' = 2\pi/\lambda_{\text{CF}}$  respectively. A double-slit is located immediately before the fields, with the top slit in front of a common antinode and the bottom slit in front of a common node. The separation distance between slits is  $0.75\lambda_{\text{QF}} = 0.25\lambda_{\text{CF}}$ .

Previous to the double slit, the spatial atomic state is realized by an atomic beam splitter (ABS) [22, 24] and an atomic mirror (AM) [5, 43], and the internal atomic state in the top path is realized by a Ramsey field (RF) [54] (figure 4.1). The reflection and transmission coefficients of the ABS are  $c_{\uparrow}$  and  $c_{\downarrow}$ , satisfying  $|c_{\uparrow}|^2 + |c_{\downarrow}|^2 = 1$ . If the atom is transmitted, it flies along the bottom path and crosses the slit at the node of the standing waves in the position  $x = 0.75\lambda_{\text{QF}}$ . On other hand, if the atom is reflected, it goes through the top slit using a AM and then a RF. The task of the RF is to prepare a superposition of the ground state  $|c\rangle$  and the intermediate state

$|b\rangle$ . Here the probability coefficients of exciting the state  $|b\rangle$  and remaining in the state  $|c\rangle$  are  $\sin^2 \phi$  and  $\cos^2 \phi$ , respectively. In this case, the atom crosses the top slit and passes through the common antinode of the fields in the position  $x = 0$ . Therefore, the top path is correlated with the internal atomic state  $|\Phi_\uparrow\rangle = \cos \phi |c\rangle + \sin \phi |b\rangle$ , while the bottom path is correlated with the state  $|\Phi_\downarrow\rangle = |c\rangle$ .

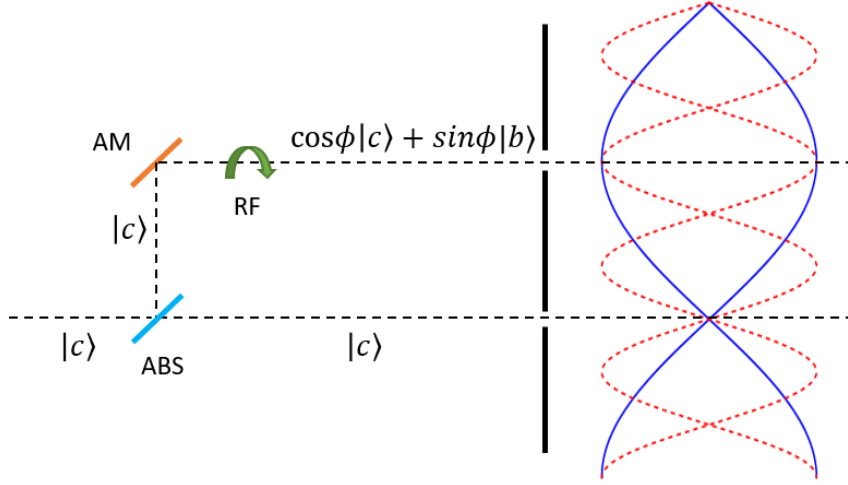


Figure 4.1: Scheme of the possible paths followed by the atom. ABS: Atomic Beam Splitter, AM: Atomic Mirror, RF: Ramsey Field. The atom is either reflected or transmitted by the ABS by taking the upper or lower path, respectively. Finally, the atom crosses the double-slit and both, quantum (red) and classical (blue) fields.

### 4.1.1 Initial state

Initially the atom is in the ground state  $|c\rangle$ . After passing through the ABS and considering the effect of the AM and the RF, the atomic state can be described as

$$\begin{aligned} |\psi(0)\rangle_{\text{atom}} &= c_\uparrow |P_\uparrow\rangle \otimes |\Phi_\uparrow\rangle + c_\downarrow |P_\downarrow\rangle \otimes |\Phi_\downarrow\rangle \\ &= c_\uparrow |P_\uparrow\rangle \otimes [\cos \phi |c\rangle + \sin \phi |b\rangle] + c_\downarrow |P_\downarrow\rangle \otimes |c\rangle, \end{aligned} \quad (4.1)$$

where the states  $|P_\uparrow\rangle$  and  $|P_\downarrow\rangle$  represent the top and bottom path of the scheme, respectively.

Immediately to the right of the double slit, a double cavity with both, classical and quantum fields is located. The quantum field before the interaction is a coherent state with amplitude  $\alpha = \sqrt{8}$  (figure 4.2),

$$|\psi(0)\rangle_{\text{field}} = |\alpha\rangle = e^{-\frac{|\alpha|^2}{2}} \sum_{m=0}^{\infty} \frac{\alpha^m}{\sqrt{m!}} |m\rangle = \sum_{m=0}^{\infty} c_m |m\rangle, \quad (4.2)$$

and the total initial system is given as

$$\begin{aligned} |\psi(0)\rangle_{\text{system}} &= |\psi(0)\rangle_{\text{atom}} \otimes |\psi(0)\rangle_{\text{field}} \\ &= \left( c_\uparrow |P_\uparrow\rangle \otimes [\cos \phi |c\rangle + \sin \phi |b\rangle] + c_\downarrow |P_\downarrow\rangle \otimes |c\rangle \right) \otimes |\alpha\rangle. \end{aligned} \quad (4.3)$$

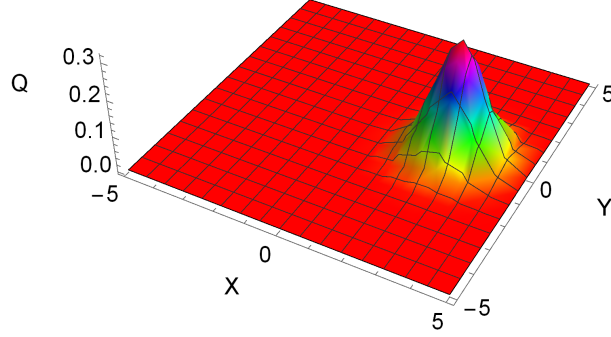


Figure 4.2: Initial phase of the quantum field  $|\alpha\rangle$  for an amplitude  $\alpha = \sqrt{8}$ , where  $X$  and  $Y$  correspond to the amplitude and phase quadrature of the field, respectively.

### 4.1.2 Time evolution of the system

After the interaction the total initial system will evolve to

$$|\psi(t)\rangle_{\text{system}} = \hat{U}|\psi(0)\rangle_{\text{system}} = e^{-\frac{i\hat{V}t}{\hbar}}|\psi(0)\rangle_{\text{system}}, \quad (4.4)$$

where  $\hat{V}$  is the Hamiltonian in the interaction framework considering a rotating wave approximation,

$$\begin{aligned} \hat{V} = & \hbar g_1 (\hat{a} e^{i\Delta t} |a\rangle \langle c| + \hat{a}^\dagger e^{-i\Delta t} |c\rangle \langle a|) \\ & + \hbar g_2 (\varepsilon e^{i\Delta t} |a\rangle \langle b| + \varepsilon^* e^{-i\Delta t} |b\rangle \langle a|). \end{aligned} \quad (4.5)$$

Here the quantum field  $\hat{a}$  couples the  $|a\rangle - |c\rangle$  transition, while the classical field  $\varepsilon$  couples the  $|a\rangle - |b\rangle$  transition with coupling constant  $g_1 = g \cos(kx)$  and  $g_2 = g' \cos(k'x)$  respectively, where  $k' = k/3$ . For both fields, the detuning  $\Delta$  is the same and it is required to be large in order to avoid photon emission and therefore, an effect on the cavity field (figure 4.3). The elements

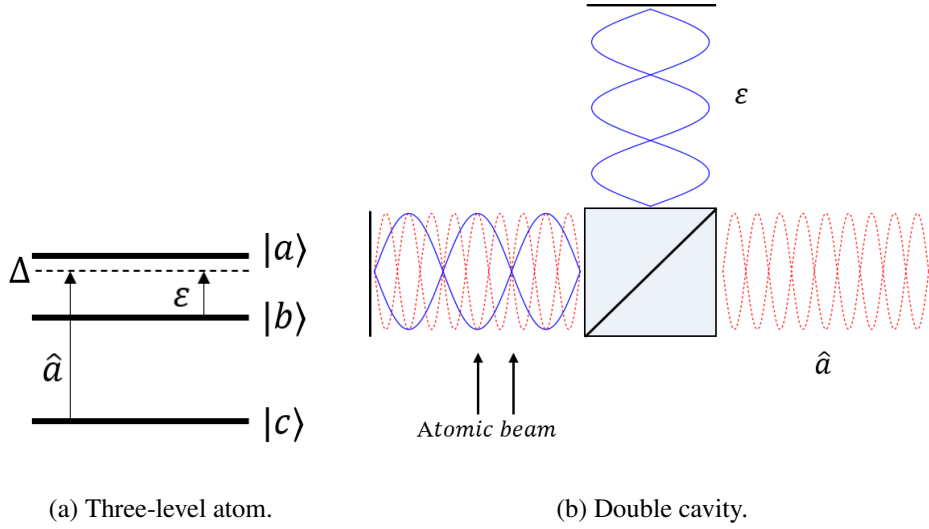


Figure 4.3: A three-level atom crosses the double cavity with a quantum (red) and a classical (blue) field.

of the evolution operator for this system are given by [51]

$$\begin{aligned}
 \bullet U_{aa} &= e^{i\Delta t/2} \left( R - \frac{i\Delta}{2} S \right) & \bullet U_{ab} &= -ig_2 \varepsilon e^{i\Delta t/2} S \\
 \bullet U_{ac} &= -ig_1 e^{i\Delta t/2} S \hat{a} & \bullet U_{ba} &= -ig_2 \varepsilon^* e^{-i\Delta t/2} S \\
 \bullet U_{bb} &= 1 + \frac{g_2^2 |\varepsilon|^2 [e^{-i\Delta t/2} (R + \frac{i\Delta}{2} S) - 1]}{\Lambda} \\
 \bullet U_{bc} &= g_1 g_2 \varepsilon^* \frac{[e^{-i\Delta t/2} (R + \frac{i\Delta}{2} S) - 1] \hat{a}}{\Lambda} \\
 \bullet U_{ca} &= -ig_1 \hat{a}^\dagger e^{-i\Delta t/2} S \\
 \bullet U_{cb} &= g_1 g_2 \varepsilon \hat{a}^\dagger \frac{[e^{-i\Delta t/2} (R + \frac{i\Delta}{2} S) - 1]}{\Lambda} \\
 \bullet U_{cc} &= 1 + \frac{g_1^2 \hat{a}^\dagger \hat{a} [e^{-i\Delta t/2} (\bar{R} + \frac{i\Delta}{2} \bar{S}) - 1]}{\bar{\Lambda}}
 \end{aligned} \tag{4.6}$$

where

$$\begin{aligned}
 \Lambda &\equiv g_2^2 |\varepsilon|^2 + g_1^2 \hat{a} \hat{a}^\dagger, & \bar{\Lambda} &\equiv g_2^2 |\varepsilon|^2 + g_1^2 \hat{a}^\dagger \hat{a}, & S &\equiv \frac{\sin \sqrt{\mu} t}{\sqrt{\mu}}, \\
 \bar{S} &\equiv \frac{\sin \sqrt{\bar{\mu}} t}{\sqrt{\bar{\mu}}}, & R &\equiv \cos \sqrt{\mu} t, & \bar{R} &\equiv \cos \sqrt{\bar{\mu}} t, \\
 \mu &\equiv g_2^2 |\varepsilon|^2 + g_1^2 \hat{a} \hat{a}^\dagger + \Delta^2/4, & \bar{\mu} &\equiv g_2^2 |\varepsilon|^2 + g_1^2 \hat{a}^\dagger \hat{a} + \Delta^2/4.
 \end{aligned} \tag{4.7}$$

For arbitrary paths, the state of the system after a time of interaction  $t$  can be written as

$$\begin{aligned}
|\psi(t)\rangle &= c_{\uparrow} \cos \phi |P_{\uparrow}\rangle \otimes \hat{U}|c\rangle \otimes |\alpha\rangle + c_{\uparrow} \sin \phi |P_{\uparrow}\rangle \otimes \hat{U}|b\rangle \otimes |\alpha\rangle \\
&+ c_{\downarrow} |P_{\downarrow}\rangle \otimes \hat{U}|c\rangle \otimes |\alpha\rangle \\
&= c_{\uparrow} \cos \phi |P_{\uparrow}\rangle \otimes [U_{bc}|b\rangle + U_{cc}|c\rangle] \otimes |\alpha\rangle \\
&+ c_{\uparrow} \sin \phi |P_{\uparrow}\rangle \otimes [U_{bb}|b\rangle + U_{cb}|c\rangle] \otimes |\alpha\rangle \\
&+ c_{\downarrow} |P_{\downarrow}\rangle \otimes [U_{bc}|b\rangle + U_{cc}|c\rangle] \otimes |\alpha\rangle \\
&= c_{\uparrow} \cos \phi |P_{\uparrow}\rangle \otimes \left[ \sum \beta_m^c |m-1\rangle |b\rangle + \sum \alpha_m^c |m\rangle |c\rangle \right] \\
&+ c_{\uparrow} \sin \phi |P_{\uparrow}\rangle \otimes \left[ \sum \alpha_m^b |m\rangle |b\rangle + \sum \beta_m^b |m+1\rangle |c\rangle \right] \\
&+ c_{\downarrow} |P_{\downarrow}\rangle \otimes \left[ \sum \beta_m^c |m-1\rangle |b\rangle + \sum \alpha_m^c |m\rangle |c\rangle \right],
\end{aligned} \tag{4.8}$$

where the coefficients  $\alpha_m^{b,c}$  and  $\beta_m^{b,c}$  depend on the internal state of atom (see appendix in section 4.3).

### 4.1.3 Quadrature measurement

In this model the which-path information depends on the phase-shift of the quantum field as a consequence of the atom's position during the interaction time  $t$ . As mentioned before, the maximum atom-field interaction is accomplished when the atom takes the top path and crosses the common antinode of both fields. In that case, we must consider the two possible internal states of the atom,  $|b\rangle$  and  $|c\rangle$ , and the effect of these on the quantum field [62]. On other hand, if the atom passes through the bottom slit and then crosses the common node, no interaction occurs, and the initial phase of the field remains the same (see 4.23 in Appendix 4.3). Therefore, considering the phase-shift caused either by the ground or intermediate atomic state in the top path, a quadrature measurement could reveal the path followed by the atom.

If the atom crosses the common antinode ( $c_{\uparrow} = 1$ ) in the state  $|b\rangle$  ( $\phi = \pi/2$ ) or  $|c\rangle$  ( $\phi = 0$ ), the final state of the total system after interaction corresponds to a superposition of the internal states  $|b\rangle$  and  $|c\rangle$  given respectively by

$$|\psi(t)\rangle_{\text{system}}^b = |P_{\uparrow}\rangle \otimes \left[ \sum_m \alpha_m^b |m\rangle |b\rangle + \sum_m \beta_m^b |m+1\rangle |c\rangle \right], \tag{4.9}$$

and

$$|\psi(t)\rangle_{\text{system}}^c = |P_{\uparrow}\rangle \otimes \left[ \sum_m \alpha_m^c |m\rangle |c\rangle + \sum_m \beta_m^c |m-1\rangle |b\rangle \right]. \tag{4.10}$$

Therefore, considering the effect of both, quantum and classical fields on the internal atomic state, the evolution of the total system can be understood as a Raman diffraction process in which the internal atomic state is changed, or a Bragg diffraction process where the internal state of the atom remains unaffected [2, 27]. These processes can be controlled by the amplitude of the classical field, since that for small values of  $\varepsilon$  the coefficients  $\beta_m^{b,c}$  decrease and it is more

probable that the atom remains in its initial state, while as  $\varepsilon$  increases, the transition from  $|b\rangle$  to  $|c\rangle$  or vice versa becomes more probable. For simplicity, we first consider only the quantum field in order to analyse the effects of the atomic state on it. For the specific values of the parameters  $\varepsilon = 0$ ,  $\alpha = \sqrt{8}$ ,  $g = g'$  and  $|g|^2 t / \Delta = \pi$ , equations (4.9) and (4.10) can be written as

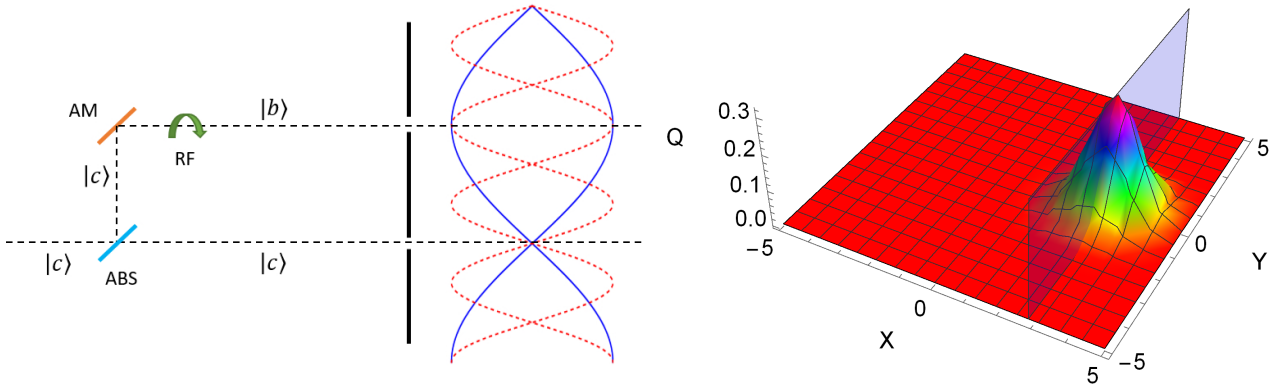
$$\begin{aligned} |\psi(t)\rangle_{\text{system}}^b &= |P_{\uparrow}\rangle \otimes \left[ \sum_m e^{-\frac{|\alpha|^2}{2}} \frac{\alpha^m}{\sqrt{m!}} |m\rangle |b\rangle \right] \\ &= |P_{\uparrow}\rangle \otimes |\alpha\rangle \otimes |b\rangle, \end{aligned} \quad (4.11)$$

and

$$\begin{aligned} |\psi(t)\rangle_{\text{system}}^c &= |P_{\uparrow}\rangle \otimes \left[ \sum_m e^{i\pi \cos^2(kx)m} e^{-\frac{|\alpha|^2}{2}} \frac{\alpha^m}{\sqrt{m!}} |m\rangle |c\rangle \right] \\ &= |P_{\uparrow}\rangle \otimes |e^{i\eta(x)}\alpha\rangle \otimes |c\rangle, \end{aligned} \quad (4.12)$$

respectively, with  $\eta(x) = \pi \cos^2(kx)$ .

Therefore, when the atom crosses the antinode of the quantum field in the intermediate state  $|b\rangle$  [figure 4.4a], there is no phase-shift [figure 4.4b] and no quadrature measurement can reveal which-path information. This is because the same phase can be obtained if the atom takes the bottom path (initial phase unaffected). In contrast, when the atom crosses the antinode in the

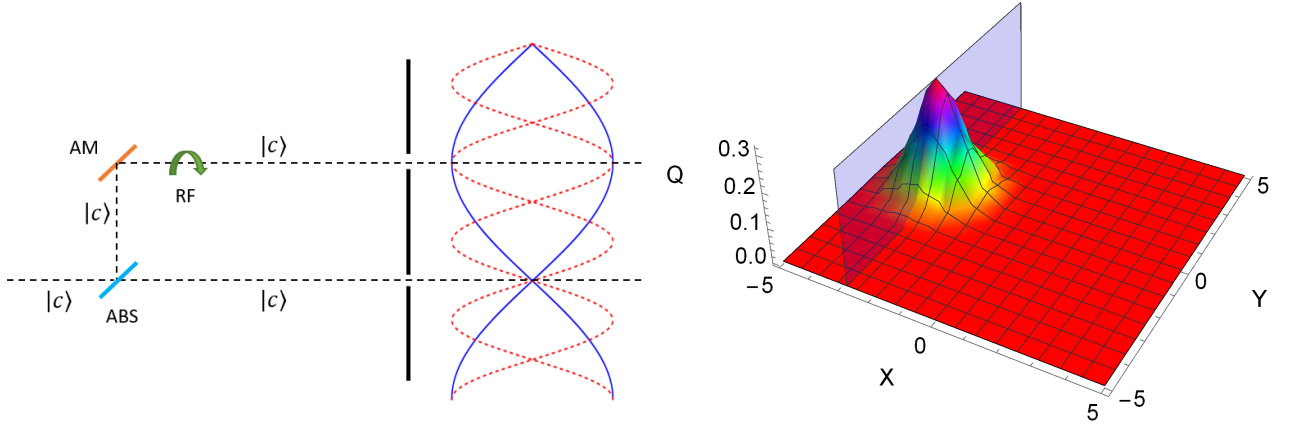


(a) Setup corresponding to the case  $\phi = \pi/2$ , in which the internal atomic state in the upper path is  $|b\rangle$ .

(b) Phase evolution after atom-field interaction for  $\phi = \pi/2$ . The initial phase remains unaffected. The blue plane shows the most probable result ( $\chi_{\theta=0} = +\alpha$ ) if a  $X$  quadrature measurement is performed.

Figure 4.4: If the internal atomic state in the top path is  $|b\rangle$ , there is no phase-shift in the quantum field for  $\alpha = \sqrt{8}$  and  $\varepsilon = 0$ . Therefore, no path-information is record on the field. However, the own internal atomic states in the top and bottom path can give information about which slit the atom passed through.

ground state  $|c\rangle$  [figure 4.5a], the phase increases from 0 to  $\pi$  [figure 4.5b]. In that case, the internal atomic state does not reveal path-information by itself. However, the path-information



(a) Setup corresponding to the case  $\phi = 0$ . In this case the internal atomic state in the upper path is  $|c\rangle$  and the interaction with the field is maximum. (b) Phase evolution after atom-field interaction for  $\phi = 0$ . The initial phase changes from 0 to  $\pi$ .

Figure 4.5: If the internal atomic state in the top path is  $|c\rangle$ , it produces a phase-shift of  $\pi$  in the quantum field, which reveals path-information. We consider  $\alpha = \sqrt{8}$  and  $\varepsilon = 0$ . In this case the most probable result for an  $X$  quadrature measurement is  $\chi_{\theta=0} = -\alpha$ .

is stored in the phase of the quantum field and can be extracted through a  $X$  quadrature measurement.

In general, if the quadrature

$$X_{\theta} = \frac{ae^{-i\theta} + a^{\dagger}e^{i\theta}}{2} \quad (4.13)$$

is measured with an eigenvalue  $\chi_{\theta}$ , the corresponding eigenstate  $|\chi_{\theta}\rangle$  is an infinitely squeezed state given by [51, 62]

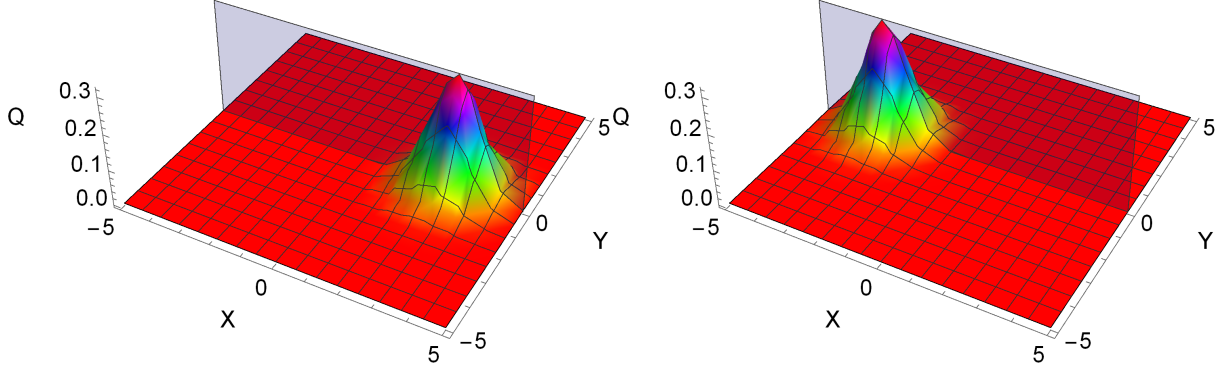
$$|\chi_{\theta}\rangle = \frac{1}{\sqrt[4]{2\pi}} \exp\left[-\frac{1}{2}(a^{\dagger}e^{i\theta} - \chi_{\theta})^2 + \frac{1}{4}\chi_{\theta}^2\right] |0\rangle = \sum_n b_n |n\rangle, \quad (4.14)$$

where

$$b_n = \frac{N}{\sqrt{n!}} \left(\frac{1}{2}e^{i\theta}\right)^{n/2} H_n(z), \quad (4.15)$$

with  $N$  being a normalization constant. The function  $H_n(z)$  corresponds to the Hermite polynomials with  $z = (\alpha e^{-i\theta} + \alpha^* e^{i\theta})/2$ .

Since we consider  $|g|^2 t/\Delta = \pi$ , a  $X_{\theta=0} = X$  quadrature measurement with values  $\chi_{\theta=0} = \pm\alpha$  determines the phase of the field and then we can know whether the atom passed through either the node or antinode (considering  $\phi = 0$ ). On other hand, if a  $X_{\theta=\pi/2} = Y$  quadrature measurement is performed, and the most probable result is obtained ( $\chi_{\theta=\pi/2} = 0$ ), no path-information is obtained and interference appears on the screen, since that from the most probable result no path information is inferred (figure 4.6).



(a) If the phase remains unaffected, the most probable result for a  $Y$  quadrature measurement is  $\chi_{\theta=\pi/2} = 0$ . (b) If the phase changes from 0 to  $\pi$ , the result of a quadrature measurement remains the same.

Figure 4.6: A  $Y$  quadrature measurement does not reveal path information, because the most probable result is obtained regardless of quantum field state.

#### 4.1.4 Particle-wave duality and concurrence

In a typical double-slit scheme we can configure several cases in order to study the quantum duality between distinguishability (particle-like) and visibility (wave-like) [17]. Now, if a correlation is established between some intrinsic property of a particle and the possible paths, the wave-particle duality can be modified depending on the degree of entanglement in the system. Recently, it has been experimentally proven the relation among distinguishability ( $D_0$ ), visibility ( $V_0$ ) and concurrence ( $C_0$ ) [53] which can be written as

$$D_0^2 + V_0^2 + C_0^2 = 1, \quad (4.16)$$

with

$$\begin{aligned} D_0 &= ||c_{\uparrow}|^2 - |c_{\downarrow}|^2| \\ V_0 &= 2|c_{\uparrow}c_{\downarrow}\gamma| \\ C_0 &= 2|c_{\uparrow}c_{\downarrow}|\sqrt{1 - |\gamma|^2}, \end{aligned} \quad (4.17)$$

[25, 31, 32, 68] where  $c_{\uparrow}$  and  $c_{\downarrow}$  are coefficients that define the probabilities for the atom of taking the top or bottom path, while  $\gamma \equiv \langle \Phi_{\uparrow} | \Phi_{\downarrow} \rangle$ , where the normalized states  $|\Phi_{\uparrow, \downarrow}\rangle$  correspond to intrinsic degrees of freedom of the particle, in our case the internal atomic state.

Cases of special interest are shown on the surface of the sphere in the figure 4.7. The point  $C_0 = 1$ , with coefficients  $c_{\uparrow} = c_{\downarrow} = 1/\sqrt{2}$  and  $\gamma = 0$ , represents a special scenario in which, based on the definitions of  $D_0$  and  $V_0$ , visibility and distinguishability are equal to zero. So, what would we expect to observe on the screen after the double slit?

In the next section we analyze different cases considering our scheme, in which the which-path information can be stored in the phase-shift of the quantum field, but also it can be controlled through the coefficients  $c_{\uparrow}$  and  $c_{\downarrow}$ , and we show the different patterns that are obtained

in each case shown on the sphere. Finally, we show how the classic field can change the initial visibility and which-path information as  $\varepsilon$  increases from 0 to higher values and how the corresponding patterns are modified.

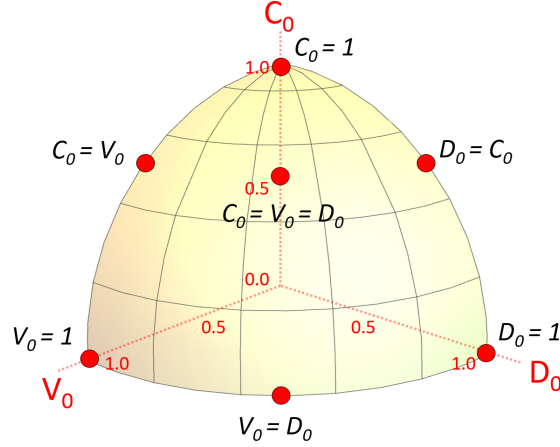


Figure 4.7: Unit sphere  $D_0^2 + V_0^2 + C_0^2 = 1$ . The extreme cases  $V_0 = 1$ ,  $D_0 = 1$ ,  $C_0 = 1$  and intermediate ones are shown on the surface by red dots.

## 4.2 Numerical results

In the previous sections we explained how the atom can modify the quantum field and how the path-information can be extracted by performing a quadrature measurement. The localization of the atom results in loss of interference and the total knowledge of the path-information. In this section we assume that once the atom leaves the cavity, it freely evolves during a time  $t'$  (in units of  $2m/\hbar k'^2$ ) to state

$$\begin{aligned} \rho_{\text{atom}}(t') &= \hat{U} \rho_{\text{atom}}(t) \hat{U}^\dagger \\ &= e^{-\frac{i\hat{H}t'}{\hbar}} \text{Tr}_{\text{field}} (|\psi(t)\rangle\langle\psi(t)|) e^{\frac{i\hat{H}t'}{\hbar}}, \end{aligned} \quad (4.18)$$

where  $\hat{H} = \frac{\hat{p}^2}{2m}$  is the free particle Hamiltonian and  $|\psi(t)\rangle$  is given by (4.8). Thus, we can obtain the atomic distribution for a specific flight time  $t'$  and observe how the initial distinguishability and visibility are tuned according to the amplitude of the quantum and classical fields. We consider that the initial atomic distribution once the atom emerges from the double-slit corresponds to two Gaussian profiles with standard deviation  $\sigma = 0.05\lambda_{\text{CF}}/2\pi$  and centred in the positions  $x = 0$  and  $x = 0.25\lambda_{\text{CF}}$ , respectively. For each studied case, the corresponding pattern on the screen is obtained considering three different stages. First, we consider a typical double-slit scheme where we can manipulate only the parameters  $c_\uparrow$ ,  $c_\downarrow$  and  $\gamma$  to define  $V_0$ ,  $D_0$  and  $C_0$  as the initial visibility, distinguishability and concurrence in absence of both fields. Subsequently, we add the quantum field and obtain the corresponding atomic distributions of each case. Finally, we consider the double slit with both, classical and quantum fields.

### 4.2.1 Stage 1: Atom passing through the double slit (no fields)

This is the simpler stage. Distinguishability, visibility and concurrence depend only on the choice of the coefficients of reflection  $c_{\uparrow}$ , transmission  $c_{\downarrow}$  and  $\gamma$ . For instance, in the case  $V_0 = 1$  the internal atomic state is  $|c\rangle$  in both paths, thus  $\phi = 0$  and  $\gamma = \cos \phi = 1$ , which ensures  $C_0 = 0$ . Furthermore, the coefficients  $c_{\uparrow}$  and  $c_{\downarrow}$  are taken to be same, then  $D_0 = 0$ . Therefore, this corresponds to a case of total interference that is shown in green in the figure 4.8a. The values  $c_{\uparrow} = 1, c_{\downarrow} = 0$  and  $0 \leq \gamma \leq 1$  correspond to other case,  $D_0 = 1$ , which does not show fringes of visibility [figure 4.8c]. Perhaps the most interesting case is  $C_0 = 1$  [figure 4.8e], in which there is no distinguishability nor visibility. In this case, the observed pattern on the screen is similar to the typical diffraction pattern of the case  $D_0 = 1$ . The rest of distributions represent intermediate cases which can be obtained considering the appropriate coefficients.

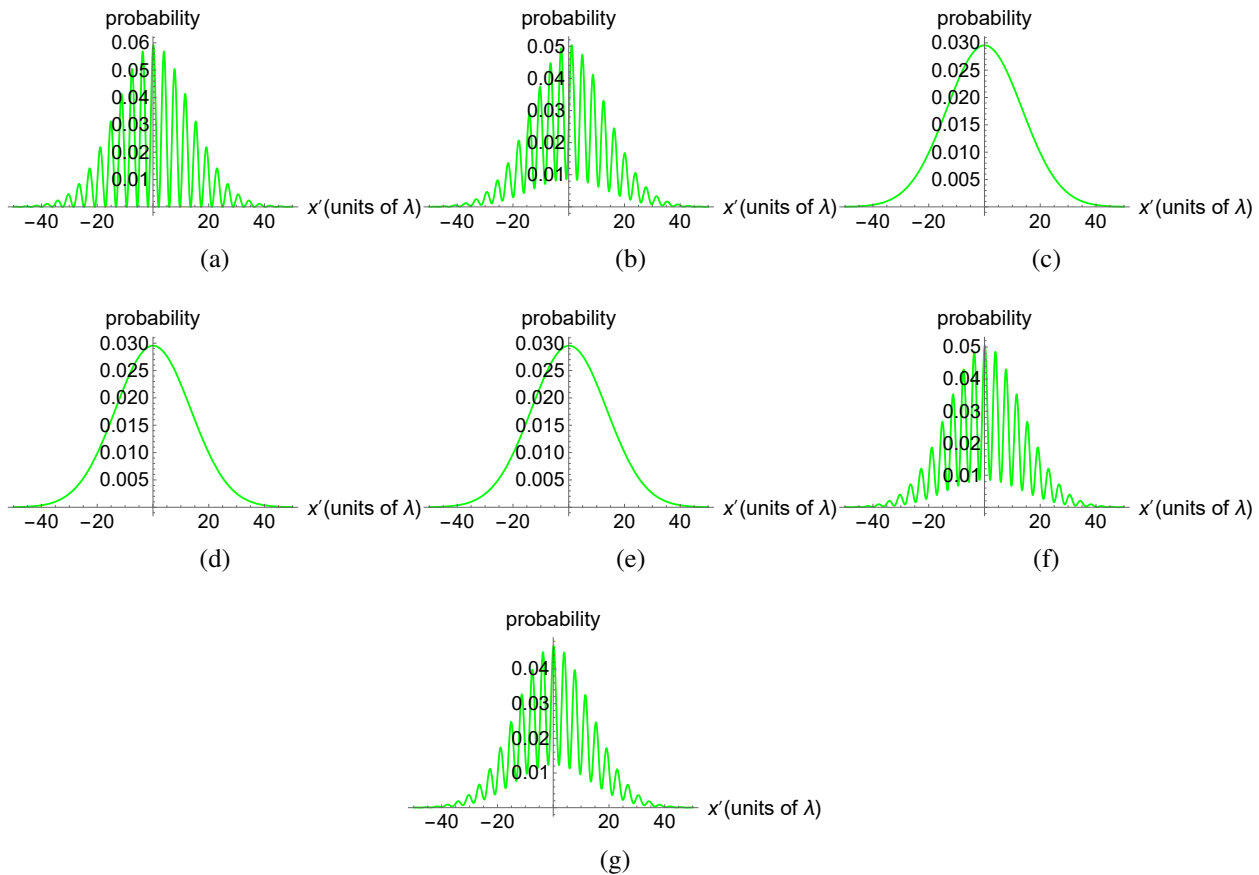


Figure 4.8: *Stage 1*: Atomic probability distribution obtained for each case shown on the sphere  $V_0^2 + D_0^2 + C_0^2 = 1$  for  $t' = 3$ . The distance  $x'$  is expressed in units of  $\lambda = \lambda_{CF}$ . a)  $V_0 = 1$ , b)  $V_0 = D_0$ , c)  $D_0 = 1$ , d)  $D_0 = C_0$ , e)  $C_0 = 1$ , f)  $C_0 = V_0$ , g)  $V_0 = D_0 = C_0$ .

### 4.2.2 Stage 2: Atom passing through the double slit with the quantum field

Here we consider the quantum field with an amplitude  $\alpha = \sqrt{8}$ , located immediately after the double-slit (see figure 4.1). As stated earlier in the Section II.C, the quantum field can store path-information in case the atom crosses the antinode in the internal state  $|c\rangle$ . Otherwise (state  $|b\rangle$  in the upper path, or state  $|c\rangle$  lower path), the phase of the quantum field remains unaffected. Thus, we have three sources of path-information: i) the choice of the coefficients  $c_\uparrow$  and  $c_\downarrow$ , ii) the possible phase-shift of the quantum field, and iii) the internal atomic state of the atom after double-slit.

- i) As in the *stage 1*, if  $c_\uparrow = 1$  and  $c_\downarrow = 0$ , we immediately get path information.
- ii) If we choose  $c_\uparrow = c_\downarrow$  and  $\phi = 0$  ( $\gamma = 1$ ), the internal atomic state in both paths is  $|c\rangle$  and the path-information is recorded in the phase of the field, and can be extracted by measuring the  $X$  quadrature.
- iii) Finally, for  $c_\uparrow = c_\downarrow$  and  $\phi = \pi/2$  ( $\gamma = 0$ ), the top and bottom paths are correlated to the atomic states  $|b\rangle$  and  $|c\rangle$ , respectively. In that case the field does not store path-information. However, path-information related to the atomic states is stored and can be obtained by measuring the internal atomic state once the atom leaves the cavity.

Therefore, in presence of the quantum field we will not observe fringes of interference in any of the cases on the sphere [see blue lines in the figure 4.9a - 4.9g], because each case corresponds either, to one of the situations i), ii), iii), or to some intermediate state. In fact, i), ii) and iii) correspond to the cases in which the coefficients  $c_{\uparrow,\downarrow}$  and  $\gamma$  satisfy  $D_0 = 1$ ,  $V_0 = 1$  and  $C_0 = 1$ , respectively. Nevertheless, fringe visibility can be restored if the path-information is erased. In order to achieve that, the first option is reducing the amplitude of the quantum field, so that the  $X$  quadrature measurement becomes ambiguous and does not reveal path-information. In this way the interference is partially restored [red lines in figure 4.9a, 4.9b, 4.9f, 4.9g]. In other cases, like  $D_0 = 1$  [figure 4.9c],  $D_0 = C_0$  [figure 4.9d] and  $C_0 = 1$  [figure 4.9e], interference cannot be restored.

A second option is performing a  $Y$  quadrature measurement of the field. In this case the path-information is completely erased and interference is restored, since we assume the outcome of our measurement as the most probable result that corresponds to  $\chi_{\theta=\pi/2} = 0$ . The green lines in the figure 4.8a - 4.8g are the distributions we would expect to see on the screen if a  $Y$  quadrature measurement is performed on the quantum field. This is the same result that we would obtain if the quantum field were not present.

### 4.2.3 Stage 3: Atom passing through the double slit with the quantum and classical fields

Finally, we consider the double-slit scheme with both quantum and classic fields. When the classical light is present, it affects the final phase of the quantum field after the interaction, because the terms whose phases depend on  $\varepsilon$  appear in the evolution operator. As a consequence, interference and path-information are altered. As in the previous stage, the phase-shift produced by  $\varepsilon$  also depends on the internal atomic state  $|c\rangle$  or  $|b\rangle$  present in the top path.

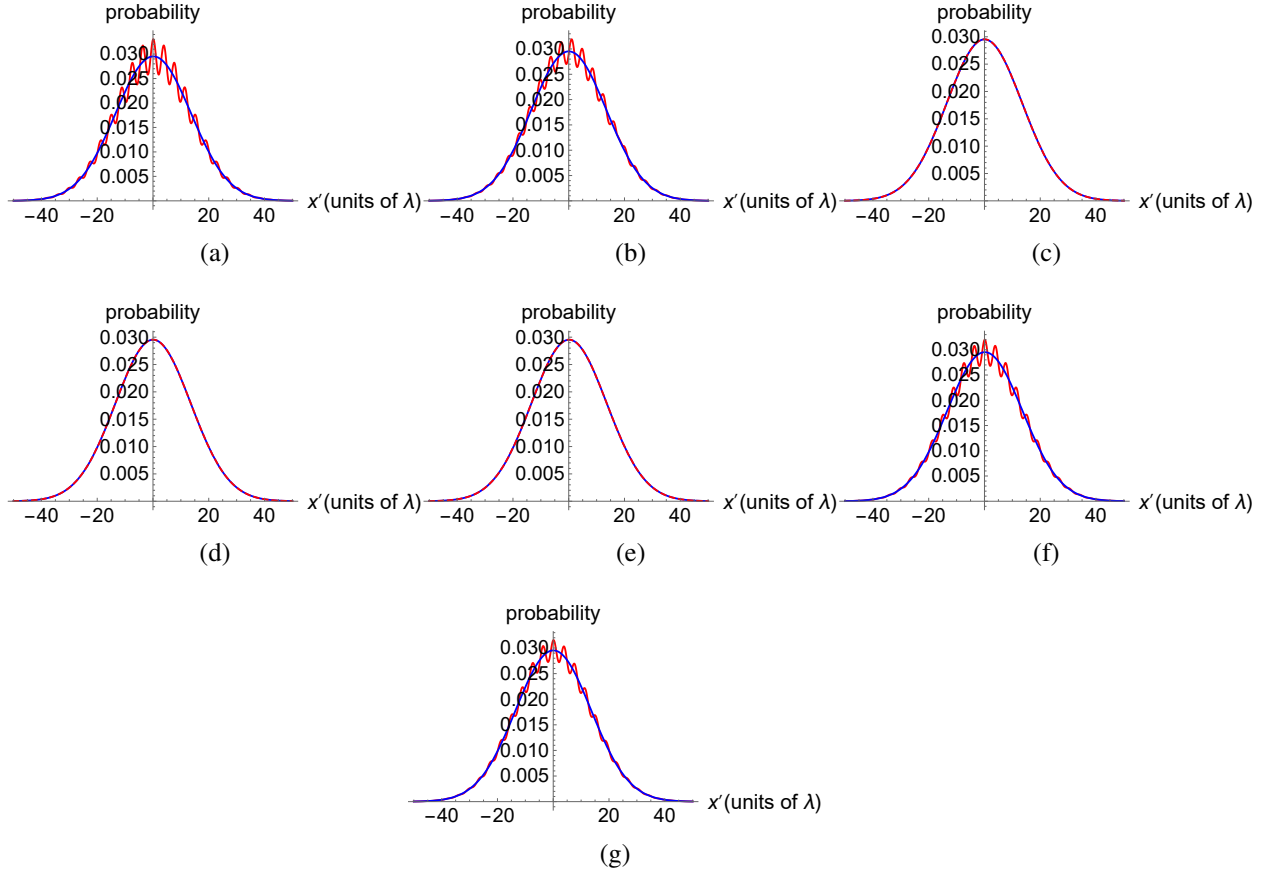


Figure 4.9: *Stage 2*: Atomic probability distribution obtained for each case shown on the sphere  $V_0^2 + D_0^2 + C_0^2 = 1$  in presence of the quantum field for  $t' = 3$  with  $\alpha = \sqrt{8}$  (blue) and  $\alpha = 1$  (red).  $x'$  is expressed in units of  $\lambda = \lambda_{CF}$ . The choice of the parameters  $c_{\uparrow,\downarrow}$  and  $\gamma$  satisfies: a)  $V_0 = 1$ , b)  $V_0 = D_0$ , c)  $D_0 = 1$ , d)  $D_0 = C_0$ , e)  $C_0 = 1$ , f)  $C_0 = V_0$ , g)  $V_0 = D_0 = C_0$ .

- *The top path and internal state  $|b\rangle$* : When  $\varepsilon = 0$ , we have already seen that the phase of the quantum field does not change and thus we cannot obtain which-path information. However, for different values of  $\varepsilon$ , the phase of the quantum field moves away from its initial value and then we are able to get distinguishability (figure 4.10). Therefore, the higher the value of  $\varepsilon$  the more path-information we get, at the expense of visibility.

- *The top path and internal state  $|c\rangle$* : In this case, starting from  $\varepsilon = 0$ , as we increase the classical field, the  $X$  quadrature measurement becomes ambiguous, decreasing the which-path information and therefore increasing the visibility(figure 4.11).

To show the effect of the classical field on the atomic distributions, we analyse the same cases shown before, considering  $\varepsilon = 3$  and  $\alpha = \sqrt{8}$ . In the figure 4.12 we can see how the visibility fringes are restored (red lines). Thus, there is less available path-information with respect to the *stage 2* (blue lines). If we look again the case  $V_0 = 1$  [figure 4.12a], we see now partial interference because now there is a probability of measuring a phase  $\eta = 0$  and get visibility, or  $\eta = \pi$  and gain path-information. Cases like  $V_0 = D_0$  [figure 4.12b],  $C_0 = V_0$  [figure 4.12f] and

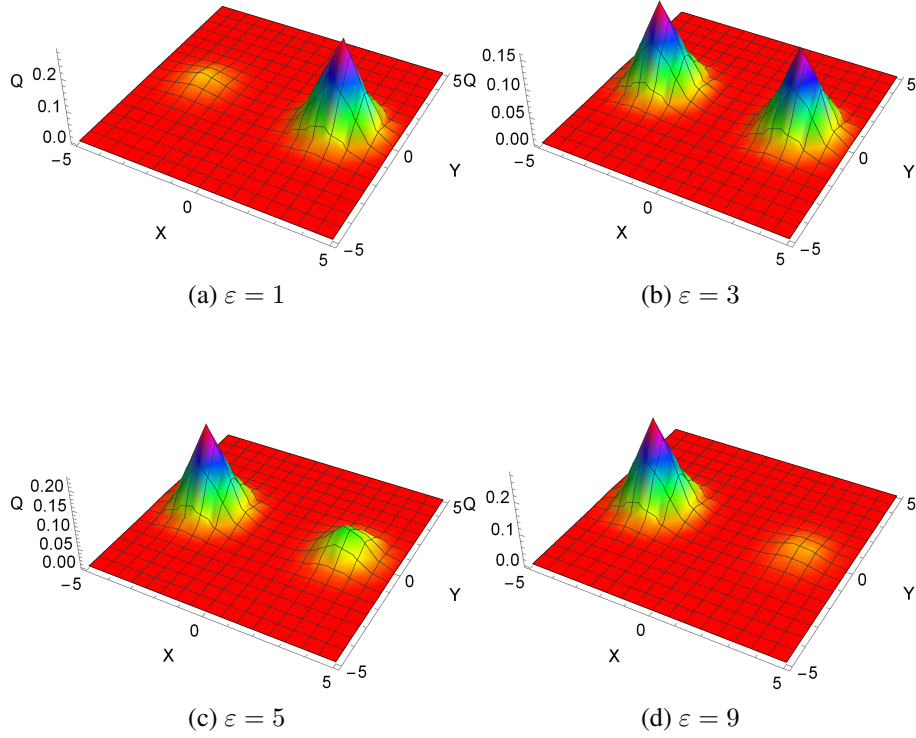


Figure 4.10: Internal atomic state  $|b\rangle$  in the top path: As the value of  $\varepsilon$  rises, the phase of the quantum field begins to differentiate from the initial phase. Thus, now a  $X$  quadrature measurement can reveal path-information.

$D_0 = C_0 = V_0$  [figure 4.12g] also show how the interference can be restored. On other hand, in the cases  $D_0 = 1$  [figure 4.12c],  $D_0 = C_0$  [figure 4.12d] and  $C_0 = 1$  [figure 4.12e] there is no interference, but these show that the atomic distributions evolve faster. This means that the initial Gaussian profiles of the atomic distribution in the position  $x = 0$  and  $x = 0.25\lambda_{CF}$  in  $t' = 0$ , interact with each other earlier as compared to the case  $\varepsilon = 0$ .

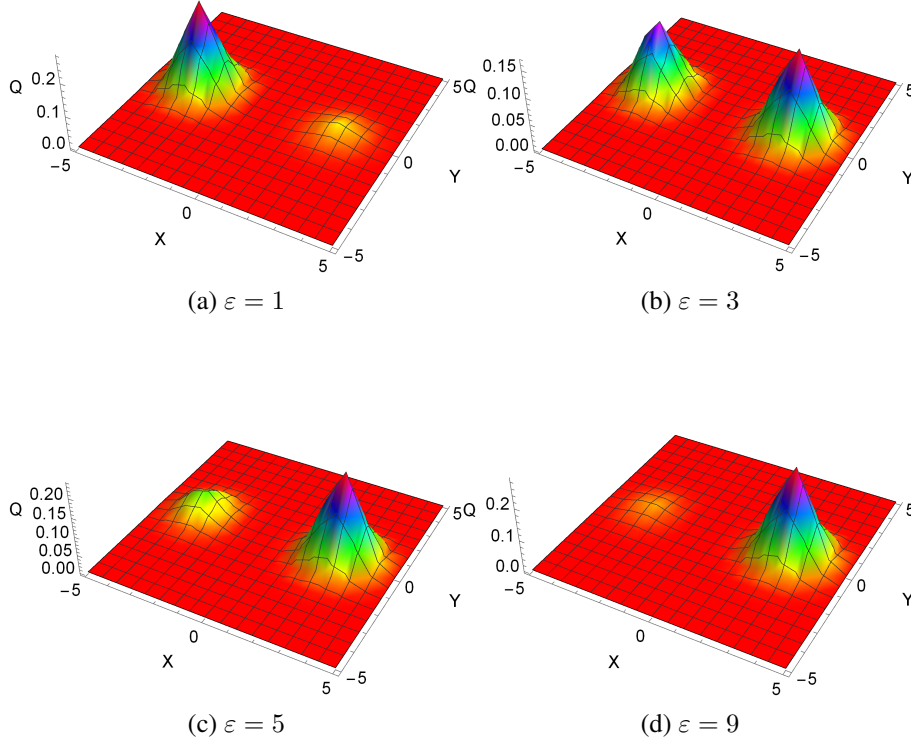


Figure 4.11: Internal atomic state  $|c\rangle$  in the top path: In this case, as  $\varepsilon$  increases, the phase of the quantum field approaches to its initial value. So now, the  $X$  quadrature measurement becomes ambiguous and the path-information decreases.

### 4.3 Effects of the evolution operator on the initial state of the quantum field $|\alpha\rangle$ [ eq. (4.8)].

The elements  $U_{bb}$  (4.19) and  $U_{cb}$  (4.20) represent the evolution of the system when the internal atomic state is  $|b\rangle$ . On other hand, the elements  $U_{cc}$  (4.21) and  $U_{bc}$  (4.22) describe the evolution when the internal state is  $|c\rangle$ . If the atom crosses the lower slit ( $c_{\downarrow} = 1$ ) and then the common node in  $x = 0.25\lambda_{CF} = 0.75\lambda_{QF}$ , no interaction occurs and the quantum field remains the same [see (4.23)].

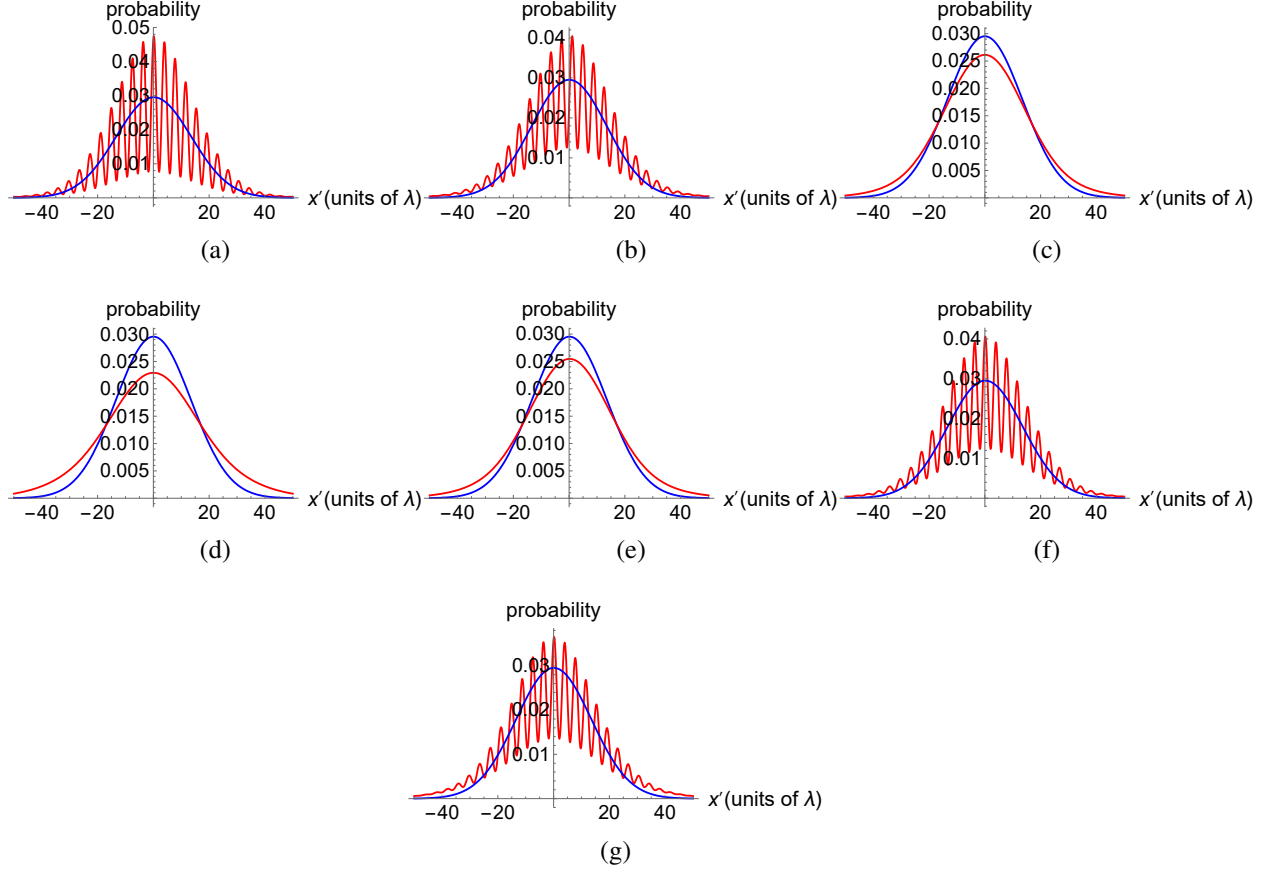


Figure 4.12: *Stage 3*: When  $\varepsilon = 3$ , the effects of the atomic states  $|b\rangle$  and  $|c\rangle$  on the phase of the quantum field are similar [see figure 4.10b and figure 4.11b]. Therefore, an  $X$  quadrature measurement cannot reveal completely path-information and the atomic distributions show partial interference in some cases and a faster evolution in other ones (red lines). Blue lines correspond to the results obtained for  $\varepsilon = 0$  in the *stage 2*. The cases a)  $V_0 = 1$ , b)  $V_0 = D_0$ , c)  $D_0 = 1$ , d)  $D_0 = C_0$ , e)  $C_0 = 1$ , f)  $C_0 = V_0$ , g)  $V_0 = D_0 = C_0$  represent the choice of the parameters used in the *stage 1*. The flight time is taken  $t' = 3$  with  $x'$  in units of  $\lambda = \lambda_{CF}$ .

$$\begin{aligned}
 \bullet U_{bb}|\alpha\rangle &= \left[ 1 + \frac{g_2^2|\varepsilon|^2 \left[ e^{-i\Delta t/2} \left( \cos \sqrt{g_2^2|\varepsilon|^2 + g_1^2 aa^\dagger + \Delta^2/4t} + \frac{i\Delta}{2} \frac{\sin \sqrt{g_2^2|\varepsilon|^2 + g_1^2 aa^\dagger + \Delta^2/4t}}{\sqrt{g_2^2|\varepsilon|^2 + g_1^2 aa^\dagger + \Delta^2/4}} \right) - 1 \right]}{g_2^2|\varepsilon|^2 + g_1^2 aa^\dagger} \right] |\alpha\rangle \\
 &= \sum_m \left[ 1 + \frac{\cos^2(k'x)|\varepsilon|^2 \left[ e^{i(g^2 \cos^2(k'x)|\varepsilon|^2 + g^2 \cos^2(kx)(1+m))t/\Delta} - 1 \right]}{\cos^2(k'x)|\varepsilon|^2 + \cos^2(kx)(1+m)} \right] e^{-\frac{|\alpha|^2}{2}} \frac{\alpha^m}{\sqrt{m!}} |m\rangle \\
 &\equiv \sum_m \alpha_m^b |m\rangle
 \end{aligned}
 \tag{4.19}$$

$$\begin{aligned}
 \bullet U_{cb}|\alpha\rangle &= \left[ g_1 g_2 \varepsilon a^\dagger \frac{[e^{-i\Delta t/2} (\cos \sqrt{g_2^2 |\varepsilon|^2 + g_1^2 a a^\dagger + \Delta^2/4t} + \frac{i\Delta}{2} \frac{\sin \sqrt{g_2^2 |\varepsilon|^2 + g_1^2 a a^\dagger + \Delta^2/4t}}{\sqrt{g_2^2 |\varepsilon|^2 + g_1^2 a a^\dagger + \Delta^2/4}}) - 1]}{g_2^2 |\varepsilon|^2 + g_1^2 a a^\dagger} - 1 \right] |\alpha\rangle \\
 &= \sum_m \left[ \cos(kx) \cos(k'x) \varepsilon \sqrt{m+1} \frac{[e^{i[g^2 \cos^2(k'x)|\varepsilon|^2 + g^2 \cos^2(kx)(1+m)]t/\Delta} - 1]}{\cos^2(k'x)|\varepsilon|^2 + \cos^2(kx)(1+m)} \right] e^{-\frac{|\alpha|^2}{2}} \frac{\alpha^m}{\sqrt{m!}} |m+1\rangle \\
 &\equiv \sum_m \beta_m^b |m+1\rangle
 \end{aligned} \tag{4.20}$$

$$\begin{aligned}
 \bullet U_{cc}|\alpha\rangle &= \left[ 1 + \frac{g_1^2 a^\dagger a [e^{-i\Delta t/2} (\cos \sqrt{g_2^2 |\varepsilon|^2 + g_1^2 a^\dagger a + \Delta^2/4t} + \frac{i\Delta}{2} \frac{\sin \sqrt{g_2^2 |\varepsilon|^2 + g_1^2 a^\dagger a + \Delta^2/4t}}{\sqrt{g_2^2 |\varepsilon|^2 + g_1^2 a^\dagger a + \Delta^2/4}}) - 1]}{g_2^2 |\varepsilon|^2 + g_1^2 a^\dagger a} \right] |\alpha\rangle \\
 &= \sum_m \left[ 1 + \frac{\cos^2(kx) m [e^{i(g^2 \cos^2(k'x)|\varepsilon|^2 + g^2 \cos^2(kx)m)t/\Delta} - 1]}{\cos^2(k'x)|\varepsilon|^2 + \cos^2(kx)m} \right] e^{-\frac{|\alpha|^2}{2}} \frac{\alpha^m}{\sqrt{m!}} |m\rangle \\
 &\equiv \sum_m \alpha_m^c |m\rangle
 \end{aligned} \tag{4.21}$$

$$\begin{aligned}
 \bullet U_{bc}|\alpha\rangle &= \left[ g_1 g_2 \varepsilon^* \frac{[e^{-i\Delta t/2} (\cos \sqrt{g_2^2 |\varepsilon|^2 + g_1^2 a a^\dagger + \Delta^2/4t} + \frac{i\Delta}{2} \frac{\sin \sqrt{g_2^2 |\varepsilon|^2 + g_1^2 a a^\dagger + \Delta^2/4t}}{\sqrt{g_2^2 |\varepsilon|^2 + g_1^2 a a^\dagger + \Delta^2/4}}) - 1]}{g_2^2 |\varepsilon|^2 + g_1^2 a a^\dagger} - 1 \right] a |\alpha\rangle \\
 &= \sum_m \left[ \cos(kx) \cos(k'x) \varepsilon^* \sqrt{m} \frac{[e^{i[g^2 \cos^2(k'x)|\varepsilon|^2 + g^2 \cos^2(kx)m)t/\Delta} - 1]}{\cos^2(k'x)|\varepsilon|^2 + \cos^2(kx)m} \right] e^{-\frac{|\alpha|^2}{2}} \frac{\alpha^m}{\sqrt{m!}} |m-1\rangle \\
 &\equiv \sum_m \beta_m^c |m-1\rangle
 \end{aligned} \tag{4.22}$$

$$\begin{aligned}
 \bullet c_\downarrow |P_\downarrow\rangle &\otimes \left[ \sum_m \beta_m^c |m-1\rangle |b\rangle + \sum_m \alpha_m^c |m\rangle |c\rangle \right] \\
 &= \int \delta(x - \lambda_{CF}/4) dx \left[ \sum_m \beta_m^c |m-1\rangle |b\rangle + \sum_m \alpha_m^c |m\rangle |c\rangle \right] \\
 &= \sum_m \left[ \cos\left(\frac{3\pi}{2}\right) \cos\left(\frac{\pi}{2}\right) \varepsilon^* \sqrt{m} \frac{[e^{i[g^2 \cos^2(\frac{\pi}{2})|\varepsilon|^2 + g^2 \cos^2(\frac{3\pi}{2})m)t/\Delta} - 1]}{\cos^2(\frac{\pi}{2})|\varepsilon|^2 + \cos^2(\frac{3\pi}{2})m} \right] e^{-\frac{|\alpha|^2}{2}} \frac{\alpha^m}{\sqrt{m!}} |m-1\rangle \\
 &+ \sum_m \left[ 1 + \frac{\cos^2(\frac{3\pi}{2}) m [e^{i(g^2 \cos^2(\frac{\pi}{2})|\varepsilon|^2 + g^2 \cos^2(\frac{3\pi}{2})m)t/\Delta} - 1]}{\cos^2(\frac{\pi}{2})|\varepsilon|^2 + \cos^2(\frac{3\pi}{2})m} \right] e^{-\frac{|\alpha|^2}{2}} \frac{\alpha^m}{\sqrt{m!}} |m\rangle \\
 &= \sum_m e^{-\frac{|\alpha|^2}{2}} \frac{\alpha^m}{\sqrt{m!}} |m\rangle \\
 &= |\alpha\rangle
 \end{aligned} \tag{4.23}$$

# Chapter 5

## Partial quantum eraser and delayed choices

Finally, we consider a double-slit scheme located immediately before a cavity with a quantum field in order to discuss some ideas about the delayed choice quantum eraser experiments. A two-level atom crosses the slits and the standing wave leaving path information stored on the quantum phase of the field, which can be extracted or erased by performing an adequate quadrature measurement once the atom leaves the system. Furthermore, we correlate the internal atomic states with the paths of the scheme, which allows us to obtain path information by measuring the internal state of the atom after the atom-field interaction. We consider both, the field and the atom, as path detectors and perform different measurements on them after the atom's position is registered. This allows us to obtain a partial quantum eraser, after which we can decide to recover or destroy the interference completely. Therefore, we propose the use of this kind of schemes in delayed choice experiments.

### 5.1 Description of the model

Our interaction model is similar to the one in Chapter 3 and is represented by the figure 5.1. We again consider that once the atom crosses the slits, it can pass through an antinode (in  $x = 0$ , with maximum atom-field interaction) or a node (in  $x = 0.25\lambda$ , with null interaction) of a standing wave, which in this case, we represent as a quantum field defined by a coherent state  $|\alpha\rangle$  with  $\alpha = |\alpha|e^{i\varphi}$  and wave number  $k = 2\pi/\lambda$ ,  $\lambda$  being the wavelength. Initially, the atom is in the groundstate  $|b\rangle$  and once it takes the upper ( $|P_\uparrow\rangle$ ) or bottom ( $|P_\downarrow\rangle$ ) path, its internal state corresponds to  $|\Phi_\uparrow\rangle = \cos\phi|b\rangle + \sin\phi|a\rangle$  and  $|\Phi_\downarrow\rangle = |b\rangle$ , respectively [45, 46]. The spatial and internal atomic state is prepared by an atomic beam splitter (ABS), an atomic mirror (AM) and a Ramsey field (RF) [5, 22, 24, 43, 54]. Therefore, the correlation between the paths and the internal atomic states is controlled by  $\phi$ , which defines the transition from  $|b\rangle$  and  $|a\rangle$  in the upper path. After passing through the ABS, the atomic state can be described as

$$\begin{aligned} |\psi(0)\rangle_{atom} &= c_\uparrow|P_\uparrow\rangle \otimes |\Phi_\uparrow\rangle + c_\downarrow|P_\downarrow\rangle \otimes |\Phi_\downarrow\rangle \\ &= c_\uparrow|P_\uparrow\rangle \otimes [\cos\phi|b\rangle + \sin\phi|a\rangle] + c_\downarrow|P_\downarrow\rangle \otimes |b\rangle. \end{aligned} \tag{5.1}$$

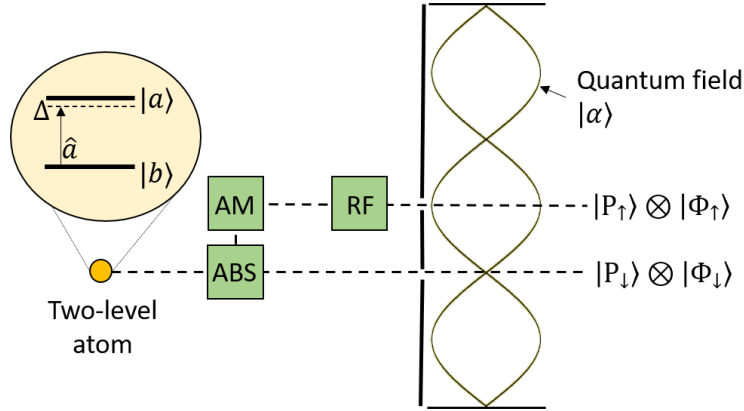


Figure 5.1: Scheme of the possible paths followed by the atom. ABS: Atomic Beam Splitter, AM: Atomic Mirror, RF: Ramsey Field. The atom is either reflected or transmitted by the ABS by taking the upper or lower path, respectively. Finally, the atom crosses the double-slit and the quantum field.

During the atom-field interaction the system will evolve according to the already known Hamiltonian  $\hat{V}$  in the interaction framework [62, 63],

$$\hat{V} = \frac{\hbar|g|^2 \cos^2(kx)}{\Delta} \hat{\sigma}_z \hat{a}^\dagger \hat{a} + \hbar\Delta \hat{\sigma}_z, \quad (5.2)$$

with  $g$  being the coupling constant and  $\Delta$  the detuning, which is required to be large in order to avoid spontaneous emission in the cavity. Therefore, the state of the system after an interaction time  $t$  can be written as [46]

$$\begin{aligned} |\psi(t)\rangle &= e^{it\Delta} c_\uparrow |P_\uparrow\rangle \otimes \cos \phi |b\rangle \otimes |e^{i\eta(x)} \alpha\rangle \\ &+ e^{-it\Delta} c_\uparrow |P_\uparrow\rangle \otimes \sin \phi |a\rangle \otimes |e^{-i\eta(x)} \alpha\rangle + e^{it\Delta} c_\downarrow |P_\downarrow\rangle \otimes |b\rangle \otimes |\alpha\rangle. \end{aligned} \quad (5.3)$$

Due to the interaction, the quantum phase of the field after the interaction can reveal information about the path taken by the atom, depending of the value of  $\eta(x)$ , which is defined as  $\eta(x) = \frac{t|g|^2}{\Delta} \cos^2(kx)$ . In this sense, the which-path information stored in the quantum field depends on the choice of the parameters  $|g|^2 t/\Delta$ . Thus, if we choose  $|g|^2 t/\Delta = \pi$  the states  $|b\rangle$  and  $|a\rangle$  have the same effect on the field, causing the same phase shift but in opposite directions. In this case, with an amplitude quadrature measurement it is possible to obtain path information since the phase of the coherent state changes only when the atom takes the upper path (figure 5.2).

When the atom crosses the node of the standing wave, the state of the field  $|\alpha\rangle$  remains the same. On other hand, for maximum atom-field interaction, the possible states of the quantum field are  $|e^{i\pi} \alpha\rangle$  and  $|e^{-i\pi} \alpha\rangle$ . Therefore, we can define  $|e^{i\pi} \alpha\rangle = |e^{-i\pi} \alpha\rangle \equiv |\alpha'\rangle$ . This allows us to identify two field states with quantum phases far enough apart. Thus, we can perform an amplitude quadrature measurement to distinguish unambiguously the initial phase from the final one and obtain path information. In contrast, if a phase quadrature measurement is performed, the probable results do not distinguish between both phases. We consider that a quadrature arbitrarily oriented defined by

$$X_\theta = \frac{ae^{-i\theta} + a^\dagger e^{i\theta}}{2} \quad (5.4)$$

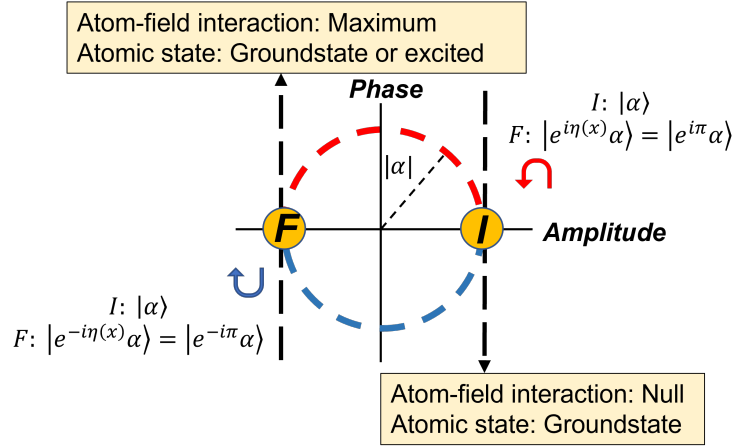


Figure 5.2: Phase shifts for maximum atom-field interaction considering  $|g|^2t/\Delta = \pi$ . If the atom crosses the upper slit is in the state  $|b\rangle$  ( $|a\rangle$ ) there is a counter-clock (clock) wise phase shift in the coherent state. If an amplitude quadrature measurement (black dotted lines) is performed, the results can give information about the path followed by the atom, but cannot always reveal the internal its internal state. On other hand, a phase quadrature measurement becomes ambiguous and it does not reveal path information or the atomic state.

is measured with an eigenvalue  $\chi_\theta$  with a corresponding eigenstate  $|\chi_\theta\rangle$  given as an infinitely squeezed state [51, 62]. On the other hand, when a correlation is established between some intrinsic property of a particle and the possible paths of the scheme, we can study the balance among visibility, distinguishability and concurrence using the relation (2.15), with

$$D = ||c_\uparrow|^2 - |c_\downarrow|^2|, \quad V = 2|c_\uparrow c_\downarrow \gamma|, \quad C = 2|c_\uparrow c_\downarrow| \sqrt{1 - |\gamma|^2}, \quad (5.5)$$

[53] where  $c_\uparrow$  and  $c_\downarrow$  are coefficients that define the probabilities for the atom of taking the top or bottom path, associated to the reflection and transmission coefficients of the atomic beam splitter, while  $\gamma \equiv \langle \Phi_\uparrow | \Phi_\downarrow \rangle$ , where the normalized states  $|\Phi_{\uparrow,\downarrow}\rangle$  correspond to intrinsic degrees of freedom of the particle which are correlated to the paths, in our case the internal atomic states. Therefore,  $\gamma$  is controlled by the atomic parameter  $\phi$ .

In order to analyse the possibilities of this scheme in the realization of delayed choice experiments, we consider for the field a coherent state with  $|\alpha| = 3$  and  $\varphi = 0$ , and for the atomic state we choose  $\phi = \pi/4$ , which ensures that, after the Ramsey field, the atom can cross the quantum field either in the state  $|b\rangle$  or  $|a\rangle$ . The coefficients  $c_\uparrow$  and  $c_\downarrow$  are taken the same and the interaction time satisfies  $|g|^2t/\Delta = \pi$ .

## 5.2 Partial quantum eraser and delayed choices

The localization of the atom via an amplitude quadrature measurement results in loss of interference and the total knowledge of the path taken by it. Therefore, the pattern obtained would correspond to a diffraction pattern. However, different effects can be observed if we consider the measurements that we can perform on the field and atom after the atom's position is registered.

In order to study the possible diffraction or interference patterns, we assume that once the atom leaves the cavity, it freely evolves during a time  $t' = 3$  (in units of  $2m/\hbar k^2$ ) to state

$$\rho(t') = |\psi(t')\rangle\langle\psi(t')| = e^{-\frac{i\hat{H}t'}{\hbar}}|\psi(t)\rangle\langle\psi(t)|e^{\frac{i\hat{H}t'}{\hbar}}, \quad (5.6)$$

where  $\hat{H} = \frac{\hat{P}^2}{2m}$  is the free particle Hamiltonian. Furthermore, we consider that the spatial atomic distribution once the atom emerges from the double-slit corresponds to two Gaussian profiles separated by  $0.25\lambda$  with a standard deviation  $\sigma = 0.05\lambda/2\pi$ , which defines the states  $|P_{\uparrow,\downarrow}\rangle$ . Thus, we can obtain the atomic distribution for a specific flight time  $t'$  as a function of the position  $x'$  in units of  $\lambda$  (figure 5.3).

If we consider that the atom's position is determined before the states of the atom and field are measured, the state of the system corresponds to

$$\begin{aligned} |\psi_x\rangle &= \langle x|\psi(t')\rangle = \frac{e^{it\Delta}}{2}\langle x|P_{\uparrow}\rangle|b\rangle \otimes |\alpha'\rangle \\ &+ \frac{e^{-it\Delta}}{2}\langle x|P_{\uparrow}\rangle|a\rangle \otimes |\alpha'\rangle + \frac{e^{it\Delta}}{\sqrt{2}}\langle x|P_{\downarrow}\rangle|b\rangle \otimes |\alpha\rangle. \end{aligned} \quad (5.7)$$

Therefore, once the atom is registered on the screen we can choose obtaining total path information from the field by measuring the  $X_0 = X$  quadrature (amplitude), or erase this information by measuring the  $X_{\pi/2} = Y$  quadrature (phase). Furthermore, we have the option to measure the internal atomic state. In the next sections, we show how the patterns observed on the screen can be modified depending on the results of the measurements performed on the field or the atom. The state of the system after a quadrature measurement with result  $\chi_\theta$  corresponds to

$$\begin{aligned} |\psi_{x,\chi_\theta}\rangle &\equiv |\chi_\theta\rangle\langle\chi_\theta|\psi_x\rangle = \frac{e^{it\Delta}}{2}\langle x|P_{\uparrow}\rangle|b\rangle\langle\chi_\theta|\alpha'\rangle|\chi_\theta\rangle \\ &+ \frac{e^{-it\Delta}}{2}\langle x|P_{\uparrow}\rangle|a\rangle\langle\chi_\theta|\alpha'\rangle|\chi_\theta\rangle + \frac{e^{it\Delta}}{\sqrt{2}}\langle x|P_{\downarrow}\rangle|b\rangle\langle\chi_\theta|\alpha\rangle|\chi_\theta\rangle. \end{aligned} \quad (5.8)$$

### 5.2.1 Reading the path information from the quantum field

Once the atom's position is registered, we can perform an  $X$  quadrature measurement on the field to obtain information about the path followed by the atom. Since we have considered a coherent state with  $\alpha = 3$ , the initial phase of the field is enough apart from the possible final phase produced by the atom-field interaction. Therefore, for an  $X$  quadrature measurement there is no overlap between both phases, which means that all possible results are unambiguous and can reveal the path followed by the atom in the double-slit scheme. We assume that an  $X$  quadrature measurement is performed with a result  $\chi_0 = \alpha$ , which locates the atom in the node of the standing wave during the atom-field interaction. The pattern observed in this case does not show fringe visibility, since the particle-like behaviour has been obtained and the path followed by the atom is completely revealed [figure 5.3b)]. A similar pattern would be observed if no quadrature measurement is performed, since although the path information is not read, it is available in the field [figure 5.3a)].

### 5.2.2 Erasing the path information from the quantum field

If instead of the  $X$  quadrature, we choose to measure the  $Y$  quadrature, then all path information initially stored in the cavity is erased. As a consequence, the quantum field can not give information about the slit through which the atom passed. In a scheme with null concurrence, this measurement leads to a complete recovery of the fringe visibility. However, in our case the paths of the scheme are correlated with the internal atomic states, which allows us to erase the path information from the quantum field and still to maintain a degree of path information in the atom. Therefore, after the  $Y$  quadrature measurement we can observe a pattern with partial interference since the internal atomic state can still reveal the path taken by the atom. In order to demonstrate this, we assume a  $Y$  quadrature measurement with result  $\chi_{\pi/2} = 0$ , which is ambiguous and can not distinguish the final phase of the field from the initial one, and thus the path followed by the atom. The pattern obtained shows partial visibility [figure 5.3d)] due to the atomic state defined initially with  $\phi = \pi/4$ .

### 5.2.3 Measuring the internal atomic state

In this section, we study the effects that the measurement of the internal atomic state causes on the pattern observed on the screen. We consider that this measurement is performed after the atom's position is registered and after the path information stored in the quantum field is erased via the  $Y$  quadrature measurement described above. In this case, the possible results of the atomic measurement can reveal total path information or total visibility. For instance, if after that the  $Y$  quadrature is measured, the atom is found in the state  $|a\rangle$ , it means that the Ramsey field in the upper path modified the initial state of the atom ( $|b\rangle$ ) and thus it crossed the antinode of the standing wave with maximum atom-field interaction. Therefore, the path followed by the atom (upper path) is completely determined and the pattern observed on the screen does not show interference [figure 5.3f)]. On the contrary, if the atom is found in the state  $|b\rangle$ , we have two options: i) The atom crossed the upper slit with maximum atom-field interaction but the Ramsey field did not modify its internal atomic state. ii) The atom crossed the bottom slit and the node of the standing wave with null atom-field interaction. Therefore, with this result we can not determine if the atom crossed the upper or bottom slit. As a consequence, total fringe visibility is observed on the screen [figure 5.3g)].

With the atomic and field measurements shown above, we can obtain patterns with different degrees of interference or path information even after the atom's position is registered. For instance, we can register the position of the atom and obtain no interference because the path information is available and stored in the field. Then, we can decide to erase this information and measure the internal atomic state and, depending on the probabilities, obtain a result that recovers the fringe visibility. This and other alternative processes can be summarized step by step considering the following order [see figure (5.3)]: 1) The atom's position is registered and no measurement is performed on the atom and field. 2) We decide to perform a measurement on the field,  $X$  or  $Y$  quadrature. 2A) If we perform an  $X$  quadrature measurement, we read the path information from the field and the path followed by the atom is determined. After this choice, the interference can not be restored. 2B) If we perform a  $Y$  quadrature measurement, we erase the path information from the field. In this case, we can still obtain path information from the atom, thus we observe partial interference, which depends on the atomic parameter  $\phi$ . 3) We

decide to measure the internal atomic state, with which we can go from partial to null or total interference. 3A) If we find the atom in the state  $|a\rangle$ , we immediately know the path followed by it. 3B) If we find the atom in the state  $|b\rangle$ , there is not path information and total interference is observed.

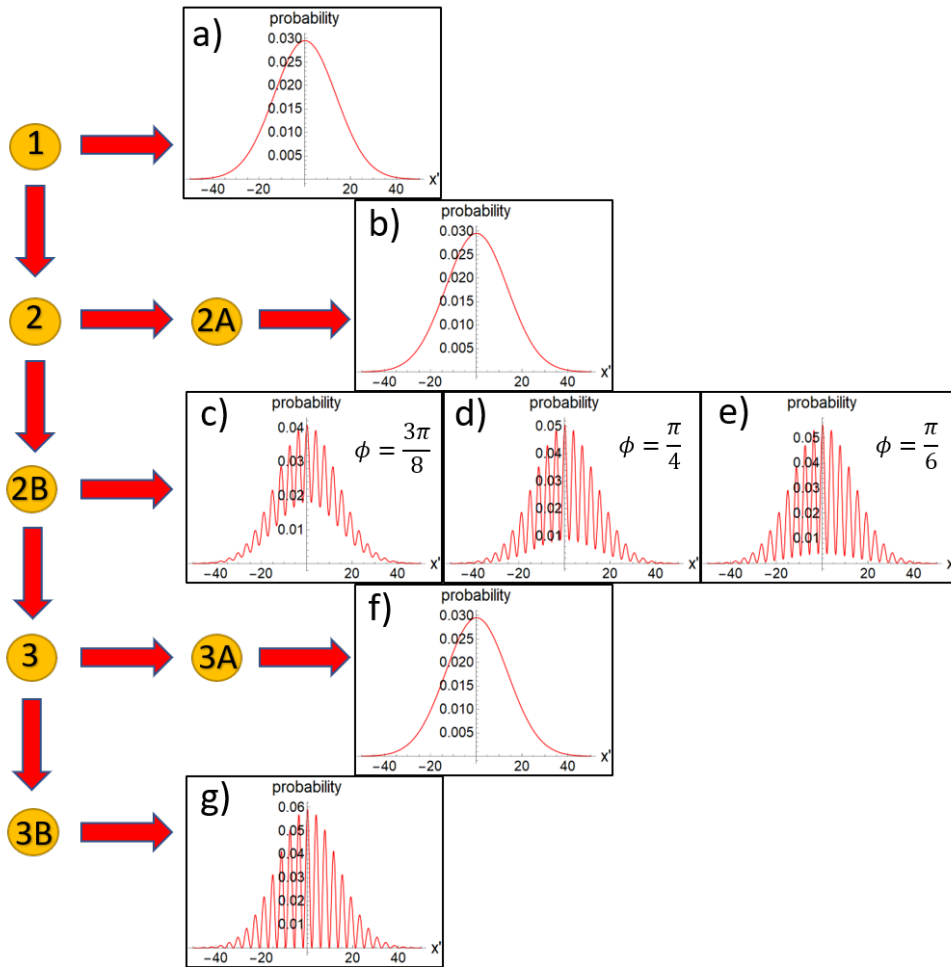


Figure 5.3: Patterns observed depending on the measurements performed on the atom and field. We consider different values of the atomic parameter  $\phi$ , in order to show more possibilities of partial fringe visibility.

# Chapter 6

## Results and conclusions

### 6.1 Controlling the wave-particle duality with quantum fields

In Chapter 3 of this thesis, we have shown that in addition to the amplitude, the initial phase  $\varphi$  of a coherent state can also control the relationship between which-path information and visibility without modifying the amplitude of the field. Secondly, in our model we have considered a field represented by a squeezed coherent state in order to study how the squeeze parameters affect the path-information and visibility. Fixing the values of the coherent amplitude  $\alpha'$  and phase  $\varphi$ , we have seen how fringe visibility can be varied and controlled via the squeeze parameters  $r$  and  $\vartheta$ . For  $\vartheta = \pi$ , as  $r$  increases, the  $X$  quadrature measurement becomes ambiguous, the which-path information reduces and partial interference appears on the screen. Nevertheless, keeping the values of the phase  $\varphi$  and the amplitudes  $\alpha'$  and  $r$ , we can reduce the fringe visibility by varying the squeeze phase  $\vartheta$ . On the other hand, we have shown that when the quantum field corresponds to a cat state and we take  $|g|^2 t / \Delta = \pi$ , we do not obtain path-information despite the fact that there is a phase-shift produced by the atom-field interaction. This is due to the symmetry of the phase of the cat states, which does not present a detectable change after a phase-shift equal to  $\pi$ . Therefore, in this case, the observed interference is the same as what we would obtain in absence of the field. However, path-information can be extracted from the phase of the cat state if we consider  $|g|^2 t / \Delta$  different from  $\pi$  which allows to differentiate the final phase from the initial one. Finally, we have analysed the possibilities that the thermal states can offer in order to control the wave-particle duality. For this kind of states we can only vary the average photon number and the final and initial phases can not be differentiated. Therefore, a thermal state by itself can not be used to control the balance between path-information and visibility. Nonetheless, based on the analysis of the squeezed coherent states, we can consider a displaced squeezed thermal state and control the duality through the average photon number  $\langle n \rangle_{th}$ , since we can generate a larger or smaller overlap between the initial and final phases of this kind of fields varying this parameter, and thus a specific quadrature measurement can become more or less ambiguous.

The fact of establishing correlations between the internal atomic states and the paths of the system allows to study the relationship between wave-particle duality and the concurrence in

different cases. Typically, the fringe visibility can vary depending on the degree of concurrence in the system, without resorting to the distinguishability. This means moving in the sphere  $VDC$  from the point  $C_0 = 1$  to the point  $V_0 = 1$  or vice versa. Therefore, we analyse the cases  $C_0 = 1$ ,  $C_0 = V_0$  and  $V_0 = 1$  where  $\phi$ , which defines the concurrence, takes the values  $\pi/2$ ,  $\pi/4$  and 0, respectively. Our results show that fringe visibility can vary without resorting to the distinguishability nor to the variation of  $\phi$ , but only considering different values of the field parameters  $\alpha'$ ,  $\varphi$ ,  $r$ ,  $\vartheta$  or  $\langle n \rangle_{th}$  in addition to the interaction time. Therefore, in a double-slit scheme with cavity field the observed interference patterns on the screen, once the atom leaves the slits-cavity setup, can be controlled through the atomic state by defining the parameter  $\phi$  in an adequate way, and also establishing different values for each one of the parameters which describe the states of the quantum field. As a consequence, these atomic and field parameters can be considered as controllers of the wave-particle duality.

Regarding to the experimental realization, our scheme presents different points which need to be considered. For instance, the time of the atom-field interaction is assumed negligible in comparison with the cavity lifetime, which along with the use of Rydberg atoms and a large detuning  $\Delta$ , allows to maintain the coherence. On other hand, the transverse distance traveled by the atom when it crosses the cavity must meet the condition  $\Delta x \ll \lambda$ . These conditions give rise to restrictions for the atom-field coupling defined by  $g$ , which also involve the values of some parameters, as the phase-shift  $\eta$ , the wavelength  $\lambda$  and the number of photons  $\langle n \rangle$  in the cavity [62]. Furthermore, since the experimental setup is crossed by one atom at a time, the experiment needs to be repeated many times in conditions as similar as possible, in order to achieve the formation of the interference patterns on the screen. This implies that the use of a velocity selector previous to the scheme becomes necessary, since a considerable difference among initial velocities of the atoms that come from a particular source could hinder the visibility of the patterns. On other hand, considering the experimental conditions and the different controllable parameters in the setup, this kind of scheme could be used in some application based on quantum information processing. For instance, for a certain distance followed by the atom between two points  $A$  and  $B$ , the interference patterns observed in the point  $B$  could reveal some information about the choice of the atomic parameters established previously in the point  $A$ . In this way, the information contained in the internal atomic state, defined in  $A$  through the choice of  $\phi$ , could be read once the atom crosses the cavity in  $B$  and the state of the quantum field is measured by homodyne detection. In this sense, the quantum field can also act as a logic quantum gate, since its state is altered only when there is interaction with the atom. Therefore, the quantum phase of the field depends on the path followed by the atom, which determines if it crosses the node or antinode of the standing wave. For example, for a coherent state  $|\alpha\rangle$ , the atom in the upper path produces a phase-shift and the final state of the field is  $|e^{\pm i\eta(x)}\alpha\rangle$ , while the atom in the bottom path does not affect the field. In the same way, if the initial state of the field is  $|e^{\pm i\eta(x)}\alpha\rangle$ , the atom modifies it (or not) if it takes the upper (or bottom) path. This can be summarized respectively as follows:  $|P_\uparrow\rangle|\alpha\rangle \mapsto |P_\uparrow\rangle|e^{\pm i\eta(x)}\alpha\rangle$ ,  $|P_\downarrow\rangle|\alpha\rangle \mapsto |P_\downarrow\rangle|\alpha\rangle$ ,  $|P_\uparrow\rangle|e^{\pm i\eta(x)}\alpha\rangle \mapsto |P_\uparrow\rangle|\alpha\rangle$  and  $|P_\downarrow\rangle|e^{\pm i\eta(x)}\alpha\rangle \mapsto |P_\downarrow\rangle|e^{\pm i\eta(x)}\alpha\rangle$ . Therefore, with an adequate representation of these states as zeros and ones, it is possible to describe these possibilities as action of a controlled not gate or CNOT [6]. In this example, we have considered  $|g|^2 t / \Delta = \pi$ .

## 6.2 Wave particle duality controlled by a classical radiation

The interaction between the three-level atom and both fields in a double cavity, added to a double-slit scheme, allows to study the relationship between wave-particle duality and concurrence in a more general context. In order to satisfy the equation (4.16), and considering a Young double-slit scheme, visibility, distinguishability and concurrence can be controlled by a correct choice of the parameters involved in the definition of each one of these quantities. However, the fact of adding both fields to the scheme implies that the gain of path-information and fringe visibility also depends on the amplitude of the classical ( $\varepsilon$ ) and quantum ( $\alpha$ ) fields. This is because the atom-field interaction can modify the initial phase of the quantum field depending on the values of these amplitudes. The phase-shift represents path-information, which can be extracted if an adequate quadrature measurement is performed. Therefore, it is possible to obtain path-information even in the case in which the choice of the parameters  $c_{\uparrow}$ ,  $c_{\downarrow}$  and  $\gamma$  satisfy  $V_0 = 1$  ( $D_0 = C_0 = 0$ ).

We have shown how the contribution of the classical radiation alters the path-information stored in the quantum field. When the atom passes by the bottom path, the interaction is null and the initial phase remains unaffected. For  $\varepsilon = 0$ , the maximum (minimum) path-information is obtained when the internal atomic state in the upper path is  $|c\rangle$  ( $|b\rangle$ ), due to the fact that atom-field interaction produces a  $\pi$  ( $0$ ) phase-shift. Therefore, in this case, a  $X$  quadrature measurement can(not) distinguish unambiguously the path followed by the atom. However, if the internal atomic state in the upper path is  $|c\rangle$ , as  $\varepsilon$  increases, the resulting phase-shift makes the  $X$  quadrature measurement ambiguous, reducing the path-information. On the contrary, if we have the internal atomic state  $|b\rangle$  in the upper path, a  $X$  quadrature measurement becomes less ambiguous, giving more path-information and less visibility. Therefore, we can consider  $\varepsilon$  as controlling parameter of the wave-particle duality. This is because the classical amplitude determines the transition probabilities between the internal states  $|b\rangle$  and  $|c\rangle$  during the atom-field interaction. For higher values of  $\varepsilon$  these transitions become more probable and thus the phases of the quantum field produced by the internal atomic states are exchanged, as it is shown in the figure 4.10 for a transition from  $|b\rangle$  to  $|c\rangle$  and in the figure 4.11 for a transition from  $|c\rangle$  to  $|b\rangle$ . In this sense, considering the possible transitions between the internal states of the atom, we can consider the classical radiation not only as a controlling parameter of the wave-particle duality but also as a controller of a single Raman diffraction process generated by both quantum and classical fields. On other hand, if we consider the presence of both fields with a small amplitude  $\varepsilon$ , the transition probabilities are reduced and the atom has a larger probability of remaining in its initial internal state. In this case the process can be described as a single Bragg diffraction process. Finally, in absence of the classical contribution, only the quantum field controls the interaction and there is no a Raman nor Bragg process.

In addition to this, and based on the different patterns observed in each case, we also conclude that for  $\varepsilon$  different from zero, the atomic distributions evolve faster as compared to the  $\varepsilon = 0$  case. This means that a certain pattern observed on the screen in absence of the classical field, can be equally obtained but in less time if it is turned on. This is because higher values of  $\varepsilon$  generate faster oscillations of the terms present in the evolution operators described in the expressions (4.19), (4.20), (4.21) and (4.22). Therefore, the initial Gaussian profiles of the atomic

distribution which emerge from the double cavity interact with each other at earlier times. In this sense, we can say that the classical field acts like a focusing device of the patterns on the screen.

A curious observation. The CV plane (figure 4.7) shows that starting from  $C_0 = 1$ , we can recover partially or completely the interference pattern by just varying the internal atomic degrees of freedom without resorting to the distinguishability ( $D_0 = 0$ ).

Finally, an interesting case is  $C_0 = 1$ , in which  $V_0$  and  $D_0$  vanish. Our scheme shows that neither visibility nor distinguishability can be restored once the maximum concurrence has been established. Therefore, this proves the sturdiness of this case against any quadrature measurement in any of the three stages presented in the previous sections.

### 6.3 Quantum eraser and delayed choices

Finally, we have studied the wave-particle duality through the atom-field interaction in a double-slit scheme that can be used in quantum eraser or delayed choice experiments. As a conclusion, in our scheme we have two sources of path information (field and atom) and we can decide the behaviour of the system even after the particle's position is registered. This is because, depending on our choices, we have the possibility to observe three different patterns: total, partial or null interference. If we decide to measure the  $X$  quadrature of the field, we immediately know the path followed by the atom and the interference can not be restored. On the contrary, if we measure the  $Y$  quadrature, the interference can be partially recovered. Therefore, after erasing the path information from the field, we can still observe both, particle-like and wave-like behaviour, unlike the previous works in which deleting the path information from the field, the interference is completely recovered. Finally, we can decide to measure the internal atomic state in order to obtain null or total interference, depending on the result of this measurement. A curious situation is produced when the atom is found in the state  $|a\rangle$ . This is because when the  $Y$  quadrature measurement is performed, we cannot know the state of the field after the interaction with the atom, since this measurement collapses its state. However, if we found that the state of the atom after the  $Y$  quadrature measurement is  $|a\rangle$ , we immediately know that the atom crossed the antinode of the quantum field and its final state  $|e^{-i\pi}\alpha\rangle$ . Therefore, in this case the internal atomic state gives us information about the state of the field post-interaction, even after that this information has been erased by the quadrature measurement  $Y$ .

# Chapter 7

## Appendix

### 7.1 Appendix subsection 2.1.3

$$\begin{aligned}
& \langle \hat{E}_a^{(-)} \hat{E}_a^{(+)} \rangle \propto p_a \\
& = \langle \hat{a}_a^\dagger e^{-i\varphi_a} \hat{a}_a e^{i\varphi_a} \rangle \\
& = [c_a^* \langle \mathbb{1}_a, \phi_a | + c_b^* \langle \mathbb{1}_b, \phi_b |] (\hat{a}_a^\dagger e^{-i\varphi_a} \hat{a}_a e^{i\varphi_a}) [c_a | \mathbb{1}_a, \phi_a \rangle + c_b | \mathbb{1}_b, \phi_b \rangle] \\
& = c_a^* c_a \langle \mathbb{1}_a, \phi_a | \hat{a}_a^\dagger \hat{a}_a | \mathbb{1}_a, \phi_a \rangle + c_b^* c_a \langle \mathbb{1}_b, \phi_b | \hat{a}_a^\dagger \hat{a}_a | \mathbb{1}_a, \phi_a \rangle + c_a^* c_b \langle \mathbb{1}_a, \phi_a | \hat{a}_a^\dagger \hat{a}_a | \mathbb{1}_b, \phi_b \rangle + c_b^* c_b \langle \mathbb{1}_b, \phi_b | \hat{a}_a^\dagger \hat{a}_a | \mathbb{1}_b, \phi_b \rangle \\
& = |c_a|^2
\end{aligned} \tag{7.1}$$

$$\begin{aligned}
& \langle \hat{E}_b^{(-)} \hat{E}_b^{(+)} \rangle \propto p_b \\
& = \langle \hat{a}_b^\dagger e^{-i\varphi_b} \hat{a}_b e^{i\varphi_b} \rangle \\
& = [c_a^* \langle \mathbb{1}_a, \phi_a | + c_b^* \langle \mathbb{1}_b, \phi_b |] (\hat{a}_b^\dagger e^{-i\varphi_b} \hat{a}_b e^{i\varphi_b}) [c_a | \mathbb{1}_a, \phi_a \rangle + c_b | \mathbb{1}_b, \phi_b \rangle] \\
& = c_a^* c_a \langle \mathbb{1}_a, \phi_a | \hat{a}_b^\dagger \hat{a}_b | \mathbb{1}_a, \phi_a \rangle + c_b^* c_a \langle \mathbb{1}_b, \phi_b | \hat{a}_b^\dagger \hat{a}_b | \mathbb{1}_a, \phi_a \rangle + c_a^* c_b \langle \mathbb{1}_a, \phi_a | \hat{a}_b^\dagger \hat{a}_b | \mathbb{1}_b, \phi_b \rangle + c_b^* c_b \langle \mathbb{1}_b, \phi_b | \hat{a}_b^\dagger \hat{a}_b | \mathbb{1}_b, \phi_b \rangle \\
& = |c_b|^2
\end{aligned} \tag{7.2}$$

$$\begin{aligned}
& \langle \hat{E}^{(-)} \hat{E}^{(+)} \rangle \propto p_c \\
& = \langle [\hat{a}_a^\dagger e^{-i\varphi_a} + \hat{a}_b^\dagger e^{-i\varphi_b}] [\hat{a}_a e^{i\varphi_a} + \hat{a}_b e^{i\varphi_b}] \rangle \\
& = \langle \hat{a}_a^\dagger \hat{a}_a + \hat{a}_a^\dagger \hat{a}_b e^{i(\varphi_b - \varphi_a)} + \hat{a}_b^\dagger \hat{a}_a e^{-i(\varphi_a - \varphi_b)} + \hat{a}_b^\dagger \hat{a}_b \rangle \\
& = [c_a^* \langle \mathbb{1}_a, \phi_a | + c_b^* \langle \mathbb{1}_b, \phi_b |] (\hat{a}_a^\dagger \hat{a}_a + \hat{a}_a^\dagger \hat{a}_b e^{i(\varphi_b - \varphi_a)} + \hat{a}_b^\dagger \hat{a}_a e^{-i(\varphi_a - \varphi_b)} + \hat{a}_b^\dagger \hat{a}_b) [c_a | \mathbb{1}_a, \phi_a \rangle + c_b | \mathbb{1}_b, \phi_b \rangle] \\
& = [c_a^* \langle \mathbb{1}_a, \phi_a | + c_b^* \langle \mathbb{1}_b, \phi_b |] \hat{a}_a^\dagger \hat{a}_a [c_a | \mathbb{1}_a, \phi_a \rangle + c_b | \mathbb{1}_b, \phi_b \rangle] + [c_a^* \langle \mathbb{1}_a, \phi_a | + c_b^* \langle \mathbb{1}_b, \phi_b |] \hat{a}_a^\dagger \hat{a}_b e^{i(\varphi_b - \varphi_a)} [c_a | \mathbb{1}_a, \phi_a \rangle + c_b | \mathbb{1}_b, \phi_b \rangle] \\
& + [c_a^* \langle \mathbb{1}_a, \phi_a | + c_b^* \langle \mathbb{1}_b, \phi_b |] \hat{a}_b^\dagger \hat{a}_a e^{-i(\varphi_a - \varphi_b)} [c_a | \mathbb{1}_a, \phi_a \rangle + c_b | \mathbb{1}_b, \phi_b \rangle] + [c_a^* \langle \mathbb{1}_a, \phi_a | + c_b^* \langle \mathbb{1}_b, \phi_b |] \hat{a}_b^\dagger \hat{a}_b [c_a | \mathbb{1}_a, \phi_a \rangle + c_b | \mathbb{1}_b, \phi_b \rangle] \\
& = c_a^* c_a \langle \mathbb{1}_a, \phi_a | \hat{a}_a^\dagger \hat{a}_a | \mathbb{1}_a, \phi_a \rangle + c_a^* c_b e^{i(\varphi_b - \varphi_a)} \langle \mathbb{1}_b, \phi_b | \hat{a}_a^\dagger \hat{a}_b | \mathbb{1}_a, \phi_a \rangle + c_b^* c_a e^{-i(\varphi_a - \varphi_b)} \langle \mathbb{1}_a, \phi_a | \hat{a}_b^\dagger \hat{a}_a | \mathbb{1}_b, \phi_b \rangle + c_b^* c_b \langle \mathbb{1}_b, \phi_b | \hat{a}_b^\dagger \hat{a}_b | \mathbb{1}_b, \phi_b \rangle \\
& = |c_a|^2 + c_a^* c_b e^{i(\varphi_b - \varphi_a)} \langle \phi_b | \phi_a \rangle + c_b^* c_a e^{-i(\varphi_a - \varphi_b)} \langle \phi_b | \phi_a \rangle + |c_b|^2 \\
& = |c_a|^2 + c_a^* c_b \gamma e^{i(\varphi_b - \varphi_a)} + c_b^* c_a \gamma^* e^{-i(\varphi_a - \varphi_b)} + |c_b|^2
\end{aligned} \tag{7.3}$$

$$D = \left| \frac{p_a - p_b}{p_a + p_b} \right| = \left| \frac{|c_a|^2 - |c_b|^2}{|c_a|^2 + |c_b|^2} \right| = \left| |c_a|^2 - |c_b|^2 \right| \quad (7.4)$$

$$\begin{aligned}
V &= \frac{p_c^{max} - p_c^{min}}{p_c^{max} + p_c^{min}} \\
&= \frac{(|c_a|^2 + c_a^* c_b \gamma + c_b^* c_a \gamma^* + |c_b|^2) - (|c_a|^2 - c_a^* c_b \gamma - c_b^* c_a \gamma^* + |c_b|^2)}{(|c_a|^2 + c_a^* c_b \gamma + c_b^* c_a \gamma^* + |c_b|^2) + (|c_a|^2 - c_a^* c_b \gamma - c_b^* c_a \gamma^* + |c_b|^2)} \\
&= \frac{2c_a^* c_b \gamma + 2c_b^* c_a \gamma^*}{2|c_a|^2 + 2|c_b|^2} \\
&= c_a^* c_b \gamma + c_b^* c_a \gamma^* \\
&= c_a^* c_b \gamma + (c_b c_a^* \gamma)^* \\
&= 2|c_a c_b \gamma|.
\end{aligned} \quad (7.5)$$

### 7.1.1 Appendix subsection 2.2.1

$$\begin{aligned}
i\hbar \frac{d}{dt} |\psi_I(t)\rangle &= i\hbar \frac{d}{dt} [\hat{U}_0^{-1} |\psi_S(t)\rangle] \\
&= i\hbar \frac{d\hat{U}_0^{-1}}{dt} |\psi_S(t)\rangle + i\hbar \hat{U}_0^{-1} \frac{d}{dt} |\psi_S(t)\rangle \\
&= i\hbar \frac{d}{dt} e^{\frac{i\hat{H}_0 t}{\hbar}} |\psi_S(t)\rangle + \hat{U}_0^{-1} (\hat{H}_0 + \hat{H}_I) |\psi_S(t)\rangle \\
&= -\hat{H}_0 \hat{U}_0^{-1} |\psi_S(t)\rangle + \hat{U}_0^{-1} \hat{H}_0 |\psi_S(t)\rangle + \hat{U}_0^{-1} \hat{H}_I |\psi_S(t)\rangle \\
&= -\hat{H}_0 \hat{U}_0^{-1} \hat{U}_0 |\psi_I(t)\rangle + \hat{U}_0^{-1} \hat{H}_0 \hat{U}_0 |\psi_I(t)\rangle + \hat{U}_0^{-1} \hat{H}_I \hat{U}_0 |\psi_I(t)\rangle \\
&= -i\hbar \hat{U}_0^{-1} \frac{d}{dt} \hat{U}_0 |\psi_I(t)\rangle + \hat{U}_0^{-1} \hat{H}_0 \hat{U}_0 |\psi_I(t)\rangle + \hat{U}_0^{-1} \hat{H}_I \hat{U}_0 |\psi_I(t)\rangle \\
&= [-i\hbar \hat{U}_0^{-1} \frac{d}{dt} \hat{U}_0 + \hat{U}_0^{-1} \hat{H} \hat{U}_0] |\psi_I(t)\rangle = \hat{W}_I(t) |\psi_I(t)\rangle,
\end{aligned} \quad (7.6)$$

$$\begin{aligned}
e^{\frac{i\hat{H}_0 t}{\hbar}} \hat{\sigma}_- \hat{a}^\dagger e^{-\frac{i\hat{H}_0 t}{\hbar}} &= \hat{\sigma}_- \hat{a}^\dagger + \left[ \frac{i\hat{H}_0 t}{\hbar}, \hat{\sigma}_- \hat{a}^\dagger \right] + \frac{1}{2!} \left[ \frac{i\hat{H}_0 t}{\hbar}, \left[ \frac{i\hat{H}_0 t}{\hbar}, \hat{\sigma}_- \hat{a}^\dagger \right] \right] + \dots \\
&= \hat{\sigma}_- \hat{a}^\dagger + \frac{it}{\hbar} \left[ \hbar \omega_a \hat{a}^\dagger \hat{a} + \frac{\hbar \omega_0 \hat{\sigma}_z}{2}, \hat{\sigma}_- \hat{a}^\dagger \right] + \frac{1}{2!} \left[ \frac{i\hat{H}_0 t}{\hbar}, \left[ \frac{i\hat{H}_0 t}{\hbar}, \hat{\sigma}_- \hat{a}^\dagger \right] \right] + \dots \\
&= \hat{\sigma}_- \hat{a}^\dagger + it \left[ (\omega_a \hat{a}^\dagger \hat{a} + \frac{\omega_0 \sigma_z}{2}) \hat{\sigma}_- \hat{a}^\dagger - \hat{\sigma}_- \hat{a}^\dagger (\omega_a \hat{a}^\dagger \hat{a} + \frac{\omega_0 \sigma_z}{2}) \right] + \dots \\
&= \hat{\sigma}_- \hat{a}^\dagger + it \left[ \omega_a (\hat{a}^\dagger \hat{a} \hat{\sigma}_- \hat{a}^\dagger - \hat{\sigma}_- \hat{a}^\dagger \hat{a} \hat{a}^\dagger) + \frac{\omega_0}{2} (\hat{\sigma}_z \hat{\sigma}_- \hat{a}^\dagger - \hat{\sigma}_- \hat{a}^\dagger \hat{\sigma}_z) \right] + \dots \\
&= \hat{\sigma}_- \hat{a}^\dagger + it \left[ \omega_a ([\hat{a} \hat{a}^\dagger - 1] \hat{\sigma}_- \hat{a}^\dagger - \hat{\sigma}_- \hat{a}^\dagger [\hat{a} \hat{a}^\dagger - 1]) + \frac{\omega_0}{2} (\hat{\sigma}_z \hat{\sigma}_- \hat{a}^\dagger - \hat{\sigma}_- \hat{a}^\dagger \hat{\sigma}_z) \right] + \dots \\
&= \hat{\sigma}_- \hat{a}^\dagger + it \left[ \omega_a (\hat{a} \hat{a}^\dagger \hat{\sigma}_- \hat{a}^\dagger - \hat{\sigma}_- \hat{a}^\dagger \hat{a} \hat{a}^\dagger) + \frac{\omega_0}{2} (-\hat{\sigma}_- \hat{a}^\dagger - \hat{\sigma}_- \hat{a}^\dagger) \right] + \dots \\
&= \hat{\sigma}_- \hat{a}^\dagger + it \left[ \omega_a (\hat{\sigma}_- [1 + \hat{a}^\dagger \hat{a}] \hat{a}^\dagger - \hat{\sigma}_- \hat{a}^\dagger \hat{a} \hat{a}^\dagger) - \omega_0 \hat{\sigma}_- \hat{a}^\dagger \right] + \frac{1}{2!} \left[ \frac{i\hat{H}_0 t}{\hbar}, \left[ \frac{i\hat{H}_0 t}{\hbar}, \hat{\sigma}_- \hat{a}^\dagger \right] \right] + \dots \\
&= \hat{\sigma}_- \hat{a}^\dagger + it \left[ \omega_a \hat{\sigma}_- \hat{a}^\dagger - \omega_0 \hat{\sigma}_- \hat{a}^\dagger \right] + \frac{1}{2!} \left[ \frac{i\hat{H}_0 t}{\hbar}, \left[ \frac{i\hat{H}_0 t}{\hbar}, \hat{\sigma}_- \hat{a}^\dagger \right] \right] + \dots \\
&= \hat{\sigma}_- \hat{a}^\dagger + it (\omega_a - \omega_0) \hat{\sigma}_- \hat{a}^\dagger + \frac{1}{2!} \left[ \frac{i\hat{H}_0 t}{\hbar}, it (\omega_a - \omega_0) \hat{\sigma}_- \hat{a}^\dagger \right] + \dots \\
&= \hat{\sigma}_- \hat{a}^\dagger - it \Delta \hat{\sigma}_- \hat{a}^\dagger + \frac{1}{2!} (-it \Delta \hat{\sigma}_- \hat{a}^\dagger)^2 + \dots \\
&= \hat{\sigma}_- \hat{a}^\dagger (1 - it \Delta + \frac{1}{2!} (-it \Delta)^2 + \dots) \\
&= \hat{\sigma}_- \hat{a}^\dagger e^{-i \Delta t}.
\end{aligned} \tag{7.7}$$

$$e^{-\frac{i}{\hbar} \int_0^t \hat{W}_I(t') dt'} = 1 - \frac{i}{\hbar} \int_0^t \hat{W}_I(t') dt' - \frac{1}{\hbar^2} \left[ \int_0^t \hat{W}_I(t') dt' \int_0^{t'} \hat{W}_I(t'') dt'' \right] + \dots \tag{7.8}$$

where

$$\begin{aligned}
\bullet \int_0^t \hat{W}_I(t') dt' &= \int_0^t \hbar \cos(kx + \xi) \left[ g^* \hat{\sigma}_- \hat{a}^\dagger e^{-i \Delta t'} + g \hat{\sigma}_+ \hat{a} e^{i \Delta t'} \right] dt' \\
&= \hbar \cos(kx + \xi) \left[ g^* \hat{\sigma}_- \hat{a}^\dagger \int_0^t e^{-i \Delta t'} dt' + g \hat{\sigma}_+ \hat{a} \int_0^t e^{i \Delta t'} dt' \right] \\
&= \hbar \cos(kx + \xi) \left[ g^* \hat{\sigma}_- \hat{a}^\dagger \left( -\frac{e^{-i \Delta t'}}{i \Delta} \right) \Big|_0^t + g \hat{\sigma}_+ \hat{a} \left( \frac{e^{i \Delta t'}}{i \Delta} \right) \Big|_0^t \right] \\
&= \frac{\hbar \cos(kx + \xi)}{i \Delta} \left[ g^* \hat{\sigma}_- \hat{a}^\dagger (1 - e^{-i \Delta t}) + g \hat{\sigma}_+ \hat{a} (e^{i \Delta t} - 1) \right]
\end{aligned} \tag{7.9}$$

$$\begin{aligned}
\bullet \int_0^t \hat{W}_I(t') dt' \int_0^{t'} \hat{W}_I(t'') dt'' &= \int_0^t \hat{W}_I(t') dt' \left( \frac{\hbar \cos(kx + \xi)}{i\Delta} \left[ g\hat{\sigma}_+\hat{a}(e^{i\Delta t'} - 1) - g^*\hat{\sigma}_-\hat{a}^\dagger(e^{-i\Delta t'} - 1) \right] \right) \\
&= \int_0^t dt' \left( \hbar \cos(kx + \xi) \left[ g^*\hat{\sigma}_-\hat{a}^\dagger e^{-i\Delta t'} + g\hat{\sigma}_+\hat{a} e^{i\Delta t'} \right] \right) \\
&\quad \left( \frac{\hbar \cos(kx + \xi)}{i\Delta} \left[ g\hat{\sigma}_+\hat{a}(e^{i\Delta t'} - 1) - g^*\hat{\sigma}_-\hat{a}^\dagger(e^{-i\Delta t'} - 1) \right] \right) \\
&= \frac{\hbar^2 \cos^2(kx + \xi)}{i\Delta} \int_0^t dt' \left[ g^*\hat{\sigma}_-\hat{a}^\dagger e^{-i\Delta t'} + g\hat{\sigma}_+\hat{a} e^{i\Delta t'} \right] \\
&\quad \left[ g\hat{\sigma}_+\hat{a} e^{i\Delta t'} - g\hat{\sigma}_+\hat{a} - g^*\hat{\sigma}_-\hat{a}^\dagger e^{-i\Delta t'} + g^*\hat{\sigma}_-\hat{a}^\dagger \right] \\
&= \frac{\hbar^2 \cos^2(kx + \xi)}{i\Delta} \int_0^t dt' \left[ |g|^2 \hat{\sigma}_-\hat{a}^\dagger \hat{\sigma}_+\hat{a} - |g|^2 \hat{\sigma}_-\hat{a}^\dagger \hat{\sigma}_+\hat{a} e^{-i\Delta t'} - g^{*2} \hat{\sigma}_-^2 \hat{a}^{\dagger 2} e^{-2i\Delta t'} \right. \\
&\quad \left. g^{*2} \hat{\sigma}_-^2 \hat{a}^{\dagger 2} e^{-i\Delta t'} + g^2 \hat{\sigma}_+^2 \hat{a}^2 e^{2i\Delta t'} - g^2 \hat{\sigma}_+^2 \hat{a}^2 e^{i\Delta t'} - |g|^2 \hat{\sigma}_+\hat{a} \hat{\sigma}_-\hat{a}^\dagger + |g|^2 \hat{\sigma}_+\hat{a} \hat{\sigma}_-\hat{a}^\dagger e^{i\Delta t'} \right] \\
&= \frac{\hbar^2 \cos^2(kx + \xi)}{i\Delta} \int_0^t dt' \left[ |g|^2 \hat{\sigma}_-\hat{a}^\dagger \hat{\sigma}_+\hat{a} - |g|^2 \hat{\sigma}_+\hat{a} \hat{\sigma}_-\hat{a}^\dagger \right] \\
&= \frac{\hbar^2 |g|^2 t \cos^2(kx + \xi)}{i\Delta} [\hat{\sigma}_-\hat{a}^\dagger, \hat{\sigma}_+\hat{a}],
\end{aligned} \tag{7.10}$$

Where the exponential terms in the penultimate equality have been omitted since when integrating them they yield values proportional to  $1/\Delta^2$  with  $\Delta$  very large. Therefore

$$\begin{aligned}
e^{-\frac{i}{\hbar} \int_0^t \hat{W}_I(t') dt'} &= 1 - \frac{i}{\hbar} \int_0^t \hat{W}_I(t') dt' - \frac{1}{\hbar^2} \left[ \int_0^t \hat{W}_I(t') dt' \int_0^{t'} \hat{W}_I(t'') dt'' \right] + \dots \\
&= 1 - \frac{i}{\hbar} \left( \frac{\hbar \cos(kx + \xi)}{i\Delta} \left[ g^*\hat{\sigma}_-\hat{a}^\dagger(1 - e^{-i\Delta t}) + g\hat{\sigma}_+\hat{a}(e^{i\Delta t} - 1) \right] \right) - \frac{1}{\hbar^2} \left( \frac{\hbar^2 |g|^2 t \cos^2(kx + \xi)}{i\Delta} [\hat{\sigma}_-\hat{a}^\dagger, \hat{\sigma}_+\hat{a}] \right) \\
&= 1 - \frac{\cos(kx + \xi)}{\Delta} \left[ g^*\hat{\sigma}_-\hat{a}^\dagger(1 - e^{-i\Delta t}) + g\hat{\sigma}_+\hat{a}(e^{i\Delta t} - 1) \right] - \frac{|g|^2 t \cos^2(kx + \xi)}{i\Delta} [\hat{\sigma}_-\hat{a}^\dagger, \hat{\sigma}_+\hat{a}] + \dots \\
&\approx 1 - \frac{|g|^2 t \cos^2(kx + \xi)}{i\Delta} [\hat{\sigma}_-\hat{a}^\dagger, \hat{\sigma}_+\hat{a}] + \dots \\
&= 1 - \frac{it}{\hbar} \left[ \frac{\hbar |g|^2 \cos^2(kx + \xi)}{\Delta} [\hat{\sigma}_+\hat{a}, \hat{\sigma}_-\hat{a}^\dagger] \right] + \dots
\end{aligned} \tag{7.11}$$

where it has been considered that if  $\langle \hat{A} \rangle \approx \langle \hat{A}^\dagger \hat{A} \rangle^{1/2}$ , with  $\hat{A} = \hat{\sigma}_+\hat{a}$ , it is not too big and

$|\frac{g}{\Delta}\langle\hat{A}^\dagger\hat{A}\rangle^{1/2}| \ll 1$  ( $\Delta$  large), then the second term can be dropped. With this we obtain that

$$\begin{aligned}
\hat{W}_{eff}^I &= \frac{\hbar|g|^2 \cos^2(kx + \xi)}{\Delta} [\hat{\sigma}_+ \hat{a}, \hat{\sigma}_- \hat{a}^\dagger] \\
&= \frac{\hbar|g|^2 \cos^2(kx + \xi)}{\Delta} (\hat{\sigma}_+ \hat{\sigma}_- \hat{a} \hat{a}^\dagger - \hat{\sigma}_- \hat{\sigma}_+ \hat{a}^\dagger \hat{a}) \\
&= \frac{\hbar|g|^2 \cos^2(kx + \xi)}{\Delta} (\hat{\sigma}_+ \hat{\sigma}_- (1 + \hat{a}^\dagger \hat{a}) - \hat{\sigma}_- \hat{\sigma}_+ \hat{a}^\dagger \hat{a}) \\
&= \frac{\hbar|g|^2 \cos^2(kx + \xi)}{\Delta} (\hat{\sigma}_+ \hat{\sigma}_- + \hat{\sigma}_+ \hat{\sigma}_- \hat{a}^\dagger \hat{a} - \hat{\sigma}_- \hat{\sigma}_+ \hat{a}^\dagger \hat{a}) \\
&= \frac{\hbar|g|^2 \cos^2(kx + \xi)}{\Delta} (\hat{\sigma}_+ \hat{\sigma}_- + \hat{\sigma}_z \hat{a}^\dagger \hat{a}) \\
&= \frac{\hbar|g|^2 \cos^2(kx + \xi)}{\Delta} \hat{\sigma}_+ \hat{\sigma}_- + \frac{\hbar|g|^2 \cos^2(kx + \xi)}{\Delta} \hat{\sigma}_z \hat{a}^\dagger \hat{a}.
\end{aligned} \tag{7.12}$$

### 7.1.2 Appendix subsection 2.2.2

$$\begin{aligned}
|\psi(t)\rangle &= \int dx \kappa(x) e^{-\frac{iVt}{\hbar}} |\alpha\rangle \otimes |x, g\rangle \\
&= \int dx \kappa(x) e^{-\frac{it}{\hbar} \left( \frac{\hbar|g|^2 \cos^2(kx + \xi)}{\Delta} \hat{\sigma}_z \hat{a}^\dagger \hat{a} + \hbar \Delta \hat{\sigma}_z \right)} |\alpha\rangle \otimes |x, g\rangle \\
&= \int dx \kappa(x) e^{-\frac{it|g|^2 \cos^2(kx + \xi)}{\Delta} \hat{\sigma}_z \hat{a}^\dagger \hat{a}} e^{-it\Delta \hat{\sigma}_z} |\alpha\rangle \otimes |x, g\rangle \\
&= \int dx \kappa(x) e^{it\Delta} e^{\frac{it|g|^2 \cos^2(kx + \xi)}{\Delta} \hat{a}^\dagger \hat{a}} |\alpha\rangle \otimes |x, g\rangle \\
&= \int dx \kappa(x) e^{it\Delta} e^{i\eta(x) \hat{a}^\dagger \hat{a}} |\alpha\rangle \otimes |x, g\rangle \quad \text{con } \eta(x) = \frac{t|g|^2 \cos^2(kx + \xi)}{\Delta} \\
&= \int dx \kappa(x) e^{it\Delta} e^{i\eta(x) \hat{a}^\dagger \hat{a}} \left[ e^{-\frac{|\alpha|^2}{2}} \sum_{n=0}^{\infty} \frac{\alpha^n}{\sqrt{n!}} |n\rangle \right] \otimes |x, g\rangle \\
&= e^{it\Delta} \int dx \kappa(x) e^{i\eta(x)n} e^{-\frac{|\alpha|^2}{2}} \sum_{n=0}^{\infty} \frac{\alpha^n}{\sqrt{n!}} |n\rangle \otimes |x, g\rangle \\
&= e^{it\Delta} \int dx \kappa(x) e^{-\frac{|\alpha|^2}{2}} e^{\frac{|\alpha e^{i\eta(x)}|^2}{2}} e^{-\frac{|\alpha e^{i\eta(x)}|^2}{2}} \sum_{n=0}^{\infty} \frac{(\alpha e^{i\eta(x)})^n}{\sqrt{n!}} |n\rangle \otimes |x, g\rangle \\
&= e^{it\Delta} \int dx \kappa(x) e^{-\frac{|\alpha e^{i\eta(x)}|^2}{2}} e^{-\frac{|\alpha|^2}{2} (1 - |e^{i\eta(x)}|^2)} \sum_{n=0}^{\infty} \frac{(\alpha e^{i\eta(x)})^n}{\sqrt{n!}} |n\rangle \otimes |x, g\rangle \\
&= e^{it\Delta} \int dx \kappa(x) \left[ e^{-\frac{|\alpha e^{i\eta(x)}|^2}{2}} \sum_{n=0}^{\infty} \frac{(\alpha e^{i\eta(x)})^n}{\sqrt{n!}} |n\rangle \right] \otimes |x, g\rangle \\
&= e^{it\Delta} \int dx \kappa(x) |\alpha e^{i\eta(x)}\rangle \otimes |x, g\rangle
\end{aligned} \tag{7.13}$$

$$\begin{aligned}
|\chi_\theta\rangle &= \frac{1}{\sqrt[4]{2\pi}} \exp\left[-\frac{1}{2}(a^\dagger e^{i\theta} - \chi_\theta)^2 + \frac{1}{4}\chi_\theta^2\right] |0\rangle \\
&= \frac{1}{\sqrt[4]{2\pi}} \exp\left[-\frac{a^{\dagger 2} e^{2i\theta}}{2} + a^\dagger e^{i\theta} \chi_\theta - \frac{1}{4}\chi_\theta^2\right] |0\rangle \\
&= \frac{1}{\sqrt[4]{2\pi}} e^{-\frac{1}{4}\chi_\theta^2} e^{-\frac{a^{\dagger 2} e^{2i\theta}}{2}} e^{a^\dagger e^{i\theta} \chi_\theta} |0\rangle \\
&= \frac{1}{\sqrt[4]{2\pi}} e^{-\frac{1}{4}\chi_\theta^2} e^{-\frac{a^{\dagger 2} e^{2i\theta}}{2}} \left[1 + a^\dagger e^{i\theta} \chi_\theta + \frac{1}{2} a^{\dagger 2} e^{2i\theta} \chi_\theta^2 + \dots\right] |0\rangle \\
&= \frac{1}{\sqrt[4]{2\pi}} e^{-\frac{1}{4}\chi_\theta^2} e^{-\frac{a^{\dagger 2} e^{2i\theta}}{2}} \left[|0\rangle + a^\dagger e^{i\theta} \chi_\theta |0\rangle + \frac{1}{2!} a^{\dagger 2} e^{2i\theta} \chi_\theta^2 |0\rangle + \frac{1}{3!} a^{\dagger 3} e^{3i\theta} \chi_\theta^3 |0\rangle + \dots\right] \\
&= \frac{1}{\sqrt[4]{2\pi}} e^{-\frac{1}{4}\chi_\theta^2} e^{-\frac{a^{\dagger 2} e^{2i\theta}}{2}} \left[|0\rangle + e^{i\theta} \chi_\theta |1\rangle + \frac{1}{\sqrt{2!}} e^{2i\theta} \chi_\theta^2 |2\rangle + \frac{1}{\sqrt{3!}} e^{3i\theta} \chi_\theta^3 |3\rangle + \dots\right] \\
&= \frac{1}{\sqrt[4]{2\pi}} e^{-\frac{1}{4}\chi_\theta^2} e^{-\frac{a^{\dagger 2} e^{2i\theta}}{2}} \sum_{n=0}^{\infty} \frac{e^{in\theta} \chi_\theta^n}{\sqrt{n!}} |n\rangle \\
&= \frac{1}{\sqrt[4]{2\pi}} e^{-\frac{1}{4}\chi_\theta^2} \left[1 - \frac{a^{\dagger 2} e^{2i\theta}}{2} + \frac{1}{2!} \frac{a^{\dagger 4} e^{4i\theta}}{4} - \frac{1}{3!} \frac{a^{\dagger 6} e^{6i\theta}}{8} + \dots\right] \sum_{n=0}^{\infty} \frac{e^{in\theta} \chi_\theta^n}{\sqrt{n!}} |n\rangle \\
&= \frac{1}{\sqrt[4]{2\pi}} e^{-\frac{1}{4}\chi_\theta^2} \left[\sum_{n=0}^{\infty} \frac{e^{in\theta} \chi_\theta^n}{\sqrt{n!}} |n\rangle - \frac{a^{\dagger 2} e^{2i\theta}}{2} \sum_{n=0}^{\infty} \frac{e^{in\theta} \chi_\theta^n}{\sqrt{n!}} |n\rangle + \frac{1}{2!} \frac{a^{\dagger 4} e^{4i\theta}}{4} \sum_{n=0}^{\infty} \frac{e^{in\theta} \chi_\theta^n}{\sqrt{n!}} |n\rangle - \frac{1}{3!} \frac{a^{\dagger 6} e^{6i\theta}}{8} \sum_{n=0}^{\infty} \frac{e^{in\theta} \chi_\theta^n}{\sqrt{n!}} |n\rangle + \dots\right] \\
&= \frac{1}{\sqrt[4]{2\pi}} e^{-\frac{1}{4}\chi_\theta^2} \left[\sum_{n=0}^{\infty} \frac{e^{in\theta} \chi_\theta^n}{\sqrt{n!}} |n\rangle - \frac{1}{2} \sum_{n=0}^{\infty} \sqrt{n+2} \sqrt{n+1} \frac{e^{i(n+2)\theta} \chi_\theta^n}{\sqrt{n!}} |n+2\rangle\right. \\
&\quad + \frac{1}{2!} \frac{1}{4} \sum_{n=0}^{\infty} \sqrt{n+4} \sqrt{n+3} \sqrt{n+2} \sqrt{n+1} \frac{e^{i(n+4)\theta} \chi_\theta^n}{\sqrt{n!}} |n+4\rangle \\
&\quad \left. - \frac{1}{3!} \frac{1}{8} \sum_{n=0}^{\infty} \sqrt{n+6} \sqrt{n+5} \sqrt{n+4} \sqrt{n+3} \sqrt{n+2} \sqrt{n+1} \frac{e^{i(n+6)\theta} \chi_\theta^n}{\sqrt{n!}} |n+6\rangle + \dots\right] \\
&= \frac{1}{\sqrt[4]{2\pi}} e^{-\frac{1}{4}\chi_\theta^2} \left[\sum_{n=0}^{\infty} \frac{e^{in\theta} \chi_\theta^n}{\sqrt{n!}} |n\rangle - \frac{1}{2} \sum_{n=0}^{\infty} \sqrt{(n+2)!} \frac{e^{i(n+2)\theta} \chi_\theta^n}{n!} |n+2\rangle\right. \\
&\quad \left. + \frac{1}{2!} \frac{1}{4} \sum_{n=0}^{\infty} \sqrt{(n+4)!} \frac{e^{i(n+4)\theta} \chi_\theta^n}{n!} |n+4\rangle - \frac{1}{3!} \frac{1}{8} \sum_{n=0}^{\infty} \sqrt{(n+6)!} \frac{e^{i(n+6)\theta} \chi_\theta^n}{n!} |n+6\rangle + \dots\right]
\end{aligned} \tag{7.14}$$

$$\begin{aligned}
\langle \chi_\theta | \alpha e^{i\eta} \rangle &= \left( \frac{1}{\sqrt[4]{2\pi}} e^{-\frac{1}{4}\chi_\theta^2} \left[ \sum_{n=0} \langle n | \frac{e^{-in\theta} \chi_\theta^n}{\sqrt{n!}} - \frac{1}{2} \sum_{n=0} \langle n+2 | \sqrt{(n+2)!} \frac{e^{-i(n+2)\theta} \chi_\theta^n}{n!} \right. \right. \\
&\quad \left. \left. + \frac{1}{2!} \frac{1}{4} \sum_{n=0} \langle n+4 | \sqrt{(n+4)!} \frac{e^{-i(n+4)\theta} \chi_\theta^n}{n!} - \frac{1}{3!} \frac{1}{8} \sum_{n=0} \langle n+6 | \sqrt{(n+6)!} \frac{e^{-i(n+6)\theta} \chi_\theta^n}{n!} + \dots \right] \right) \\
&\quad \left( e^{-\frac{|\alpha e^{i\eta}|^2}{2}} \sum_{m=0} \frac{(\alpha e^{i\eta})^m}{\sqrt{m!}} |m\rangle \right) \\
&= \frac{1}{\sqrt[4]{2\pi}} e^{-\frac{1}{4}\chi_\theta^2} \left[ \left( \sum_{n=0} \langle n | \frac{e^{-in\theta} \chi_\theta^n}{\sqrt{n!}} \right) \left( e^{-\frac{|\alpha e^{i\eta}|^2}{2}} \sum_{m=0} \frac{(\alpha e^{i\eta})^m}{\sqrt{m!}} |m\rangle \right) \right. \\
&\quad - \frac{1}{2} \left( \sum_{n=0} \langle n+2 | \sqrt{(n+2)!} \frac{e^{-i(n+2)\theta} \chi_\theta^n}{n!} \right) \left( e^{-\frac{|\alpha e^{i\eta}|^2}{2}} \sum_{m=0} \frac{(\alpha e^{i\eta})^m}{\sqrt{m!}} |m\rangle \right) \\
&\quad + \frac{1}{2!} \frac{1}{4} \left( \sum_{n=0} \langle n+4 | \sqrt{(n+4)!} \frac{e^{-i(n+4)\theta} \chi_\theta^n}{n!} \right) \left( e^{-\frac{|\alpha e^{i\eta}|^2}{2}} \sum_{m=0} \frac{(\alpha e^{i\eta})^m}{\sqrt{m!}} |m\rangle \right) \\
&\quad \left. - \frac{1}{3!} \frac{1}{8} \left( \sum_{n=0} \langle n+6 | \sqrt{(n+6)!} \frac{e^{-i(n+6)\theta} \chi_\theta^n}{n!} \right) \left( e^{-\frac{|\alpha e^{i\eta}|^2}{2}} \sum_{m=0} \frac{(\alpha e^{i\eta})^m}{\sqrt{m!}} |m\rangle \right) + \dots \right] \\
&= \frac{1}{\sqrt[4]{2\pi}} e^{-\frac{1}{4}\chi_\theta^2} e^{-\frac{|\alpha e^{i\eta}|^2}{2}} \left[ \left( \sum_{n,m=0} \frac{e^{-in\theta} \chi_\theta^n (\alpha e^{i\eta})^m}{\sqrt{n!} \sqrt{m!}} \langle n|m\rangle \right) - \frac{1}{2} \left( \sum_{n,m=0} \frac{\sqrt{(n+2)!} e^{-i(n+2)\theta} \chi_\theta^n (\alpha e^{i\eta})^m}{n! \sqrt{m!}} \langle n+2|m\rangle \right) \right. \\
&\quad \left. + \frac{1}{2!} \frac{1}{4} \left( \sum_{n,m=0} \frac{\sqrt{(n+4)!} e^{-i(n+4)\theta} \chi_\theta^n (\alpha e^{i\eta})^m}{n! \sqrt{m!}} \langle n+4|m\rangle \right) - \frac{1}{3!} \frac{1}{8} \left( \sum_{n,m=0} \frac{\sqrt{(n+6)!} e^{-i(n+6)\theta} \chi_\theta^n (\alpha e^{i\eta})^m}{n! \sqrt{m!}} \langle n+6|m\rangle \right) + \dots \right] \\
&= \frac{1}{\sqrt[4]{2\pi}} e^{-\frac{1}{4}\chi_\theta^2} e^{-\frac{|\alpha e^{i\eta}|^2}{2}} \left[ \left( \sum_{n=0} \frac{(\chi_\theta \alpha e^{i(\eta-\theta)})^n}{n!} \right) - \frac{1}{2} \left( \sum_{n=0} \frac{\sqrt{(n+2)!} e^{-i(n+2)\theta} \chi_\theta^n (\alpha e^{i\eta})^{n+2}}{n! \sqrt{(n+2)!}} \right) \right. \\
&\quad \left. + \frac{1}{8} \left( \sum_{n=0} \frac{\sqrt{(n+4)!} e^{-i(n+4)\theta} \chi_\theta^n (\alpha e^{i\eta})^{n+4}}{n! \sqrt{(n+4)!}} \right) - \frac{1}{48} \left( \sum_{n=0} \frac{\sqrt{(n+6)!} e^{-i(n+6)\theta} \chi_\theta^n (\alpha e^{i\eta})^{n+6}}{n! \sqrt{(n+6)!}} \right) + \dots \right] \\
&= \frac{1}{\sqrt[4]{2\pi}} e^{-\frac{1}{4}\chi_\theta^2} e^{-\frac{|\alpha e^{i\eta}|^2}{2}} \left[ \left( \sum_{n=0} \frac{(\chi_\theta \alpha e^{i(\eta-\theta)})^n}{n!} \right) - \frac{1}{2} \chi_\theta^{-2} \left( \sum_{n=0} \frac{e^{-i(n+2)\theta} (\chi_\theta \alpha e^{i\eta})^{n+2}}{n!} \right) \right. \\
&\quad \left. + \frac{1}{8} \chi_\theta^{-4} \left( \sum_{n=0} \frac{e^{-i(n+4)\theta} (\chi_\theta \alpha e^{i\eta})^{n+4}}{n!} \right) - \frac{1}{48} \chi_\theta^{-6} \left( \sum_{n=0} \frac{e^{-i(n+6)\theta} (\chi_\theta \alpha e^{i\eta})^{n+6}}{n!} \right) + \dots \right] \\
&= \frac{1}{\sqrt[4]{2\pi}} e^{-\frac{1}{4}\chi_\theta^2} e^{-\frac{|\alpha e^{i\eta}|^2}{2}} \left[ \left( \sum_{n=0} \frac{(\chi_\theta \alpha e^{i(\eta-\theta)})^n}{n!} \right) - \frac{1}{2} \chi_\theta^{-2} \left( \sum_{n=0} \frac{(\chi_\theta \alpha e^{i(\eta-\theta)})^{n+2}}{n!} \right) \right. \\
&\quad \left. + \frac{1}{8} \chi_\theta^{-4} \left( \sum_{n=0} \frac{(\chi_\theta \alpha e^{i(\eta-\theta)})^{n+4}}{n!} \right) - \frac{1}{48} \chi_\theta^{-6} \left( \sum_{n=0} \frac{(\chi_\theta \alpha e^{i(\eta-\theta)})^{n+6}}{n!} \right) + \dots \right] \\
&= \frac{1}{\sqrt[4]{2\pi}} e^{-\frac{1}{4}\chi_\theta^2} e^{-\frac{|\alpha e^{i\eta}|^2}{2}} \left[ \left( \sum_{n=0} \frac{(\chi_\theta \alpha e^{i(\eta-\theta)})^n}{n!} \right) - \frac{1}{2} \chi_\theta^{-2} (\chi_\theta \alpha e^{i(\eta-\theta)})^2 \left( \sum_{n=0} \frac{(\chi_\theta \alpha e^{i(\eta-\theta)})^n}{n!} \right) \right. \\
&\quad \left. + \frac{1}{8} \chi_\theta^{-4} (\chi_\theta \alpha e^{i(\eta-\theta)})^4 \left( \sum_{n=0} \frac{(\chi_\theta \alpha e^{i(\eta-\theta)})^n}{n!} \right) - \frac{1}{48} \chi_\theta^{-6} (\chi_\theta \alpha e^{i(\eta-\theta)})^6 \left( \sum_{n=0} \frac{(\chi_\theta \alpha e^{i(\eta-\theta)})^n}{n!} \right) + \dots \right]
\end{aligned} \tag{7.15}$$

$$\begin{aligned}
\langle \chi_\theta | \alpha e^{i\eta} \rangle &= \frac{1}{\sqrt[4]{2\pi}} e^{-\frac{1}{4}\chi_\theta^2} e^{-\frac{|\alpha e^{i\eta}|^2}{2}} \left[ \left( \sum_{n=0}^{\infty} \frac{(\chi_\theta \alpha e^{i(\eta-\theta)})^n}{n!} \right) - \frac{1}{2} \chi_\theta^{-2} \left( \sum_{n=0}^{\infty} \frac{(\chi_\theta \alpha e^{i(\eta-\theta)})^{n+2}}{n!} \right) \right. \\
&\quad \left. + \frac{1}{8} \chi_\theta^{-4} \left( \sum_{n=0}^{\infty} \frac{(\chi_\theta \alpha e^{i(\eta-\theta)})^{n+4}}{n!} \right) - \frac{1}{48} \chi_\theta^{-6} \left( \sum_{n=0}^{\infty} \frac{(\chi_\theta \alpha e^{i(\eta-\theta)})^{n+6}}{n!} \right) + \dots \right] \\
&= \frac{1}{\sqrt[4]{2\pi}} e^{-\frac{1}{4}\chi_\theta^2} e^{-\frac{|\alpha e^{i\eta}|^2}{2}} \left[ \left( \sum_{n=0}^{\infty} \frac{(\chi_\theta \alpha e^{i(\eta-\theta)})^n}{n!} \right) - \frac{1}{2} \chi_\theta^{-2} (\chi_\theta \alpha e^{i(\eta-\theta)})^2 \left( \sum_{n=0}^{\infty} \frac{(\chi_\theta \alpha e^{i(\eta-\theta)})^n}{n!} \right) \right. \\
&\quad \left. + \frac{1}{8} \chi_\theta^{-4} (\chi_\theta \alpha e^{i(\eta-\theta)})^4 \left( \sum_{n=0}^{\infty} \frac{(\chi_\theta \alpha e^{i(\eta-\theta)})^n}{n!} \right) - \frac{1}{48} \chi_\theta^{-6} (\chi_\theta \alpha e^{i(\eta-\theta)})^6 \left( \sum_{n=0}^{\infty} \frac{(\chi_\theta \alpha e^{i(\eta-\theta)})^n}{n!} \right) + \dots \right] \\
&= \frac{1}{\sqrt[4]{2\pi}} e^{-\frac{1}{4}\chi_\theta^2} e^{-\frac{|\alpha e^{i\eta}|^2}{2}} e^{\chi_\theta \alpha e^{i(\eta-\theta)}} \left[ 1 - \frac{1}{2} (\alpha e^{i(\eta-\theta)})^2 + \frac{1}{8} (\alpha e^{i(\eta-\theta)})^4 - \frac{1}{48} (\alpha e^{i(\eta-\theta)})^6 + \dots \right] \\
&= \frac{1}{\sqrt[4]{2\pi}} e^{-\frac{1}{4}\chi_\theta^2} e^{-\frac{|\alpha e^{i\eta}|^2}{2}} e^{\chi_\theta \alpha e^{i(\eta-\theta)}} \sum_{n=0}^{\infty} \frac{(-\frac{1}{2} (\alpha e^{i(\eta-\theta)})^2)^n}{n!} \\
&= \frac{1}{\sqrt[4]{2\pi}} e^{-\frac{1}{4}\chi_\theta^2} e^{-\frac{|\alpha e^{i\eta}|^2}{2}} e^{\chi_\theta \alpha e^{i(\eta-\theta)}} e^{-\frac{1}{2} (\alpha e^{i(\eta-\theta)})^2} \\
&= \frac{1}{\sqrt[4]{2\pi}} e^{-\frac{|\alpha|^2}{2}} e^{-\frac{1}{4}\chi_\theta^2} e^{\chi_\theta (\alpha_1 + i\alpha_2)} e^{-\frac{1}{2} (\alpha_1 + i\alpha_2)^2} \quad (\text{where } \alpha_1 + i\alpha_2 \equiv \alpha e^{i[(|g|^2 t / \Delta) \cos^2(kx + \xi) - \theta]}) = \alpha e^{i(\eta - \theta)} \\
&= \frac{1}{\sqrt[4]{2\pi}} e^{-\frac{(\alpha_1^2 + \alpha_2^2)}{2} - \frac{1}{4}\chi_\theta^2 + \chi_\theta \alpha_1 + i\chi_\theta \alpha_2 - \frac{1}{2}(\alpha_1^2 + 2i\alpha_1 \alpha_2 - \alpha_2^2)} \\
&= \frac{1}{\sqrt[4]{2\pi}} e^{-\alpha_1^2 - \frac{1}{4}\chi_\theta^2 + \chi_\theta \alpha_1 + i\chi_\theta \alpha_2 - i\alpha_1 \alpha_2} \\
&= \frac{1}{\sqrt[4]{2\pi}} e^{-[(\alpha_1 - \frac{\chi_\theta}{2})^2 + i\alpha_2(\alpha_1 - \chi_\theta)]}
\end{aligned}$$

$$\begin{aligned}
\langle \psi(t) | \psi(t) \rangle &= \left[ N \int dx \kappa^*(x) \frac{1}{\sqrt[4]{2\pi}} e^{-[(\alpha_1 - \frac{\chi_\theta}{2})^2 - i\alpha_2(\alpha_1 - \chi_\theta)]} \langle x, g | \right] \left[ N \int dx \kappa(x) \frac{1}{\sqrt[4]{2\pi}} e^{-[(\alpha_1 - \frac{\chi_\theta}{2})^2 + i\alpha_2(\alpha_1 - \chi_\theta)]} \right] \\
&= \int \frac{N^2 |\kappa(x)|^2}{\sqrt{2\pi}} e^{-2[\alpha_1 - \frac{\chi_\theta}{2}]^2} dx, \quad \text{with } \chi_\theta = 0. \\
&= \frac{N^2 |\kappa|^2}{\sqrt{2\pi}} \int_{-0.25}^{0.25} e^{-2[\alpha_1]^2} dx \\
&= \frac{N^2 |\kappa|^2}{\sqrt{2\pi}} \int_{-0.25}^{0.25} e^{-2[\alpha \cos[\pi \cos^2(kx + \xi)]]^2} dx, \quad \text{with } \alpha = \sqrt{8}, y \xi = 0. \\
&= \frac{N^2 |\kappa|^2}{\sqrt{2\pi}} \int_{-0.25}^{0.25} e^{-16 \cos^2[\pi \cos^2(kx)]} dx \\
&= \frac{N^2 |\kappa|^2}{\sqrt{2\pi}} (4.59769x10^{-2}) = 1.
\end{aligned} \tag{7.17}$$

$$\begin{aligned}
N^2 &= \frac{\sqrt{2\pi}}{|\kappa|^2 (4.59769x10^{-2})} \\
N &= \frac{\sqrt[4]{2\pi}}{|\kappa| \sqrt{4.59769x10^{-2}}} \\
&= \frac{\sqrt[4]{2\pi}}{|\kappa| \sqrt{C}}, \quad \text{with } C = 4.59769x10^{-2}.
\end{aligned} \tag{7.18}$$

$$\begin{aligned}
\langle x', g | \psi(t') \rangle &= \psi(x', t') = \int dx \langle x', g | e^{-\frac{it'}{\hbar} \frac{p^2}{2m}} | x, g \rangle \langle x, g | \psi(t) \rangle \\
&= \int dx \langle x', g | \int dp' | p' \rangle \langle p' | e^{-\frac{it'}{\hbar} \frac{p^2}{2m}} \int dp | p \rangle \langle p | x, g \rangle \psi(x, t) \\
&= \int dx \int dp' \int dp \langle x', g | p' \rangle \langle p' | e^{-\frac{it'}{\hbar} \frac{p^2}{2m}} | p \rangle \langle p | x, g \rangle \psi(x, t) \\
&= \int dx \int dp' \int dp \frac{1}{\sqrt{2\pi\hbar}} e^{i\frac{x'p'}{\hbar}} e^{-\frac{it'}{\hbar} \frac{p^2}{2m}} \delta(p' - p) \frac{1}{\sqrt{2\pi\hbar}} e^{-i\frac{xp}{\hbar}} \psi(x, t) \\
&= \frac{1}{2\pi\hbar} \int dx \int dp e^{-\frac{it'}{\hbar} \frac{p^2}{2m}} e^{i\frac{p}{\hbar}(x'-x)} \psi(x, t) \\
&= \frac{1}{2\pi\hbar} \int dx e^{\frac{im}{2\hbar t'}(x'-x)^2} \int dp e^{-\frac{it'}{2m\hbar}(p - \frac{m}{t'}(x'-x))^2} \psi(x, t) \\
&= \frac{1}{2\pi\hbar} \int dx e^{\frac{im}{2\hbar t'}(x'-x)^2} \sqrt{\frac{2\pi m\hbar}{it'}} \psi(x, t) \\
&= \sqrt{\frac{m}{2\pi i\hbar t'}} \int dx e^{\frac{im}{2\hbar t'}(x'-x)^2} \psi(x, t) \\
&= \sqrt{\frac{m}{2\pi i\hbar t'}} N \int dx e^{\frac{im}{2\hbar t'}(x'-x)^2} \kappa(x) \frac{1}{\sqrt[4]{2\pi}} e^{-[\alpha_1^2(x) + i\alpha_2(x)\alpha_1(x)]} \\
&= \sqrt{\frac{m}{2\pi i\hbar t'}} \frac{1}{\sqrt[4]{2\pi}} N \int dx e^{\frac{im}{2\hbar t'}(x'-x)^2} \kappa(x) e^{-[\alpha_1^2(x) + i\alpha_2(x)\alpha_1(x)]} \\
&= \sqrt{\frac{m}{2\pi i\hbar t'}} \frac{1}{\sqrt[4]{2\pi}} N \int dx e^{\frac{im}{2\hbar t'}(x'-x)^2} \kappa(x) e^{-[\alpha^2 \cos^2(\pi \cos^2(kx)) + i\alpha^2 \cos(\pi \cos^2(kx)) \sin(\pi \cos^2(kx))]} \\
&= \sqrt{\frac{m}{2\pi i\hbar t'}} \frac{1}{\sqrt[4]{2\pi}} N \int dx e^{\frac{im}{2\hbar t'}(x'-x)^2} \kappa(x) e^{-[\alpha^2 \cos^2(\pi \cos^2(kx)) + i\alpha^2 \frac{1}{2} \sin(2\pi \cos^2(kx))]} \\
&= \sqrt{\frac{m}{2\pi i\hbar t'}} \frac{1}{\sqrt[4]{2\pi}} N \int dx e^{\frac{im}{2\hbar t'}(x'-x)^2} \kappa(x) e^{-\alpha^2 \cos^2(\pi \cos^2(kx))} e^{-i\alpha^2 \frac{1}{2} \sin(2\pi \cos^2(kx))} \\
&= \sqrt{\frac{m}{2\pi i\hbar t'}} \frac{1}{\sqrt[4]{2\pi}} N \int dx e^{\frac{im}{2\hbar t'}(x'-x)^2} \kappa(x) e^{-8 \cos^2(\pi \cos^2(kx))} e^{-i4 \sin(2\pi \cos^2(kx))} \\
&= \sqrt{\frac{m}{2\pi i\hbar t'}} \frac{1}{\sqrt[4]{2\pi}} N \int dx \kappa(x) e^{i[\frac{m}{2\hbar t'}(x'-x)^2 - 4 \sin(2\pi \cos^2(kx))]} e^{-8 \cos^2(\pi \cos^2(kx))}
\end{aligned}$$

(7.19)

$$\begin{aligned}
\psi(x', t') &= \sqrt{\frac{m}{2\pi i \hbar t'}} \frac{1}{\sqrt[4]{2\pi}} N \int dx \kappa(x) e^{i[\frac{m}{2\hbar t'}(x'-x)^2 - 4 \sin(2\pi \cos^2(kx))]} e^{-8 \cos^2(\pi \cos^2(kx))} \\
&= \sqrt{\frac{m}{2\pi i \hbar t'}} \frac{1}{\sqrt[4]{2\pi}} N \int_{-0.25\lambda}^{0.25\lambda} dx \kappa(x) e^{i[\frac{m}{2\hbar t'}(x'-x)^2 - 4 \sin(2\pi \cos^2(kx))]} e^{-8 \cos^2(\pi \cos^2(kx))} \quad \text{with } N = \frac{\sqrt[4]{2\pi}}{|\kappa|\sqrt{C}} \\
&= \sqrt{\frac{m}{2\pi i \hbar t'}} \sqrt{\frac{2k^2}{2k^2}} \frac{1}{\sqrt[4]{2\pi}} \left( \frac{\sqrt[4]{2\pi}}{|\kappa|\sqrt{C}} \right) \kappa \int_{-0.25\lambda}^{0.25\lambda} dx e^{i[\frac{m}{2\hbar t'} \frac{2k^2}{2k^2}(x'-x)^2 - 4 \sin(2\pi \cos^2(kx))]} e^{-8 \cos^2(\pi \cos^2(kx))} \\
&= \frac{k}{\sqrt{4C\pi i t'}} \int_{-0.25\lambda}^{0.25\lambda} dx e^{i[\frac{1}{4t'}(kx'-kx)^2 - 4 \sin(2\pi \cos^2(kx))]} e^{-8 \cos^2(\pi \cos^2(kx))}, \quad \text{Let this be } u = kx, dx = \frac{du}{k} \\
&= \frac{k}{\sqrt{4C\pi i t'}} \int_{-0.25\lambda k}^{0.25\lambda k} \frac{du}{k} e^{i[\frac{1}{4t'}(kx'-u)^2 - 4 \sin(2\pi \cos^2(u))]} e^{-8 \cos^2(\pi \cos^2(u))} \\
&= \frac{1}{\sqrt{4C\pi i t'}} \int_{-0.25 \cdot 2\pi}^{0.25 \cdot 2\pi} du e^{i[\frac{1}{4t'}(kx'-u)^2 - 4 \sin(2\pi \cos^2(u))]} e^{-8 \cos^2(\pi \cos^2(u))} \\
&= \frac{1}{\sqrt{4C\pi i t'}} \int_{-0.25 \cdot 2\pi}^{0.25 \cdot 2\pi} du e^{i[\frac{1}{4t'}(2\pi x' - u)^2 - 4 \sin(2\pi \cos^2(u))]} e^{-8 \cos^2(\pi \cos^2(u))}
\end{aligned} \tag{7.20}$$

$$\begin{aligned}
\langle \psi(t) | \psi(t) \rangle &= \left[ N \int dx \kappa^*(x) \frac{1}{\sqrt[4]{2\pi}} e^{-[(\alpha_1 - \frac{\chi_\theta}{2})^2 - i\alpha_2(\alpha_1 - \chi_\theta)]} \langle x, g | \right] \left[ N \int dx \kappa(x) \frac{1}{\sqrt[4]{2\pi}} e^{-[(\alpha_1 - \frac{\chi_\theta}{2})^2 + i\alpha_2(\alpha_1 - \chi_\theta)]} \right] \\
&= \int \frac{N^2 |\kappa(x)|^2}{\sqrt{2\pi}} e^{-2[\alpha_1 - \frac{\chi_\theta}{2}]^2} dx, \quad \text{with } \chi_\theta = 0. \\
&= \frac{N^2 |\kappa|^2}{\sqrt{2\pi}} \int_{-0.375}^{0.375} e^{-2[\alpha_1]^2} dx \\
&= \frac{N^2 |\kappa|^2}{\sqrt{2\pi}} \int_{-0.375}^{0.375} e^{-2[\alpha \cos[\pi \cos^2(kx + \xi)]]^2} dx, \quad \text{with } \alpha = \sqrt{8}, \text{ y } \xi = 1/8. \\
&= \frac{N^2 |\kappa|^2}{\sqrt{2\pi}} \int_{-0.375}^{0.375} e^{-16 \cos^2[\pi \cos^2(kx + 1/8)]} dx \\
&= \frac{N^2 |\kappa|^2}{\sqrt{2\pi}} (6.89653 \times 10^{-2}) = 1.
\end{aligned} \tag{7.21}$$

$$\begin{aligned}
N^2 &= \frac{\sqrt{2\pi}}{|\kappa|^2 (6.89653 \times 10^{-2})} \\
N &= \frac{\sqrt[4]{2\pi}}{|\kappa| \sqrt{6.89653 \times 10^{-2}}} \\
&= \frac{\sqrt[4]{2\pi}}{|\kappa| \sqrt{C}}, \quad \text{with } C = 6.89653 \times 10^{-2}.
\end{aligned} \tag{7.22}$$

$$\begin{aligned}
\psi(x', t') &= \sqrt{\frac{m}{2\pi i\hbar t'}} \frac{1}{\sqrt[4]{2\pi}} N \int dx \kappa(x) e^{i[\frac{m}{2\hbar t'}(x'-x)^2 - 4 \sin(2\pi \cos^2(k[x+1/8]))]} e^{-8 \cos^2(\pi \cos^2(k[x+1/8]))} \\
&= \sqrt{\frac{m}{2\pi i\hbar t'}} \frac{1}{\sqrt[4]{2\pi}} N \int_{-0.375\lambda}^{0.375\lambda} dx \kappa(x) e^{i[\frac{m}{2\hbar t'}(x'-x)^2 - 4 \sin(2\pi \cos^2(k[x+1/8]))]} e^{-8 \cos^2(\pi \cos^2(k[x+1/8]))} \quad \text{with } N = \frac{\sqrt[4]{2\pi}}{|\kappa|\sqrt{C}} \\
&= \sqrt{\frac{m}{2\pi i\hbar t'}} \sqrt{\frac{2k^2}{2k^2}} \frac{1}{\sqrt[4]{2\pi}} \left( \frac{\sqrt[4]{2\pi}}{|\kappa|\sqrt{C}} \right) \kappa \int_{-0.375\lambda}^{0.375\lambda} dx e^{i[\frac{m}{2\hbar t'} \frac{2k^2}{2k^2} (x'-x)^2 - 4 \sin(2\pi \cos^2(k[x+1/8]))]} e^{-8 \cos^2(\pi \cos^2(k[x+1/8]))} \\
&= \frac{k}{\sqrt{4C\pi i t'}} \int_{-0.375\lambda}^{0.375\lambda} dx e^{i[\frac{1}{4t'}(kx'-kx)^2 - 4 \sin(2\pi \cos^2(k[x+1/8]))]} e^{-8 \cos^2(\pi \cos^2(k[x+1/8]))}, \quad \text{Let this be } u = k[x + 1/8] \\
&= \frac{k}{\sqrt{4C\pi i t'}} \int_{[-0.375+1/8]\lambda k}^{[0.375+1/8]\lambda k} \frac{du}{k} e^{i[\frac{1}{4t'}(kx'-[u-k/8])^2 - 4 \sin(2\pi \cos^2(u))]} e^{-8 \cos^2(\pi \cos^2(u))} \\
&= \frac{1}{\sqrt{4C\pi i t'}} \int_{[-0.375+1/8]\cdot 2\pi}^{[0.375+1/8]\cdot 2\pi} du e^{i[\frac{1}{4t'}(kx'-[u-k/8])^2 - 4 \sin(2\pi \cos^2(u))]} e^{-8 \cos^2(\pi \cos^2(u))} \\
&= \frac{1}{\sqrt{4C\pi i t'}} \int_{[-0.375+1/8]\cdot 2\pi}^{[0.375+1/8]\cdot 2\pi} du e^{i[\frac{1}{4t'}(2\pi x' - [u-2\pi/8])^2 - 4 \sin(2\pi \cos^2(u))]} e^{-8 \cos^2(\pi \cos^2(u))}
\end{aligned} \tag{7.23}$$

### 7.1.3 Appendix chapter 3

$$\begin{aligned}
|\psi(t)\rangle &= \hat{U} (|\psi(0)\rangle_{atom} \otimes |\psi(0)\rangle_{field}) \\
&= e^{-\frac{i\hat{V}t}{\hbar}} \left( c_{\uparrow}|P_{\uparrow}\rangle \otimes [\cos \phi|b\rangle + \sin \phi|a\rangle] + c_{\downarrow}|P_{\downarrow}\rangle \otimes |b\rangle \right) \\
&\otimes |\alpha, \xi\rangle \\
&= e^{-\frac{it|g|^2 \cos^2(kx+\xi)}{\Delta} \hat{\sigma}_z \hat{a}^\dagger \hat{a}} e^{-it\Delta \hat{\sigma}_z} \left( c_{\uparrow}|P_{\uparrow}\rangle \otimes [\cos \phi|b\rangle + \sin \phi|a\rangle] \right. \\
&\left. + c_{\downarrow}|P_{\downarrow}\rangle \otimes |b\rangle \right) \otimes |\alpha, \xi\rangle \\
&= c_{\uparrow}|P_{\uparrow}\rangle \otimes \cos \phi e^{i\eta(x)n} e^{it\Delta}|b\rangle \otimes |\alpha, \xi\rangle \\
&+ c_{\uparrow}|P_{\uparrow}\rangle \otimes \sin \phi e^{-i\eta(x)n} e^{-it\Delta}|a\rangle \otimes |\alpha, \xi\rangle \\
&+ c_{\downarrow}|P_{\downarrow}\rangle \otimes e^{i\eta(x)n} e^{it\Delta}|b\rangle \otimes |\alpha, \xi\rangle \\
&= e^{it\Delta} c_{\uparrow}|P_{\uparrow}\rangle \otimes \cos \phi|b\rangle \otimes |e^{i\eta(x)}\alpha, \xi\rangle \\
&+ e^{-it\Delta} c_{\uparrow}|P_{\uparrow}\rangle \otimes \sin \phi|a\rangle \otimes |e^{-i\eta(x)}\alpha, \xi\rangle \\
&+ e^{it\Delta} c_{\downarrow}|P_{\downarrow}\rangle \otimes |b\rangle \otimes |e^{i\eta(x)}\alpha, \xi\rangle
\end{aligned} \tag{7.24}$$

$$\begin{aligned}
|\psi(t)\rangle &= \hat{U} (|\psi(0)\rangle_{atom} \otimes |\psi(0)\rangle_{field}) \\
&= e^{-\frac{i\hat{V}t}{\hbar}} \left( c_{\uparrow}|P_{\uparrow}\rangle \otimes [\cos \phi|b\rangle + \sin \phi|a\rangle] + c_{\downarrow}|P_{\downarrow}\rangle \otimes |b\rangle \right) \\
&\otimes |cat\rangle_{o,e} \\
&= e^{-\frac{it|g|^2 \cos^2(kx+\xi)}{\Delta} \hat{\sigma}_z \hat{a}^\dagger \hat{a}} e^{-it\Delta \hat{\sigma}_z} \left( c_{\uparrow}|P_{\uparrow}\rangle \otimes [\cos \phi|b\rangle + \sin \phi|a\rangle] \right. \\
&\left. + c_{\downarrow}|P_{\downarrow}\rangle \otimes |b\rangle \right) \otimes \left( \frac{|\alpha\rangle \pm |-\alpha\rangle}{\sqrt{2(1+e^{-2|\alpha|^2})}} \right) \\
&= e^{it\Delta} c_{\uparrow}|P_{\uparrow}\rangle \otimes \cos \phi|b\rangle \otimes \left( \frac{|e^{i\eta(x)}\alpha\rangle \pm | - e^{i\eta(x)}\alpha\rangle}{\sqrt{2(1+e^{-2|\alpha|^2})}} \right) \\
&+ e^{-it\Delta} c_{\uparrow}|P_{\uparrow}\rangle \otimes \sin \phi|a\rangle \otimes \left( \frac{|e^{-i\eta(x)}\alpha\rangle \pm | - e^{-i\eta(x)}\alpha\rangle}{\sqrt{2(1+e^{-2|\alpha|^2})}} \right) \\
&+ e^{it\Delta} c_{\downarrow}|P_{\downarrow}\rangle \otimes |b\rangle \otimes \left( \frac{|e^{i\eta(x)}\alpha\rangle \pm | - e^{i\eta(x)}\alpha\rangle}{\sqrt{2(1+e^{-2|\alpha|^2})}} \right).
\end{aligned} \tag{7.25}$$

# Bibliography

- [1] (1756). *The History of the Royal Society of London for Improving of Natural Knowledge ... as a Supplement to The Philosophical Transactions. By Thomas Birch ... Vol. 1. (-4.)*. Number v. 1.
- [2] Abend, S., Gersemann, M., Schubert, C., Schlippert, D., Rasel, E. M., Zimmermann, M., Efremov, M. A., Roura, A., Narducci, F. A., and Schleich, W. P. (2020). Atom interferometry and its applications.
- [3] Achard, F. (2005). Chapter 44 - james clerk maxwell, a treatise on electricity and magnetism, first edition (1873). In Grattan-Guinness, I., Cooke, R., Corry, L., Crépel, P., and Guicciardini, N., editors, *Landmark Writings in Western Mathematics 1640-1940*, pages 564–587. Elsevier Science, Amsterdam.
- [4] Aharonov, Y. and Zebairy, M. S. (2005). Time and the quantum: Erasing the past and impacting the future. *Science*, 307(5711):875–879.
- [5] Balykin, V. I., Letokhov, V. S., Ovchinnikov, Y. B., and Sidorov, A. I. (1988). Quantum-state-selective mirror reflection of atoms by laser light. *Phys. Rev. Lett.*, 60:2137–2140.
- [6] Bergou, J. A. and Hillery, M. (2013). *Introduction to the theory of quantum information processing*. Springer Science & Business Media.
- [7] Bohr, N. (1928). The quantum postulate and the recent development of atomic theory. *Nature*, 121:580–590.
- [8] Brownson, C. (1981). Euclid’s optics and its compatibility with linear perspective. *Archive for history of Exact Sciences*, 24(3):165–194.
- [9] Burton, H. E. (1945). The optics of euclid1. *JOSA*, 35(5):357–372.
- [10] Cooper, M. and Hunter, M. (2006). *Robert Hooke: Tercentennial Studies*. Ashgate.
- [11] Cottingham, J., Stoothoff, R., Murdoch, D., Kenny, A., et al. (1985). *The philosophical writings of Descartes*, volume 1. Cambridge University Press Cambridge.
- [12] Davisson, C. J. and Germer, L. H. (1928). Reflection of electrons by a crystal of nickel. *Proceedings of the National Academy of Sciences of the United States of America*, 14(4):317.

- [13] De Broglie, L. (1924). *Recherches sur la théorie des quanta*, Doct. PhD thesis, thesis, Univ. Paris.
- [14] Eden, A. (1992). The search for christian doppler. In *The Search for Christian Doppler*, pages 1–4. Springer.
- [15] Einstein, A. (2005). Über einen die erzeugung und verwandlung des lichtes betreffenden heuristischen gesichtspunkt [adp 17, 132 (1905)]. *Annalen der Physik*, 14(S1 1):164–181.
- [16] Einstein, A., Podolsky, B., and Rosen, N. (1935). Can quantum-mechanical description of physical reality be considered complete? *Phys. Rev.*, 47:777–780.
- [17] Englert, B.-G. (1996). Fringe visibility and which-way information: An inequality. *Phys. Rev. Lett.*, 77:2154–2157.
- [18] Estermann, I. and Stern, O. (1930). Beugung von molekularstrahlen. *Zeitschrift für Physik*, 61(1):95–125.
- [19] Evans, R. D. (1958). Compton effect. In *Corpuscles and Radiation in Matter II/Korpuskeln und Strahlung in Materie II*, pages 218–298. Springer.
- [20] Fresnel, A. (1868). *Oeuvres complètes d'augustin Fresnel*, volume 2. Imprimerie impériale.
- [21] Gerry, C., Knight, P., and Knight, P. L. (2005). *Introductory quantum optics*. Cambridge university press.
- [22] Glasgow, S., Meystre, P., Wilkens, M., and Wright, E. M. (1991). Theory of an atomic beam splitter based on velocity-tuned resonances. *Phys. Rev. A*, 43:2455–2463.
- [23] Gong, J. J. and Aravind, P. K. (1990). Expansion coefficients of a squeezed coherent state in the number state basis. *American Journal of Physics*, 58(10):1003–1006.
- [24] Gould, P. L., Ruff, G. A., and Pritchard, D. E. (1986). Diffraction of atoms by light: The near-resonant kapitza-dirac effect. *Phys. Rev. Lett.*, 56:827–830.
- [25] Greenberger, D. M. and Yasin, A. (1988). Simultaneous wave and particle knowledge in a neutron interferometer. *Physics Letters A*, 128(8):391 – 394.
- [26] Haroche, S. and Kleppner, D. (1989). Cavity quantum electrodynamics. *Phys. Today*, 42(1):24–30.
- [27] Hartmann, S., Jenewein, J., Giese, E., Abend, S., Roura, A., Rasel, E. M., and Schleich, W. P. (2020). Regimes of atomic diffraction: Raman versus bragg diffraction in retroreflective geometries. *Phys. Rev. A*, 101:053610.
- [28] Hertz, H. (1990). *Las ondas electromagnéticas*, volume 2. Univ. Autònoma de Barcelona.
- [29] Huygens, C. (1690). *Traite de la lumiere: Où sont expliquées les causes de ce qui luy arrive dans la reflexion, & dans la refraction. Et particulièrement dans l'etrange refraction du cristal d'Islande*. Chez Pierre vander Aa.

- [30] Huygens, C. (1955). *Treatise on Light: In which are Explained the Causes of that which Occurs in Reflexion, & in Refraction, and Particularly in the Strange Refraction of Iceland Crystal : Rendered Into English by Silvanus P. Thompson*. University of Chicago Press.
- [31] Jaeger, G., Horne, M. A., and Shimony, A. (1993). Complementarity of one-particle and two-particle interference. *Phys. Rev. A*, 48:1023–1027.
- [32] Jaeger, G., Shimony, A., and Vaidman, L. (1995). Two interferometric complementarities. *Phys. Rev. A*, 51:54–67.
- [33] Jakob, M. and Bergou, J. A. (2003). Quantitative complementarity relations in bipartite systems.
- [34] Jakob, M. and Bergou, J. A. (2007). Complementarity and entanglement in bipartite qudit systems. *Phys. Rev. A*, 76:052107.
- [35] Jakob, M. and Bergou, J. A. (2010). Quantitative complementarity relations in bipartite systems: Entanglement as a physical reality. *Optics Communications*, 283(5):827 – 830.
- [36] Jönsson, C. (1974). Electron diffraction at multiple slits. *American Journal of Physics*, 42(1):4–11.
- [37] Klein, M. J. (1973). The development of boltzmann’s statistical ideas. In *The Boltzmann Equation*, pages 53–106. Springer.
- [38] Kragh, H. (2000). Max planck: the reluctant revolutionary. *Physics World*, 13(12):31.
- [39] Kragh, H. (2020). *Quantum generations*. Princeton University Press.
- [40] Kwan, A., Dudley, J., and Lantz, E. (2002). Who really discovered snell’s law? *Physics World*, 15(4):64.
- [41] Libri, G. (1838). *Histoire des sciences mathématiques en Italie, depuis la renaissance des lettres jusqu’à la fin du dix-septième siècle*. Number v. 2 in *Histoire des sciences mathématiques en Italie, depuis la renaissance des lettres jusqu’à la fin du dix-septième siècle*. J. Renouard.
- [42] Maxwell, J. (1873). *A Treatise on Electricity and Magnetism*. Number v. 1 in *A Treatise on Electricity and Magnetism*. Clarendon Press.
- [43] Merimeche, H. (2006). Atomic beam focusing with a curved magnetic mirror. *Journal of Physics B: Atomic, Molecular and Optical Physics*, 39(18):3723–3731.
- [44] Meyer, C. (1949). *The Diffraction of Light, X-rays, and Material Particles: An Introductory Treatment*. J. W. Edwards.
- [45] Miranda, M. and Orszag, M. (2020). Control of interference and diffraction of a three-level atom in a double-slit scheme with cavity fields. *Phys. Rev. A*, 102:033723.
- [46] Miranda, M. and Orszag, M. (2021). Controlling parameters of the wave-particle duality of a two-level atom in a double-slit scheme with cavity field. *JOSA B*, 38(2):652–661.

- [47] Newton, I. (1672). Newton isaac 1672mr. isaac newtons answer to some considerations upon his doctrine of light and colors. *Phil. Trans. R. Soc.*, page 75084–5103.
- [48] Newton, I. (1718). *Opticks: Or, A Treatise of the Reflections, Refractions, Inflections and Colours of Light*. W. and J. Innys .
- [49] Olivares, S. (2012). Quantum optics in the phase space. *The European Physical Journal Special Topics*, 203(1):3–24.
- [50] Orszag, M. (2016). Quantum optics.
- [51] Orszag, M., Ramirez, R., Retamal, J. C., and Saavedra, C. (1995). On the atomic microscope. *Quantum and Semiclassical Optics: Journal of the European Optical Society Part B*, 7(4):455–459.
- [52] Planck, M. (1900). On an improvement of wien’s equation for the spectrum. *Ann. Physik*, 1:719–721.
- [53] Qian, X.-F., Konthasinghe, K., Manikandan, S. K., Spiecker, D., Vamivakas, A. N., and Eberly, J. H. (2020). Turning off quantum duality. *Phys. Rev. Research*, 2:012016.
- [54] Ramsey, N. F. (1950). A molecular beam resonance method with separated oscillating fields. *Phys. Rev.*, 78:695–699.
- [55] Robertson, H. P. (1929). The uncertainty principle. *Physical Review*, 34(1):163.
- [56] Scully, M. O. and Drühl, K. (1982). Quantum eraser: A proposed photon correlation experiment concerning observation and ”delayed choice” in quantum mechanics. *Phys. Rev. A*, 25:2208–2213.
- [57] Scully, M. O., Englert, B.-G., and Walther, H. (1991). Quantum optical tests of complementarity. *Nature*, 351(6322):111–116.
- [58] Scully, M. O. and Zubairy, M. S. (1997). Quantum optics.
- [59] Stachel, J. J. (2005). Einstein’s miraculous year: five papers that changed the face of physics.
- [60] Stites, D. (1970). *Study of Fresnel Diffraction*. Independent studies.
- [61] Storey, P., Collett, M., and Walls, D. (1992). Measurement-induced diffraction and interference of atoms. *Phys. Rev. Lett.*, 68:472–475.
- [62] Storey, P., Collett, M., and Walls, D. (1993). Atomic-position resolution by quadrature-field measurement. *Phys. Rev. A*, 47:405–418.
- [63] Walls, D. F. and Milburn, G. J. (2007). *Quantum optics*. Springer Science & Business Media.
- [64] Wheaton, B. R. (1978). Philipp lenard and the photoelectric effect, 1889-1911. *Historical Studies in the Physical Sciences*, 9:299–322.

- [65] Wheaton, B. R. (2009). Photoelectric effect. In *Compendium of Quantum Physics*, pages 472–475. Springer.
- [66] Wolf, E. (2007). The influence of young’s interference experiment on the development of statistical optics. *Progress in Optics*, 50:251–273.
- [67] Wootters, W. K. (1998). Entanglement of formation of an arbitrary state of two qubits. *Phys. Rev. Lett.*, 80:2245–2248.
- [68] Wootters, W. K. and Zurek, W. H. (1979). Complementarity in the double-slit experiment: Quantum nonseparability and a quantitative statement of bohr’s principle. *Phys. Rev. D*, 19:473–484.
- [69] Young, T. (1804). Experimental demonstration of the general law of the interference of light. *Philosophical Transactions of the Royal society of London*, 94(1804):1.